FINITE ELEMENT MODELING APPROACHES AND COMPARATIVE STUDY ON THE NONLINEAR BEHAVIOR OF STEEL SHEAR-LINKS

A THESIS SUBMITTED TO
THE GRADUATE SCHOOL OF NATURAL AND APPLIED SCIENCES
OF
MIDDLE EAST TECHNICAL UNIVERSITY

YAŞAM KIZILDAĞ

IN PARTIAL FULFILLMENT OF THE REQUIREMENTS
FOR
THE DEGREE OF MASTER OF SCIENCE
IN
CIVIL ENGINEERING

AUGUST 2013

Approval of the thesis:

FINITE ELEMENT MODELING APPROACHES AND COMPARATIVE STUDY ON THE NONLINEAR BEHAVIOR OF STEEL SHEAR-LINKS

Submitted by **YAŞAM KIZILDAĞ** in partial fulfillment of the requirements for the degree of **Master of Science in Civil Engineering Department, Middle East Technical University** by,

Prof. Dr. Canan ÖZGEN
Dean, Graduate School of **Natural and Applied Sciences** _____________

Prof. Dr. Ahmet Cevdet YALÇINER
Head of Department, **Civil Engineering** _____________

Assoc. Prof. Dr. Afşin SARITAŞ
Supervisor, **Civil Engineering Dept., METU** _____________

Examining Committee Members

Prof. Dr. Cem TOPKAYA
Civil Engineering Dept., METU _____________

Assoc. Prof. Dr. Afşin SARITAŞ
Civil Engineering Dept., METU _____________

Assoc. Prof. Dr. Özgür KURÇ
Civil Engineering Dept., METU _____________

Asst. Prof. Dr. Serdar GÖKTEPE
Civil Engineering Dept., METU _____________

Dr. Cenk TORT
Miteng _____________

Date : 29.08.2013

I hereby declare that all information in this document has been obtained and presented in accordance with academic rules and ethical conduct. I also declare that, as required by these rules and conduct, I have fully cited and referenced all material and results that are not original to this work.

Name, Last name: **Yaşam KIZILDAĞ**

Signature:

ABSTRACT

FINITE ELEMENT MODELING APPROACHES AND COMPARATIVE STUDY ON THE NONLINEAR BEHAVIOR OF STEEL SHEAR-LINKS

KIZILDAĞ, Yaşam

M.S., Department of Civil Engineering

Supervisor: Assoc. Prof. Dr. Afşin SARITAŞ

August 2013, 75 pages

This study deals with the finite element modeling of the nonlinear behavior of shear links under various loading and boundary conditions. Shear-links are the most important part of an eccentrically braced steel frame system, and provide fuse in terms of reducing the forces acting on the rest of the members such as columns and braces in the framing system. Shear-links are designed for dissipation of large amounts of energy in case of overloading; therefore construction of buildings with eccentrically braced frames is suitable for earthquake resistant design. Since strength, stiffness and ductility characteristics of shear links dominate the behavior of eccentrically braced frames, having full knowledge of the behavior of shear-links is an important research topic.

The early research on eccentrically braced frames in literature were generally based on experimental studies that were costly to conduct, but nowadays the use of advanced finite element software packages provide opportunity for the assessment and simulation of the nonlinear behavior of shear-links under various loading and boundary conditions.

Such a study has been undertaken in this thesis, and the shear links are modeled and analyzed in finite element program ANSYS Workbench with 2-D and 3-D elements. First, a verification study is conducted, where shear-links from past experiments are considered and the results obtained from the analysis are compared with experimental data. The shear links are modeled according to the original dimensions and boundary conditions. The material properties are calibrated based on the cyclic behavior of steel with some assumptions that are described in detail in the thesis.

After this verification study, a detailed comparative finite element study has been conducted. In this part of the thesis, the links are analyzed not only with the proposed finite element modeling approach, i.e. the utilization of 2-D and 3-D elements and cyclic calibration of steel material through the use of ANSYS Workbench, but also with a frame element that can capture spread of plasticity both along element length and section depth. In the first part of

the comparative study, the contribution of flange to the overall shear force carrying capacity of shear-links is assessed through both finite element modeling approaches. With this comparison, a realistic description of flange shear strain for the frame finite element model is suggested. In the second part of the comparative study, the influence of unsymmetrical loading protocols on the nonlinear behavior of shear-links is studied through the use of both finite element modeling approaches, and the results are compared to each other and the accuracy of the frame finite element model is assessed.

Keywords: Steel, eccentrically braced frames, shear-links, finite element method, cyclic material behavior, cyclic loading, nonlinear structural analysis

ÖZ

ÇELİK BAĞ KİRİŞLERİN DOĞRUSAL OLMAYAN DAVRANIŞLARI ÜSTÜNE SONLU ELEMANLARLA MODELLEME YAKLAŞIMLARI VE KARŞILAŞTIRMALI ÇALIŞMA

KIZILDAĞ, Yaşam

Yüksek Lisans, İnşaat Mühendisliği Bölümü

Tez Yöneticisi: Doç. Dr. Afşin SARITAŞ

Ağustos 2013, 75 sayfa

Bu çalışma, dışmerkez çaprazlı çelik çerçevelerin en önemli parçası olan bağ kirişlerin farklı yüklemeler altında doğrusal olmayan davranışlarını incelemektedir. Bağ kirişler, dışmerkez çaprazlı çelik çerçeve sistemlerin en önemli parçasını oluştururlar ve kolon ve çapraz elemanlar üzerine potansiyel olarak etki edebilecek yüklerin düşürülmesinde sigorta görevi görürler. Doğru tasarlanmış bağ kirişler ciddi yüklemeler altında bile yüksek seviyede enerji sönümleyebilir, bu sebeple dışmerkez çaprazlı çelik çerçeveler depreme dayanıklı yapı tasarımında cazip bir alternatif sistem olarak ortaya çıkmaktadır. Dışmerkez çaprazlı çelik çerçevelerin davranışını belirleyen en önemli etmen bağ kirişinin dayanımı, rijitliği ve süneklik özellikleri olduğu için bağ kirişinin doğrusal olmayan davranışının tam olarak bilinmesi önemli bir araştırma konusudur.

Literatürde dışmerkez çaprazlı çelik çerçeveler üzerine başlarda yapılan araştırmalar daha çok deneysel yöntemlere dayanmıştır. Bu tür çalışmaların yürütülmesinin pahalı ve zahmetli olabilmesinden ötürü ve günümüzde artık gelişmiş sonlu elemanlar yöntemleri ile analiz olanakları sağlayan yazılım paketlerinin kullanımı ile bağ kirişlerin doğrusal olmayan davranışının sayısal olarak tespit edilmesi ciddi araştırma olanakları sunmaktadır.

Bu sebeple, bu tez kapsamında, bağ kirişler 2 ve 3 boyutlu elemanlar kullanılarak, sonlu elemanlar analiz programı ANSYS Workbench ile modellenip analiz edilmiştir. Geliştirilen modellerin doğruluğunun tespit edilmesi için öncelikli olarak literatürde var olan deneysel çalışmalarla karşılaştırma çalışması yürütülmüştür. Bağ kirişler, orijinal boyutları ve sınır koşullarına bağlı kalınarak modellenmiştir. Çelik malzeme özellikleri ise bu tezde detaylı bir şekilde belirtilen bazı kabullerle döngüsel yüklere göre kalibre edilmiştir.

Doğrulama çalışmasının ardından, sonlu elemanlar yönteminde birden fazla yaklaşım tarzı denenerek karşılaştırmalı çalışma yürütülmüştür. Yaklaşımlardan ilki yukarıda da belirtildiği üzere ANSYS Workbench platformunun kullanılmasıyla 2 ve 3 boyutlu sonlu elemanlarla

modelleme ve döngüsel malzeme modelinin kalibre edilmesine dayanmaktadır. İkinci yaklaşım ise daha önceden geliştirilmiş olan ve eleman boyunca ve kesit derinliğinde yayılı plastisiteyi yakalayabilen bir çerçeve elemanı modellenin kullanılması olmuştur. Karşılaştırmalı çalışmanın ilk etabında, bağ kirişinin flanjının kalınlığının değiştirilmesi ile kirişin taşıdığı toplam kesme kuvvetindeki değişim her iki sayısal yöntemle incelenmiştir. Bu karşılaştırmalı çalışmanın sonucu olarak da çerçeve elemanı modelinde kullanılmak üzere kesitte flanja etki edecek kesme birim deformasyonu tavsiyesi verilmiştir. Karşılaştırmalı çalışmanın ikinci etabında ise, simetrik olmayan yüklemelerin etki etmesi durumunda bağ kirişlerin doğrusal olmayan davranışının her iki sayısal yöntem kullanılarak tespit edilmesi amaçlanmış ve çerçeve eleman modelinin tepkilerinin doğruluğu üzerine sonuca varılmıştır.

Anahtar Kelimeler: Çelik, dışmerkez çaprazlı çelik çerçeve, bağ kiriş, sonlu elemanlar yöntemi, döngüsel malzeme davranışı, döngüsel yükleme, doğrusal olmayan yapısal analiz

ACKNOWLEDGMENTS

First and foremost, I offer my most sincere gratitude to my supervisor, Assoc. Prof. Dr. Afşin SARITAŞ for his excellent guidance, understanding, patience and encouragement during my graduate studies. I have been amazingly fortunate to have an advisor who cared so much about my work, and who responded to my questions and queries so selflessly.

I would like to express my thanks to the professors and faculty members whom I have interacted during the course of my graduate studies. They supported me a lot and gave valuable knowledge during not only my graduation period but also my undergraduate years. In particular, I would like to express my sincere thanks to Assoc. Prof. Dr. Ayşegül ASKAN GÜNDOĞAN for her valuable advises, support and friendship.

I wish to express my sincerely thanks to Murat AZAP, who is one of the most important peeople in my life. He has been a brother and a true friend from the beginning of the high school to the end of my life. This thesis would not have been written without him.

I am also grateful to Gamze Didem ÖGET for her limitless support, patience, help and inspirations during my thesis and graduation. I am very lucky to meet her at the first day of school at METU. She is a perfect housemate and workfellow and one of the people who made me who I am.

I am thankful to my friends at MEGA Mühendislik for giving me endless support, patience and friendship. In particular, I am thankful to my chief Kamil ERGÜNER, my ex-chief Doğu BOZALİOĞLU, my dear fellows Ali Günalp GÖRGÜLÜ, Hatice ERGİN, Kübra BEZGİN, Mustafa PAZARBAŞIOĞLU for their helps, tolerations and encouragements.

Many friends have helped me continue my study through these difficult years. I greatly value their friendship and I deeply appreciate their belief in me. I want to specially thank to Ufuk OKUMUŞ and Begüm TUR who did not leave me alone during my endless study hours. They have supported me and helped me stay focused on my study. I also want to thank my dear friends Tuğçe TÜTÜNCÜBAŞI, Cenk ONARAL, Anıl EKİCİ, Deniz KARAER ARIK, Ali Can ARIK, Baran ÇOBANOĞLU, Ali Ersin DİNÇER for their help, support and friendship during my graduate study.

Most importantly, none of these would have been possible without the love and patience of my family to whom this thesis is dedicated. In this regards, I would like to thank my mother Canan KIZILDAĞ, my father Hasan KIZILDAĞ, my sister Yelda KIZILDAĞ ÖZDEMİRLİ and my brother Tolga ÖZDEMİRLİ for their love, understanding, toleration and support. Especially, I wish to give special thanks to my little nephew Nova ÖZDEMİRLİ for being my source of joy in my study time.

TABLE OF CONTENTS

LIST OF TABLES

TABLES

LIST OF FIGURES

FIGURES

CHAPTER 1

INTRODUCTION

1.1. General

Ductility is one of the most important design criteria of a structural system. A ductile structure may take damage during an earthquake but will not collapse if it is in the required strength limits. To meet these requirements, a structure should have sufficient strength, stiffness and energy dissipation capacity, and these requirements basically yielded to the popular use of moment resisting steel framed structures and concentrically braced steel framed structures in construction industry.

Moment resisting frames (MRF) (Fig. 1.1) are designed based on strong column-weak beam design approach. As a result of this design methodology, plastic hinges occur in beam ends, near the beam column joints during a major earthquake and the inelastic action distributed in the structure at beam ends can dissipate large amount of energy. Through this, MRFs can be designed to remain ductile and survive from a major earthquake without failure. However, there are also some disadvantages of this framing system. Since the beams have large flexural deformation capacity, large lateral drifts can be observed. Increasing the element sizes can be a solution to this problem but it may also be uneconomical. The second problem about moment resisting frames is distortion at column panel zones due to the large shear forces that occurs by transferring of moment from beam to column. This situation increases the lateral drift of the system and results in larger P-Δ effects. To strengthen the columns, web doubler plates are generally used in column panel zones. Consequently, the cost of the structure increases with these expenses.

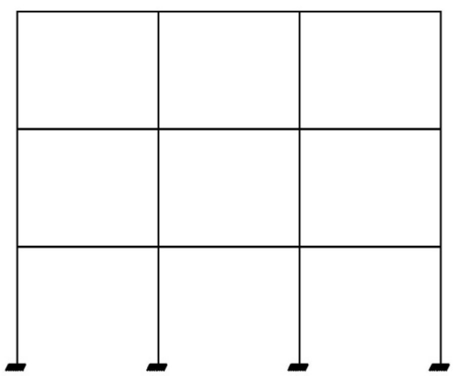

Fig. 1.1 Moment Resisting Frame

In order to control lateral drifts, concentric braced frames (CBF) (Fig. 1.2) can be used. Since diagonal braces increase the lateral stiffness of the system, CBF can resist against lateral forces during minor and moderate earthquakes. Using this kind of structures is generally more economical than increasing element sizes and using doubler plates. However, during a major earthquake, these lateral forces can increase significantly and generally diagonal bracing struts buckle due to the cyclic axial load. The plastic behavior of bracing struts results in a decrease of buckling strength and energy dissipation capacity after continued load cycles. As a result, an unstable behavior may be expected in the structure due to the reduction of lateral load carrying capacity. To eliminate this problem, the slenderness ratio of bracings can be increased by using larger sized elements which is also an uneconomical solution.

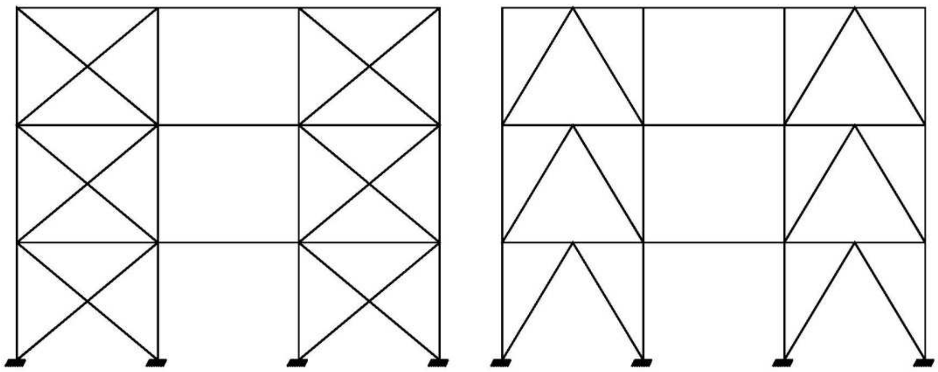

Fig. 1.2 Concentrically Braced Frames

Due to the problems faced in CBFs and MRFs, Popov and his associates at University of California, Berkeley developed an alternative structural system that have large energy dissipation capacity and sufficient stiffness to resist lateral cyclic loads in ductility limits. This system is called as Eccentrically Braced Frame (EBF). Initial research studies conducted on this new framing system were undertaken in the thesis studies by Hjelmstad (1983) and Kasai (1985) and in the report by Roeder and Popov (1977), Ricles and Popov (1987a). For a complete citation, it is also important to mention the papers by Roeder and Popov (1978), Hjelmstad and Popov (1983), Malley and Popov (1984), Kasai and Popov (1986a), Kasai and Popov (1986b). EBFs can be designed as different types such as D-braced, K-braced and V-braced. In this kind of bracing system, an active link (called as shear-link) is located as a part of the beam. The purpose of this link is to transfer the shear and bending forces on the beam to the bracing strut as axial force. Thus, the maximum force that can be conveyed to the brace depends on the shear capacity of the shear-link. The link element is designed to remain elastic in minor ground motions, and to yield during major ground motions so that the structural system can dissipate large amount of energy. Yielding of the shear-link limits the axial force on braces and prevents buckling of the braces.

Understanding strength, stiffness and ductility properties of EBFs requires studying the nonlinear behavior of shear-links. Research studies show that behavior of shear links are fairly complicated and affected by various parameters, and as a result significant amount of research interest has been directed towards both experimental and numerical determination of the nonlinear behavior and cyclic energy dissipation characteristics of shear-links. Experimental studies usually provide more reliable means to assess the behavior, but conducting experimental studies may not be economical in some cases. Furthermore, experimental studies are usually limited in terms of loading and boundary conditions as well as material and geometric properties of tested specimens. Therefore, development of finite element models or the use of already available finite element programs could provide means for this purpose. In this regards, finite element analysis programs nowadays enable modeling all kinds of nonlinearities that may be present in structures. Nevertheless, the reliability of a finite element model should be checked attentively.

In this thesis, a comparative numerical study on the estimation of the nonlinear behavior of steel shear-links subjected to cyclic loading will be carried out through the use of 2-D (shell) and 3-D (solid) finite element models and also through the use of 1-D (frame) finite element model. 2-D and 3-D finite element analyses are carried out by using ANSYS Workbench software package. In order to check the validity of the aforementioned modeling and analyses in ANSYS, first, a validation study with the experiments conducted in literature is undertaken, where the experimental specimens are selected from the studies of Kasai (1985) and Hjelmstad (1983). In order to get a close estimate of the nonlinear behavior and cyclic energy dissipation characteristics of shear-links, it is imperative to use an accurate and calibrated cyclic material model for steel. Utmost effort is given in this regards to accurately capture the Bauschinger effect observed in steel material. In order to check the reliability of the finite element models, same loading protocols are used with Kasai and Hjelmstad, where these loading protocols fall into the symmetric type. Then, unsymmetrical cyclic loading protocols, which are called as “near-fault loading protocol” in literature (Krawinkler et al. (2000)), are also applied to the same finite element models. The results obtained from ANSYS are compared with the numerical results obtained from a frame finite element model developed by Saritas and Filippou (2009a). In order to assess the accuracy of numerical models, comparison with experimental data is usually needed and preferred. In the absence of such data, comparison of a 1-D (frame) finite element approach with 2-D (shell) or 3-D (solid) finite element modeling approaches could provide means for assessing the accuracy of results obtained from 1-D models. This comparative study is conducted first on the influence of flange thickness on the over-strengthening of shear-link behavior, then on the influence of cyclic loading protocols of shear-link behavior.

1.2. Organization of Thesis

This thesis contains seven chapters. The introduction chapter involves brief information about the study conducted in this thesis and the objectives of the thesis.

In second chapter, behavior and design of shear links and previous experimental and numerical studies on shear link behavior are explained. In this chapter, detailed information about the yield mechanism of EBFs and some important points on design of EBFs are given, and the differences between EBFs, CBFs and MRFs are presented. The previous studies are examined in two different headings; experimental studies and analytical studies and the aim and procedure of both types of studies are summarized

Third chapter of the thesis gives information about the finite element program ANSYS Workbench and also the tools of the program used while modeling of the shear-links. This part does not cover all properties and capabilities of ANSYS Workbench but gives general information about the program and introduces the tools used in this study.

The fourth chapter of the thesis includes verification study on the finite element modeling approach undertaken by the use of ANSYS Workbench. Numerical results obtained from finite element simulations are compared with experimental data for the specimens of Hjelmstad (1983) and Kasai (1985). In this chapter, the material and dimensional properties of the specimens, loading protocol and the experiment results of the specimens are presented. In the last part of the fourth chapter, the analysis results of the specimen are compared to the experimental results to prove the validity of the models and some remarks on the results are discussed.

In the fifth chapter, a 1-D (frame) finite element model which is developed by Saritas and Filippou (2009a) is introduced. First part of the chapter describes the formulation of the element, approximation of shear distribution and material model. The specimens of Hjelmstad (1983) and Kasai (1985) modeled with the 1-D finite element model and are also analyzed under same loading history. The second part of the chapter includes the results of the analysis and the comparison with the experimental results.

The sixth chapter of the study is presented in two parts. In first part the contribution of flange to the shear carrying capacity of link is investigated. For this purpose, the link is modeled with solid and shell elements in ANSYS Workbench and also with 1-D (frame) finite element. The diagrams that show the change in shear capacity with the increase of flange thickness are represented in this part. In the second part of the sixth chapter, the behavior of the link under unsymmetrical cyclic loading is investigated with 2-D (shell) and 1-D (frame) finite element models and the results of the analysis are compared to each other.

Finally, the conclusion chapter presents a brief summary of the studies undertaken within the scope of the thesis and includes a demonstration of results and concluding remarks and comments on the study.

CHAPTER 2

BACKGROUND ON SHEAR-LINKS

This chapter aims to give information on eccentrically braced frames (EBFs) and shear-links and summarize previous studies conducted on this subject. First part of the chapter focuses on discussing the physical behavior and design of EBFs. In this context, differences between moment resisting frames, concentrically braced frames, and eccentrically braced frames will be given. Then, yielding mechanisms observed in EBFs and important considerations related to the design of shear-links are presented. Second part of this chapter focuses on the presentation of previous experimental and analytical studies conducted on the determination and estimation of nonlinear behavior of shear-links.

2.1. Behavior and Design of Eccentrically Braced Frames

2.1.1. Behavior of Eccentrically Braced Frames

Eccentrically braced frame (EBF) is a hybrid system which is a combination of moment resisting frame (MRF) and concentrically braced frame (CBF) (Okazaki (2004)). With a proper design, ductility of a MRF and drift control capacity of a CBF can be obtained economically through the use of an eccentrically braced frame.

As mentioned in the study of Hjelmstad and Popov (1984), another advantage of using EBFs is compliance to architectural requirements while limiting the drifts since the braces can be placed in different variations to allow for architectural openings (Fig. 2.1).

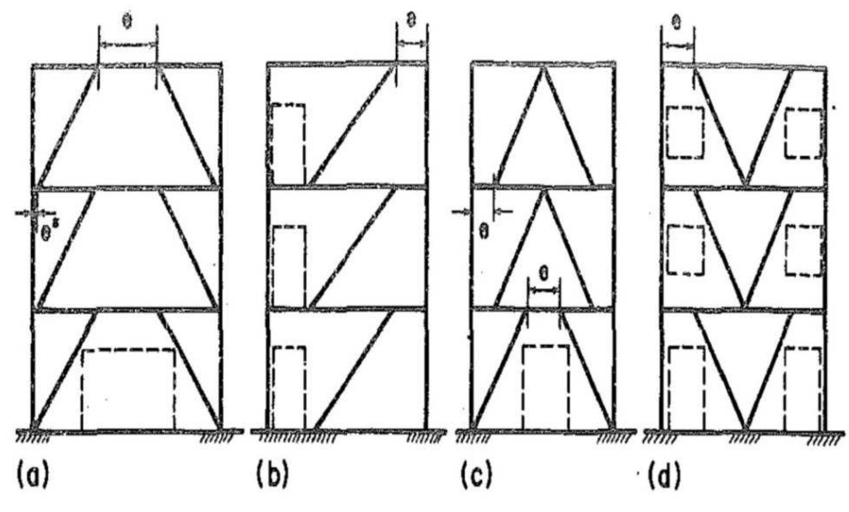

Fig. 2.1 Alternative Bracing Arrangements for Eccentrically Braced Frames (Hjelmstad and Popov (1984))

Working principle of eccentrically braced frames relies on the transfer of the moment and shear forces on a segment of the beam through the brace to column or another brace as axial force. This beam segment is called as active link or shear link. The link member yields after severe cyclic movement and dissipate large amount of energy (Hjelmstad and Popov (1984)). Comparing Fig. 2.2 and Fig. 2.3 the energy dissipation mechanism of EBFs and difference between CBFs and EBFs can be observed more clearly as a result of the differences in the yielding mechanism. Generally, inelastic behavior of shorter links is dominated by shear yielding of web; however, in longer links, yielding behavior of the link element is between the shear yielding case in short beams and the flexural yielding case of long beams typically occurring in MRFs. With an optimum design of EBFs, the system can satisfy both ductility and stiffness limits, as well as strength criteria.

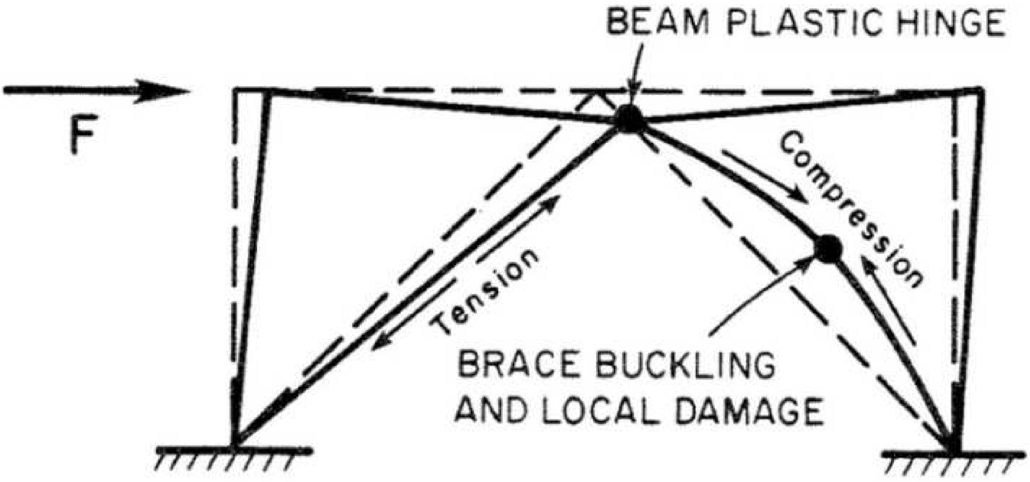

Fig. 2.2 Inelastic behavior of concentrically braced frames during a major earthquake (Kasai and Popov (1986c))

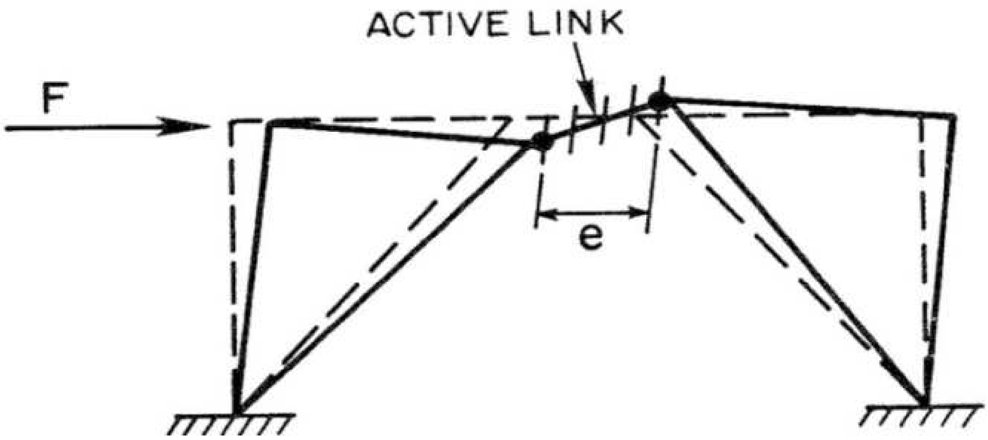

Fig. 2.3 Plastic deformation of K-braced frames (Kasai and Popov (1986c))

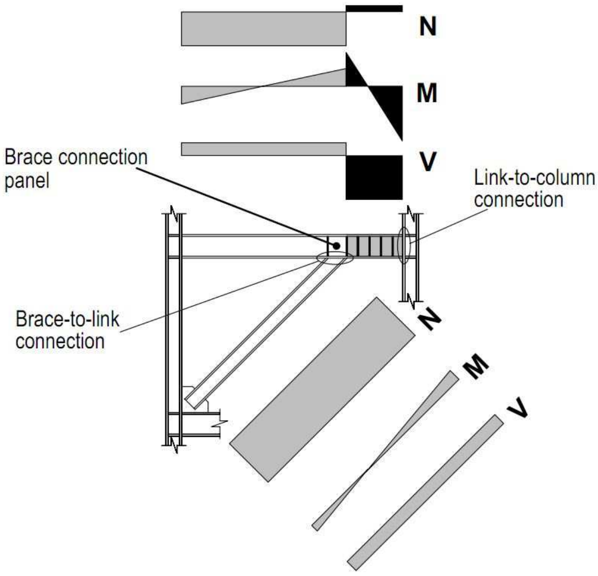

Fig. 2.4 Typical force distribution in an EBF (Okazaki (2004))

The force distribution in an eccentrically braced frame under lateral forces is illustrated in Fig. 2.4 . Generally, constant shear, reverse curvature moment and small axial force are observed along a shear-link, and axial force is dominant in a brace member of EBF system.

Behavior of the eccentrically braced frames can change depending on the length of the shear-link and other parameters of the structure. This length is generally marked as “e” (Fig. 2.5). According to Hjelmstad and Popov (1984), by changing the ratio of link length to bay length, i.e. e/L, between 0 and 1, the arrangement of structure varies between CBF and MRF. In case of e/L=1, structure acts as MRF, but if e/L reduces to 0, the structure can be identified as CBF. EBFs should be designed with a reasonable link length to meet both the ductility and stiffness conditions.

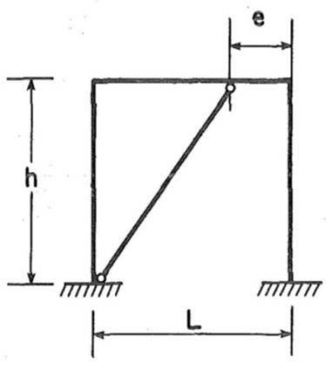

Fig. 2.5 Simplest Eccentrically Braced Frame (Hjelmstad and Popov (1984))

Fig. 2.6 shows the end moments (M_B and M_C) and the shear force (V) that may develop on a link element, and since the axial force is small it may be safely assumed negligible and zero. The moments developed at the ends of the beam may be different from each other, but for end moments being equal, i.e. $M_B = M_C = M$, the equation $2M = V \times e$ can be easily obtained from static equilibrium. This equation may be transformed to get the shear-link length $e = 2M_p/V_p$ for an elastic perfectly plastic link, in case no interaction between shear and flexure is present, where V_p and M_p are plastic shear and plastic moment capacities, respectively (Okazaki (2004)). Higher moments are concentrated at the ends of the link and yielding of the link due to the presence of bending moment should result in the restriction of plastic deformation at link ends if the length of the link is sufficiently long enough. On the other hand, shear-links are expected to first yield due to high shear forces that are uniformly distributed along the link. With the web panel maintaining a stable deformed shape due to the presence of web stiffeners, yielding due to high shear forces can be sustained in the link. This action forces the link member to deform in shear rather than bend. Kasai and Popov (1986a) indicate a formula to ensure shear yielding through providing the following link length:

$$e \leq 1.6 \frac{M_p}{V_p} \tag{1}$$

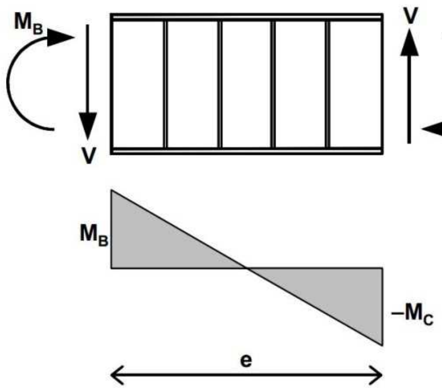

Fig. 2.6 Free body diagram of link (Okazaki (2004))

Overall behavior of an eccentrically braced frame is illustrated in Fig. 2.7 by Okazaki. Based on these diagrams, relation between plastic drift angle θ_p and plastic link rotation γ_p can be obtained from following equation:

$$\gamma_p = \frac{L}{e} \theta_p \tag{2}$$

As indicated in above equation, link rotation capacity depends on L/e ratio. According to this equation, it can be said that higher the L/e ratio is, higher the rotational capacity would be. Comparing to MRFs, for same plastic drift angle, EBF should have higher rotational capacity then the plastic hinge rotation that may be present at beam ends in a MRF system. This also shows the importance of choosing the length of a link, so that link rotational capacity will be greater than the rotation amount that will be present in an EBF frame.

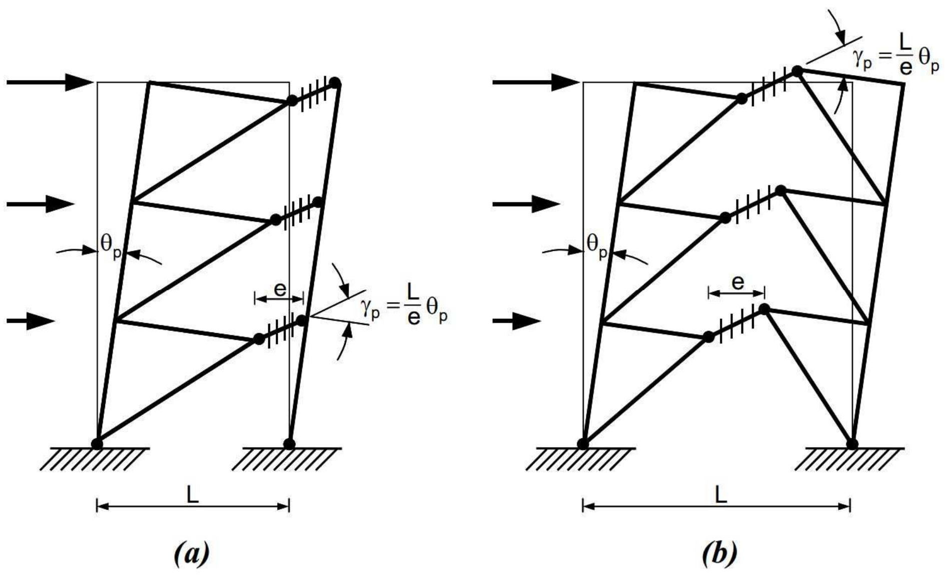

Fig. 2.7 Energy dissipation mechanisms (Okazaki (2004))

In order to provide sufficient rotational capacity and ductility to shear-link elements, web stiffeners should be used and the dimensions of web and flange of the link are the first parameters that become important in the design. The width to thickness ratio of flanges and webs should satisfy the high ductility requirements specified in Section D1.1 of AISC (2010).

AISC (2010) also categorize the links according to their lengths to define the inelastic behavior of shear-links. AISC Seismic Provisions indicate that there are three types of links that are shear links which yields due to shear, moment links which yields due to flexure and intermediate links that are affected both from shear and moment yielding. The limitations about these links are specified such as, the link length $e \leq 1.6M_p/V_p$ for shear-links, $e \geq 2.6M_p/V_p$ for moment links, and $1.6M_p/V_p < e < 2.6M_p/V_p$ for intermediate links. Rotation limit is identified as 0.08 rad for shear-links, 0.02 rad for moment links and for intermediate links can be evaluated by interpolation between 0.08 rad and 0.02 rad depending on the link length.

In this thesis, both short and relatively long shear-link members will be analyzed in order to assess the accuracy of finite element models in capturing both the shear dominant yielding and shear-flexure interaction yielding.

2.1.2. Design of Eccentrically Braced Frames

Link members should be the most ductile segment of an eccentrically braced frame system. Beside this requirement, the links should be designed so that the inelastic behavior and damage of the link should be limited. In such design of EBF, the link acts as a fuse that both dissipates energy of the system and limits the forces developed on other members of the system (Engelhardt and Popov (1989)).

Engelhardt and Popov (1989) constituted a design procedure based on capacity design. According to this method, the dimensions and properties of the link are chosen based on the codes but other elements in the structure are designed for the loads developed in the structure when the link is fully yielded and strain hardened, and where ultimate shear and moment capacity of a frame can be estimated according to Seismic Provisions AISC (2010) .

Another important issue about eccentrically braced frames is the intersection angle of brace and the beam. Small intersection angles may develop large axial forces outside of the beam. Engelhardt and Popov (1989) indicated that high magnitudes of moment and axial force on the beam cause instability of beam before it reaches its full strength. To avoid this problem, the angle between the beam and brace should not be less than 35°.

Under the assumption of perfect-plasticity, strain hardening is not observed and shear moment interaction of the link is neglected. According to Engelhardt and Popov (1989), to design a perfectly plastic link, it is important to determine the yield strength of the link. The dimensions of a link are determined so that link does not yield under the shear loads generated by lateral loads specified in codes. Engelhardt and Popov (1989) suggested the following equations to determine the shear yield strength:

$$V_p \quad \text{for} \quad e \leq 2\frac{M_p}{V_p} \tag{3}$$

$$\frac{2M_p}{e} \quad \text{for} \quad e \geq 2\frac{M_p}{V_p} \tag{4}$$

These values are given for the factored lateral loads, but for the load given by an allowable stress design code the values should be calibrated.

Equations (3) and (4) are valid for the case of small axial force acting on the links, such as $P / P_y < 0.15$. In case of higher axial forces, the equations should be reduced considering shear axial force and shear moment interaction equations. Higher axial forces affect inelastic rotational capacity, as well.

When analyzing a shear link connected to a column, very large elastic moments can be observed at the link end adjacent to column of the link. However, large elastic moments should not be the design load of a link. Previous experimental studies show that a plastic hinge occurs at the end of the link due to the high elastic moments and moment redistributes along the link. Therefore, maximum moment on the link does not reach flexural yield strength of the link before it yields due to shear. Thus, the shear yield strength should be considered rather than flexural yield strength while designing the link.

2.2. Literature Review on Shear-Links

2.2.1. Experimental studies

Hjelmstad (1983) in his Ph.D. thesis conducted experiments to determine the energy dissipation capacity of shear-links, the effect of web buckling on energy dissipation capacity and the magnitude of inelastic deformation of a link. Hjelmstad (1983) tested shear-link specimens with different lengths and different stiffener numbers with a testing arrangement that causes equal end moments at link ends. Hysteretic behavior of specimens showed that the stiffening of shear-links plays an important role to control inelastic web buckling. As part of his Ph.D. thesis, Hjelmstad (1983) also proposed a displacement-based frame finite element model to assess the monotonic behavior of shear-links.

Malley and Popov (1983) performed experiments on shear-links in order to determine stiffener design and spacing that is both economical and resistant to shear forces. Test results showed that type and application of loading can affect the energy dissipation capacity since loading conditions affect web buckling. In their study, Malley and Popov (1983) also worked on the importance of welding and fabrication of the link to provide full shear capacity.

Distinct from Hjelmstad (1983), the experimental studies performed by Kasai (1985) included also the effects of strain hardening and axial loading on the plastic capacity of shear-links. It was observed that unsymmetrical flange buckling may be prevented in presence of axial force and reduction of plastic moment capacity is not observed due to the strain hardening under high shear loading. Loading and boundary conditions of Kasai's specimens resulted in unsymmetrical moments at beam ends and variation of the end moments due to the shear yielding of the link. Kasai (1985), indicated that the stiffener spacing and height to thickness ratio is very important for elastic behavior. In addition, he used random unsymmetrical loading protocols in their experiments; however the experimental load-deflection curves for these tests were not presented.

Ricles and Popov (1987b) investigated the behavior of links with composite slabs under cyclic loading. In this scope, 8 tests are conducted with EBFs that have different bracing systems and composite slabs or bare links. As a conclusion of the study, energy dissipation capacity and shear capacity of composite links was observed to be greater than bare links. At the end of the tests, larger end moments are observed in composite links than bare links due to the strain hardening. In this study, Ricles determined a link deformation value, γ_b, at which web buckling is observed. They also indicated that, specimens subjected to cyclic deformation represent irreversible web buckling even if adverse deformation is applied, in case of an early large impulse. These specimens cannot reach the γ_b value due to the web damage occurred in early stages.

Engelhardt and Popov (1992) performed experiments on long links to investigate their yielding mechanisms and plastic rotation capacity. The experiments are performed with two different sections which are W12x16 and W12x22 and the cyclic loading is applied to the specimens. As a result of 12 experiments the dominant failure mode of the long links were observed to be the fracture of the flange near the column connection. Another important conclusion of the study is that long links are generally not suitable for using next to column but if properly designed they can be located between two braces.

Okazaki and Engelhardt (2007) tested specimens constructed of A992 steel with different sections and lengths to examine strain hardening and buckling of flanges. 4 different cyclic loading protocols are used during the experiments. After the experiments they observed that the loading protocol has importance on inelastic rotation of the active links. They also gave some new techniques to stiffener to web connections to limit the web fractions. At the end of the tests, Okazaki reaches some conclusions on influence of over strength factor on the link behavior. The overstrength factors of the specimens varies between 1.05 to 1.62 and test results shows that the specimens that have higher over strength factor are more suitable for short links with heavy flanges.

Berman and Bruneau (2007) conducted tests on hollow rectangular links that are expected to provide more torsional stiffness. Necessity of stiffener, shear and moment capacities and design considerations were examined in the study. The experiments show that the hybrid tubular links which have similar ductility levels with wide-flange links can achieve even exceed the maximum rotation values specified in AISC (2005). Another point from the study is the contribution of flange to the shear carrying capacity of link. The calculated ultimate plastic strength values by using web material are exceeded in the experiments, since some shear carries by flange of the link. In the scope of this study, also analysis results of the shear-links with a finite element analysis program are compared with test and analysis results.

2.2.2. Analytical and Numerical studies

Finite element analysis on shear-links can be divided into two categories. In the first category, researchers try to develop their own finite element formulations and models and then they later assess the reliability of the proposed models by comparing with experimental data. In the second category, researchers also attempt to use already developed and available advanced finite element software packages such as ANSYS and ABAQUS. In the latter category, mostly shell (2-D) or solid (3-D) type finite elements are used in conjunction with the nonlinear material models available in the aforementioned programs.

The study conducted in this thesis basically focuses on the use of 2-D/3-D finite element models present in ANSYS, and also uses a previously developed 1-D (frame) finite element model by Saritas and Filippou (2009a). Since the thesis study is not intended to develop a new finite element formulation, literature survey will focus on the use of finite element programs to model shear-link behavior. Detailed literature survey on the development of frame finite element models for the analysis of shear-links is available in the thesis by Saritas (2006).

Ghobarah and Ramadan (1990) considered a finite element model with shell elements to observe the behavior of the link after yield up to the ultimate point. The aim of the study was to understand the effect of the axial forces on a link that is subjected to cyclic end displacements. They compared the model with previous experimental studies for verification the model accuracy. After the analysis, a reduction in the load carrying, rotation and energy dissipation capacities and ductility of the beams that were subjected to axial force was observed. According to the analysis results, they suggested that only short shear links should be used in case of existence of an axial force.

Ramadan and Ghobarah (1991) examined the ultimate capacity of wide flange links under cyclic loading. To determine the nonlinear behavior, Ramadan and Ghobarah (1991) modeled links with the finite element program ADINA by using shell elements. The models are analyzed under cyclic loading. Multi-linear elastic-plastic material model is chosen for the model and the hardening region was defined as linear isotropic. After the analysis, the results were compared with the experimental results. The results of this study show that the model can be used for investigation under different loading conditions.

The study of Itani et al. (2003) was on built-up shear links under large deformations. The study aimed to evaluate the finite element program capability to determine the ultimate shear strength of the link, to determine the stress strain distribution along the link under large deformations and the influence of changing dimensional parameters on plastic rotation capacity of the link. In this scope, the links were modeled with ADINA by using eight node-shell elements and bilinear plastic material model. The ultimate capacities obtained from analysis are compared with experiment and a good agreement between analysis and experiments were indicated. Also some notes are expressed on behavior of built-up sections.

Prinz and Richards (2009) made evaluations for links with reduced web sections subjected to cyclic loading. As finite element analysis program, ABAQUS is used and the results obtained from the program are compared with experimental data. The flanges of links and columns are modeled with solid elements while the webs are modeled with shell elements. The region outside the link is modeled with a frame element, since no yielding is expected this area. All material properties are defined according to nonlinear kinematic hardening properties. Although the detailed data is not given in the study, the material was calibrated with the parameters of Kaufmann et al. (2001). After the analyses, it can be said that the rotation capacity of the links with reduced web section show similarities with normal links but the failure modes of the reduced sections are different.

The most recent analytical study on finite element modeling of shear-link is conducted by Della Corte et al. (2013). They modeled the HE and IPE sections with different end conditions to examine the plastic shear over strength of short links more detailed. They compared the finite element analysis results with the test results obtained from previous studies in the literature. For modeling of the specimens shell elements with 6 nodes are used in finite element program ABAQUS. In a similar way with the study of Prinz and Richards (2009), the material model used in analysis is calibrated according to the experimental data of Kaufmann et al. (2001) and defined in program using kinematic hardening law. The analyses show the importance of axial forces, flange-web area ratio and link length cross section depth for the shear over strength. They also observed that the tensile axial forces developed due to the restraints, have significant effects on shear over strength.

In addition to these analytical studies, some of researchers mentioned in experimental studies section, conducted also analytical studies that support the experimental results. Kasai and Popov (1986a), Ricles and Popov (1987b), Okazaki (2004) and Berman and Bruneau (2007) modeled specimens with 1-D, 2-D elements and gave place to some comparative studies in their publications. The aim of the analytical study parts was obtaining detailed strain stress distribution, behavior of connections and the proof and validation of the analytical methods.

CHAPTER 3

FINITE ELEMENT MODELING OF SHEAR-LINKS

Modeling and analysis of shear-links are performed with ANSYS Workbench in this thesis. ANSYS is an advanced software package that aims to model the interaction of different disciplines such as physics, structural, vibration, fluid dynamics, heat transfer and electromagnetic for engineers. In order to gain relative simplicity and user friendliness, the graphical user interface version of ANSYS, named as ANSYS Workbench can be used.

ANSYS Workbench has various analysis systems provided in its toolbox and Static Structural is one of them that suited to the finite element analysis study performed in this thesis. This tool has the capability of performing linear and nonlinear analysis, detection of contacts automatically and simplifies the parametric analysis (ANSYS (November, 2009)).

Capabilities of Static Structural analysis toolbox relevant to this thesis are presented in detail in the rest of this chapter.

3.1. Modeling of Material

There are number of different parameters that affect the nonlinear material behavior of a structure. At different load levels, as the stiffness of the structure changes, the response of the structure will be different. In order to simulate nonlinear material behavior, ANSYS allows single use or collocation of the following models:

- Multi-linear elasticity material model
- Plasticity
- Hyper elasticity material model
- Bergstrom-Boyce hyper viscoelastic material model
- Mullins effect material model
- Anisotropic hyper elasticity material model
- Creep material model
- Shape memory alloy material model
- Viscoelasticity
- Viscoplasticity
- Swelling material model
- User-defined material model

In this study plastic material option is used for the cyclic simulations of steel shear-links. Steel mostly exhibits linear stress-strain relationship up to a stress level which is called as proportional limit. Between the proportional limit and yield point, material behaves nonlinear, but not necessarily plastic. After the stress exceeds the yield stress, material becomes plastic, and it cannot recover the strain completely upon removal of the stress.

Since there is little difference between proportional limit and yield point, these two points can be assumed to coincide as shown in Fig. 3.1.

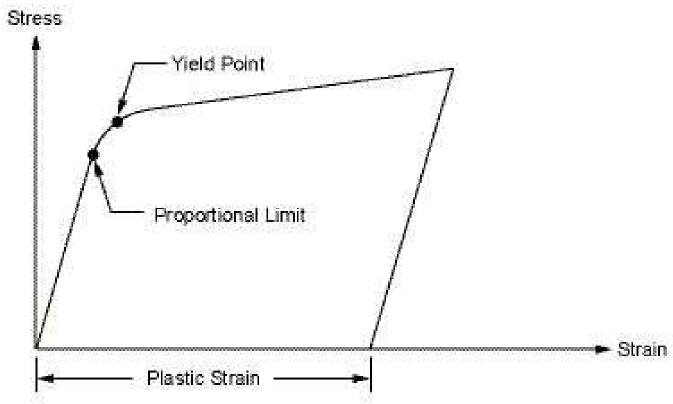

Fig. 3.1 Elasto-plastic Stress-Strain Curve (ANSYS (November, 2009))

Since, plasticity is non-conservative and path-dependent, order of the applied loads and responses have an important role on the response of the material. Therefore to obtain the plastic response accurately, the load should be applied in a series of small incremental load steps or time steps. ANSYS automatically generates time steps to reduce the step size in case of large number of iterations or large plastic strain increment. If the step is still too large to respond plasticity, ANSYS bisect and resolves with a smaller step size.

The following plastic material models are available in ANSYS:

- Bilinear kinematic hardening
- Multi-linear kinematic hardening
- Nonlinear kinematic hardening
- Bilinear isotropic hardening
- Multi-linear isotropic hardening
- Nonlinear isotropic hardening
- Anisotropic
- Hill anisotropy
- Drucker-Prager
- Extended Drucker-Prager
- Gurson plasticity
- Cast iron

In order to describe the inelastic action present in steel members analyzed in this thesis, kinematic hardening plasticity model is employed in order to accurately capture Bauschinger effect in steel, where isotropic hardening is assumed to be non-existing. Bilinear kinematic hardening (Fig. 3.2) cannot sufficiently capture the cyclic energy dissipation characteristic of steel if a good match between experimental data and finite element simulations is sought. In this regards, the best option is to use nonlinear kinematic hardening models suggested in literature, and such a response can be replicated through the use of multi-linear kinematic hardening model provided in ANSYS (Fig. 3.3). Multi-linear kinematic hardening option allows defining stress-plastic strain curves with several points.

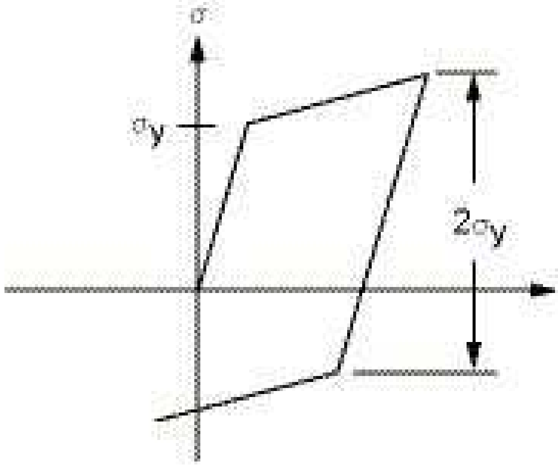

Fig. 3.2 Bauschinger Effect (ANSYS (November, 2009))

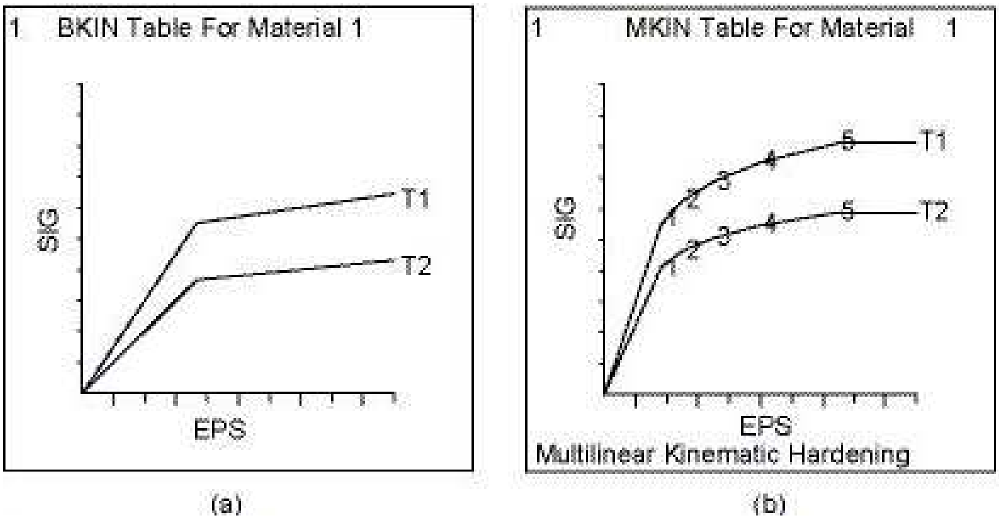

Fig. 3.3 Bilinear Kinematic Hardening and Multilinear Kinematic Hardening (ANSYS (November, 2009))

The material property input can be edited to the Engineering Data module of Static Structural analysis toolbox (Fig. 3.4). In this module, different material definitions can be used as mentioned above. After the material name is defined, the properties such as density, elasticity, plasticity etc. are given by the user. In case of multi-linear kinematic hardening, the plastic strain and corresponding stress values are defined for each point. The plastic strain starts just after the yielding point, so that the plastic strain is accepted as zero and the other strain values should be corrected considering the original zero reference value. When the data is given to the program, ANSYS Workbench represents the stress strain diagram of the material as shown in Fig. 3.5.

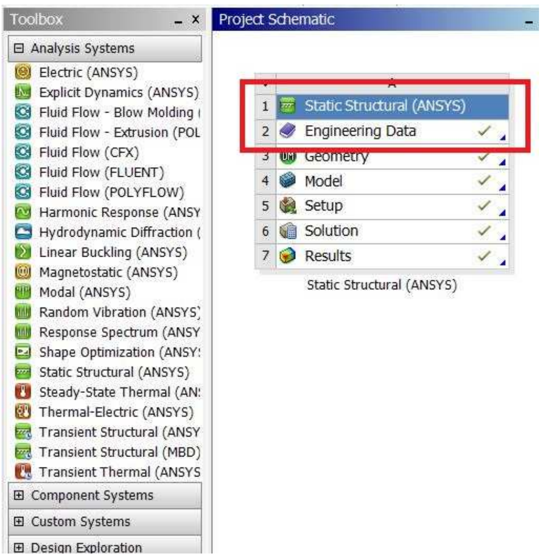

Fig. 3.4 Engineering Data on ANSYS Workbench (Inc. (2009))

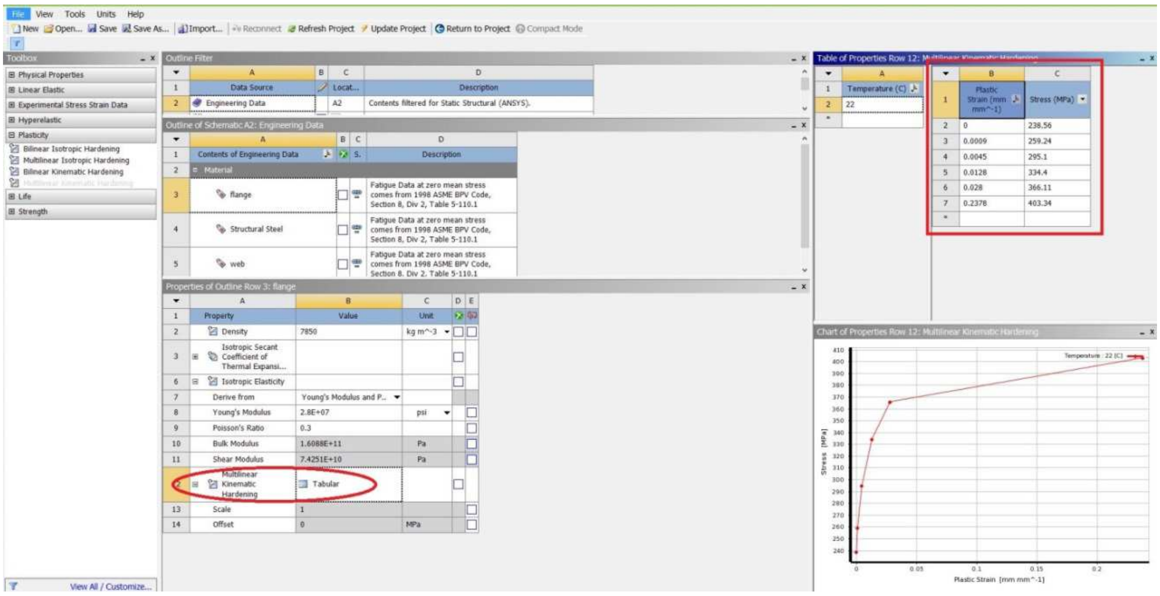

Fig. 3.5 Material Properties in ANSYS Workbench

3.2. Elements

ANSYS Workbench defines the component of the structure as “body” (Fig. 3.6). In design modeler application, five different types of bodies can be used:

- Solid
- Surface
- Line
- Planar
- Winding

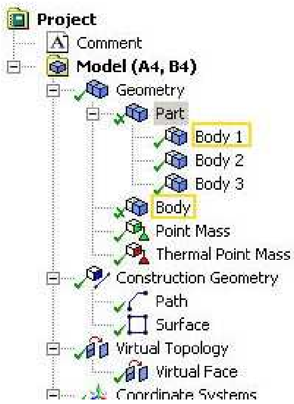

Fig. 3.6 ANSYS Workbench work tree

In this study, link elements are modeled by using surface body to simplify the model and shorten the analysis time. Surface body is a 2-D element, where the thickness of the element is assigned by the user (Fig. 3.7). Surface body is also called as shell element.

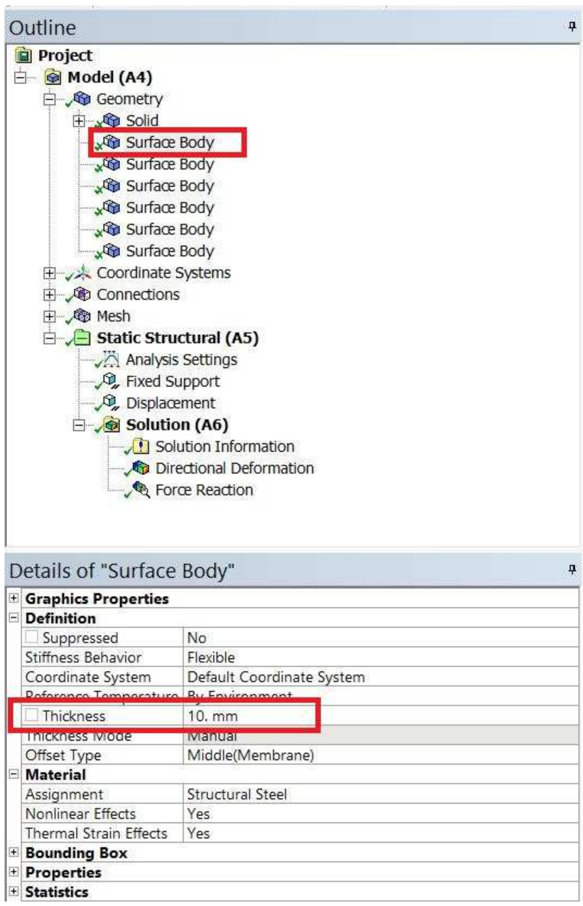

Fig. 3.7 Mechanical Application- Details of a surface body

ANSYS Workbench uses shell elements named “SHELL181” as default. SHELL181 is a 4-node element with six degrees of freedom at each node; translations in x, y, z directions, and rotations about the x, y, z directions (FIG 3.8). SHELL181 is suitable for analyzing thin to moderately-thick shell structures and can be preferred for large strain nonlinear applications.

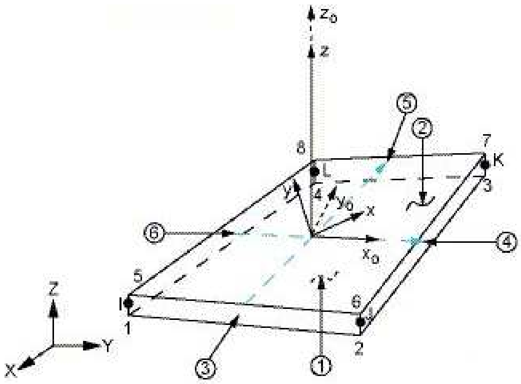

Fig. 3.8 SHELL181 Geometry (ANSYS (2009))

As ANSYS Workbench provides a visual interface, the geometry of a structure with various parts and members can be drawn relatively easily through Design Modeler module (Fig. 3.9). ANSYS Workbench has many options to simplify the geometrical modeling of structures. A shell model can be easily created by sketching the boundaries and converting them into a surface.

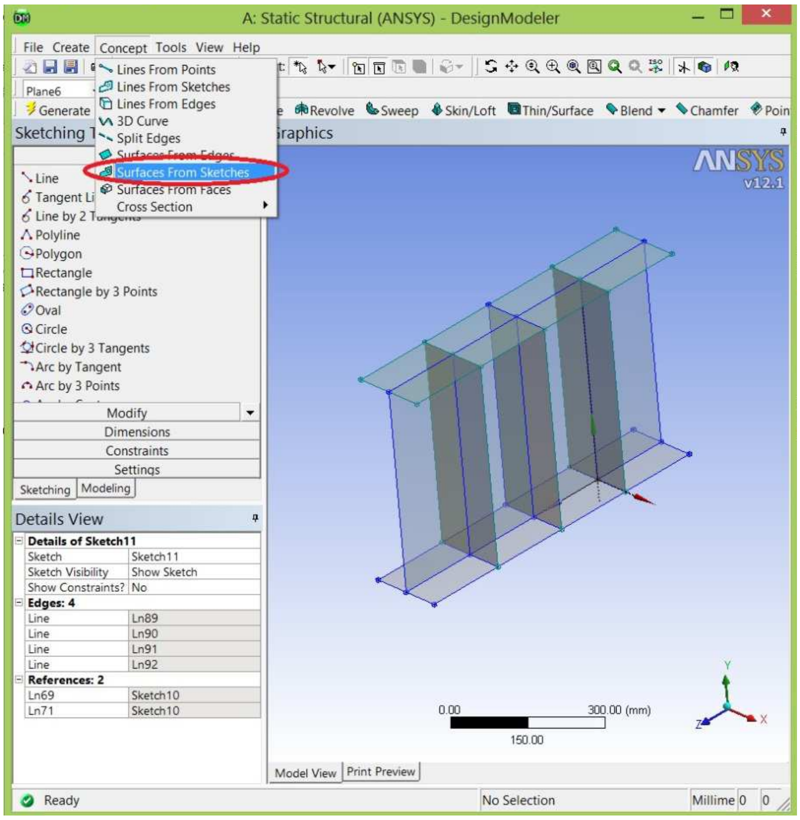

Fig. 3.9 Modeling of structure in ANSYS Workbench with design modeler program

3.3. Meshing

ANSYS Workbench provides meshing module that allows easy mesh generation of a drawn structure. The purpose of meshing in a numerical simulation is to discretize a continuous domain, which actually contains infinite number of points, as finite number of regions. Meshing module enables the user to generate meshing automatically or manually with different level of precision. Size, shape and refinement of the mesh can be controlled as shown in Fig. 3.10.

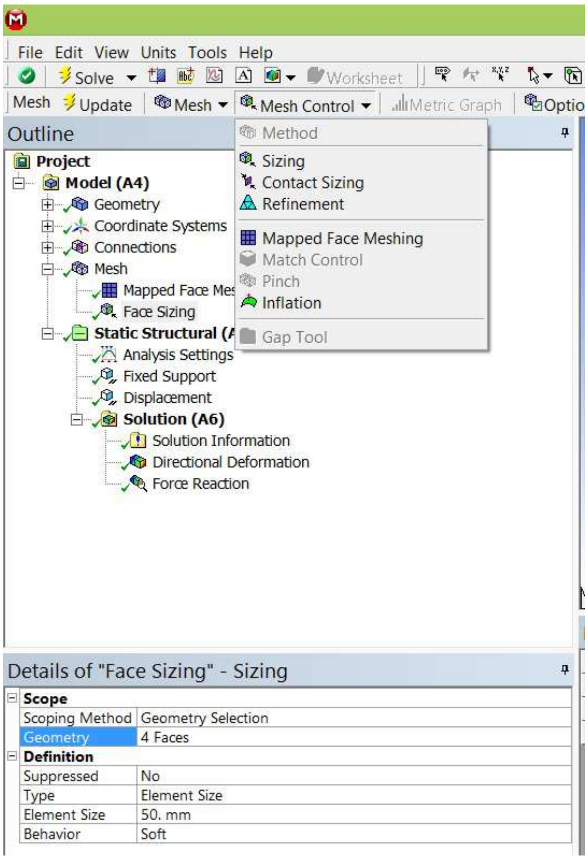

Fig. 3.10 Mesh Control

Since surface body is a 2-D (shell) element, there are two meshing types which are quadrilaterals and triangles. By selecting bodies separately, different mesh types can be assigned to different parts of the structure. By selecting mapped face meshing, a structure can be easily meshed by adjusting the mesh size (Fig. 3.11). The size and shape of the meshes should be selected carefully, because meshing directly affects the accuracy of results. On the other hand too small meshing size results in increased computation time, and in this regards three levels of mesh refinement should always be tested in order to assess the influence of mesh refinement on results.

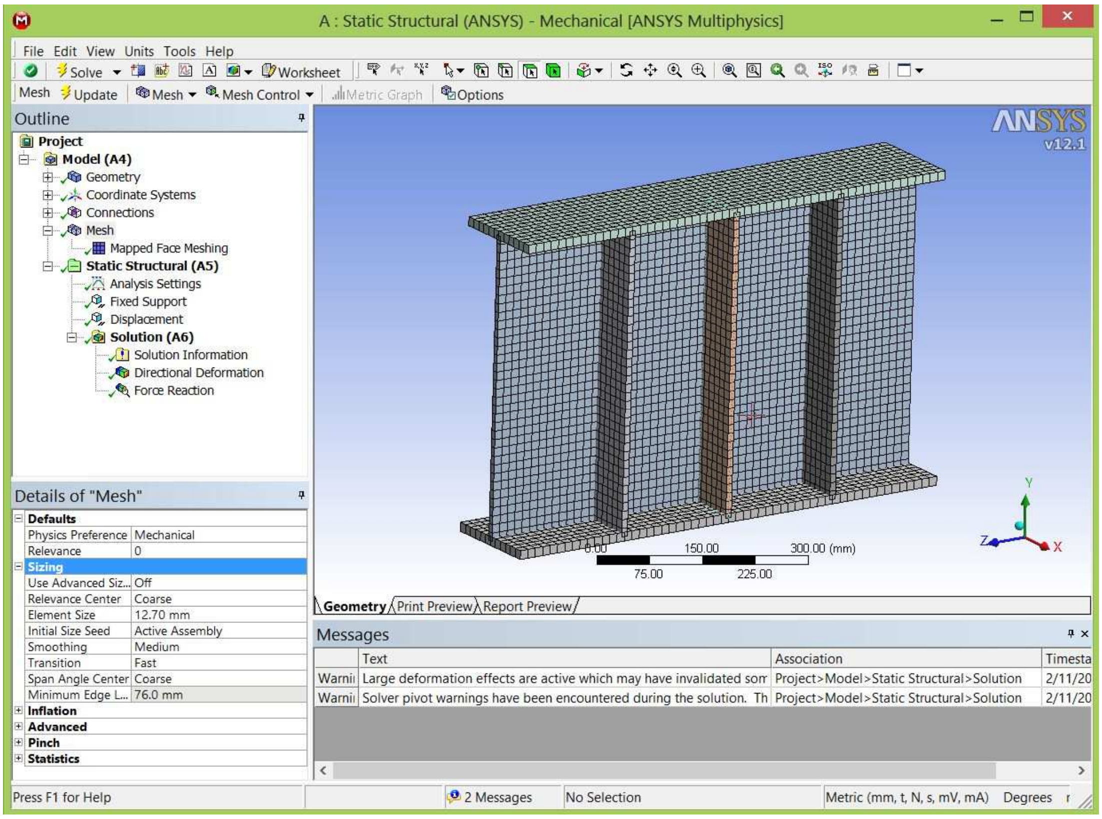

Fig. 3.11 Mapped face meshing

3.4. Contact

Contact properties between each part/member of a structure should be well defined in ANSYS. Contact properties can be assigned by using the contact menu in mechanical module. Contact between the parts can be defined as bonded, no separation, frictionless, frictional or rough. Choosing the correct type of contact is important in terms of simulating the physical problem realistically.

Steel beam profiles can be produced as rolled or built-up. In this thesis, it is assumed that bonded contact between all parts can be assumed whether welding is used to connect parts. Bonded contact is the default contact type in ANSYS Workbench, where separation or sliding of elements is not allowed so the elements behave monolithically.

Contact information is assigned to the elements by selecting the target surfaces and contact edges of the other surface that intersects with target then the type of the contact is defined as shown in Fig. 3.12.

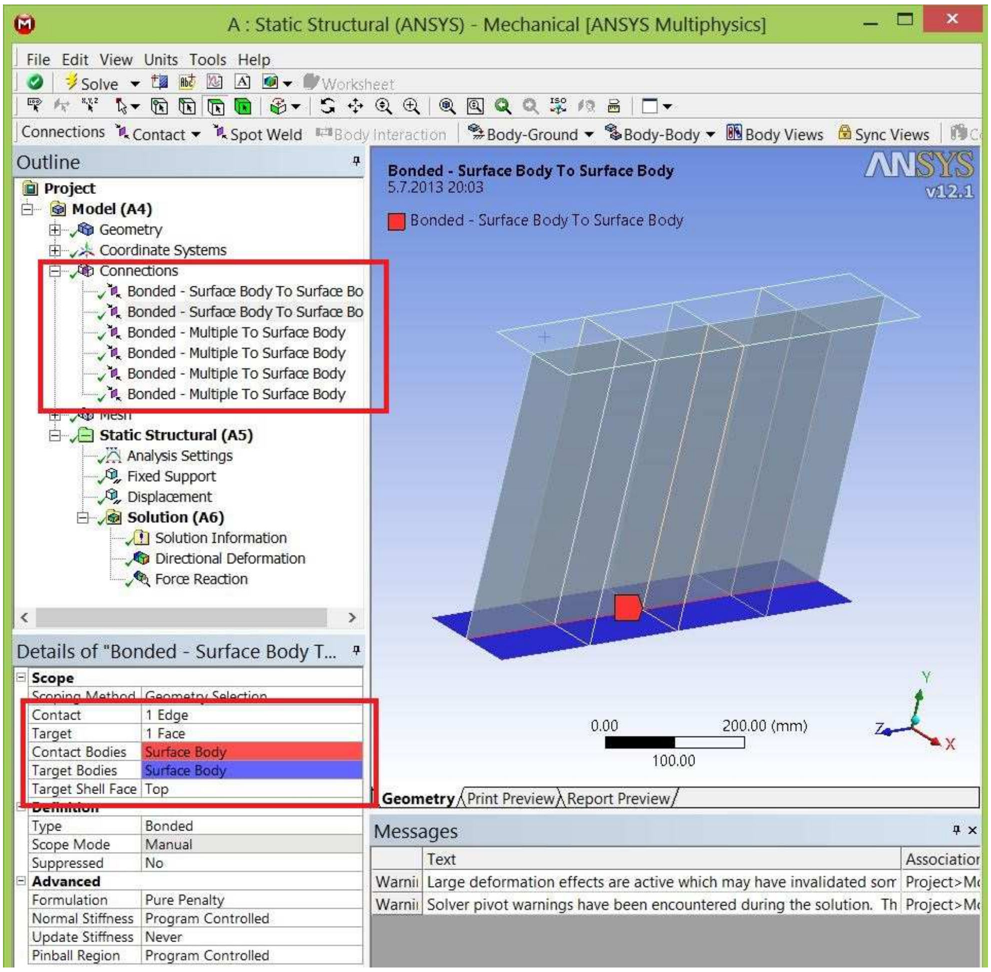

Fig. 3.12 Defining contact information

3.5. Boundary Conditions

ANSYS Workbench makes possible to simulate different boundary conditions through its support options (Fig. 3.13). In mechanical program, a support can be assigned to a point, edge or surface. Also support displacements can be defined from these options. Displacement can be assigned with different values for each step and in different direction so that the cyclic displacement can easily be defined (Fig. 3.14). While the modeling of the active links, fixed support is assigned one end of the link and at the other end displacement is applied according to the test procedure.

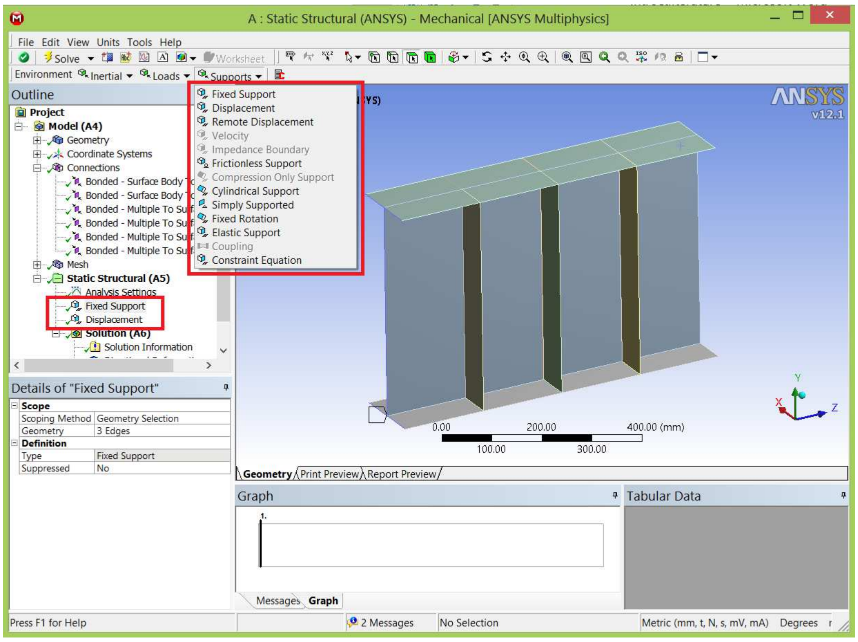

Fig. 3.13 Support options

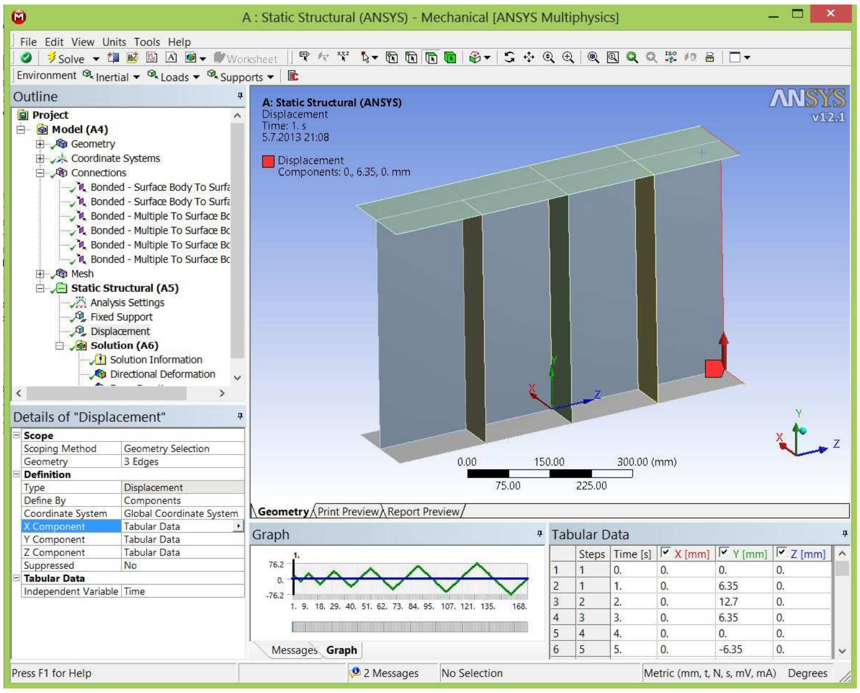

Fig. 3.14 Defining displacement data

CHAPTER 4

VERIFICATION STUDY

In this chapter, experiments conducted on shear-links by Hjelmstad (1983) and Kasai (1985) are considered for verification of the calibrated material parameters and finite element modeling approach presented in Chapter 3. Numerical results obtained from finite element simulations by using ANSYS Workbench are compared with experimental data. For purpose of comparison, only the specimens that show stable hysteretic performances are considered, since the same specimens will also be used in the next chapter for comparative purposes with a frame finite element model that can only capture stable shear-link behavior.

4.1. Hjelmstad's Experiments

4.1.1. Specimens and Test Setups

Specimen 4 of Hjelmstad (1983) is considered for verification in this thesis. Experimental setup used by Hjelmstad was such that equal end moments were applied to the ends of a shear-link specimen. The section used in Specimen 4 was W18x40, which had a flange thickness of 13.23 mm, web thickness of 7.98 mm, height of 454.15 mm and flange width of 152 mm. Total length of the link was 711.2 mm. The a/t_w ratio, i.e. the ratio of dimension of panel zone to thickness of the web, was 21.4 mm and with this value Specimen 4 had the lowest a/t_w ratio among the specimens tested by Hjelmstad, and in this regards showed a perfectly stable response under nonlinear behavior.

Transverse web stiffeners were used to decrease the possibility of inelastic buckling of the web of shear-links in the study of Hjelmstad (1983). Transverse thickness of the transverse stiffener is 9.525 mm and each stiffener is welded to the web and the flanges.

Hjelmstad (1983) prepared a testing system as shown in Fig. 4.1. An L-shaped rigid element that was supported by three Teflon coated support transferred the load to the link. The aim of using Teflon coated supports was to eliminate the frictional forces. Stability of the system was provided by the side arms. End connections of the specimens were designed so that their capacity was greater than the plastic capacity of the links, and this allowed observation of strain hardening effects in the shear-links. The connections were also designed to prevent brittle failure which could have influenced the ductile behavior of the links negatively.

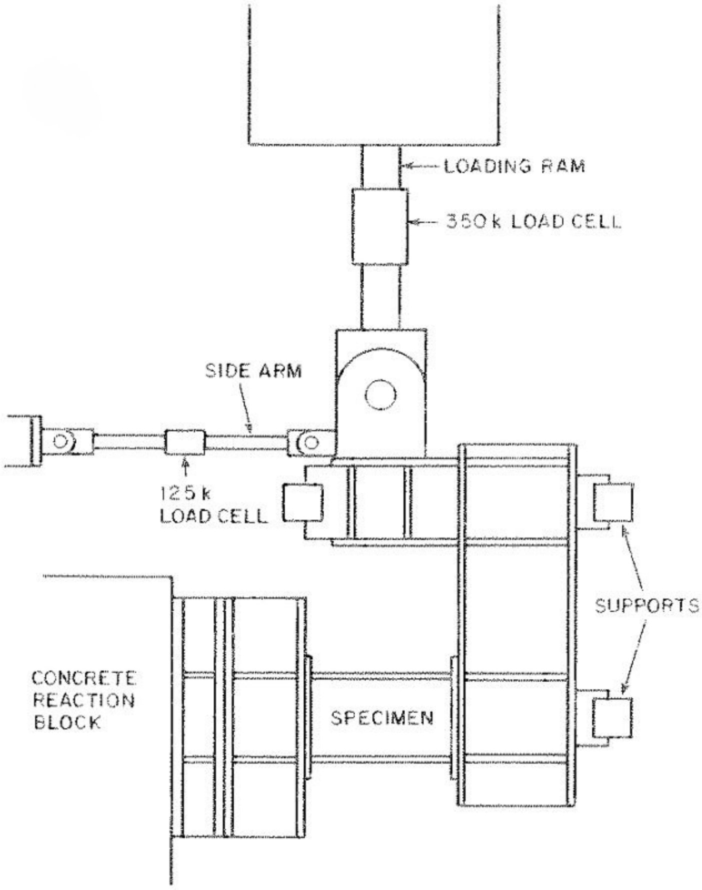

Fig. 4.1 Testing arrangement by Hjelmstad (1983)

The geometry of finite element model in ANSYS Workbench is created based on the dimensions of Specimen 4 by Hjelmstad (1983). Three web stiffeners are placed at exact locations, and all of the parts of the specimen are defined as surface body, which is a shell element (2-D element). The main reason of selecting 2-D element type rather than 3-D element is simplicity and of modeling and shorter computation time, besides the results of 2-D elements are similar to the results obtained from 3-D elements. The chapter 5 of this thesis will give detailed information about this subject. All body parts (web, flanges and stiffeners) are connected to each other through bonded contact (Fig. 4.2).

The end plates of the specimens are not modeled in the finite element model because these parts of the specimen were designed by Hjelmstad (1983) such that they had greater capacity than the link, and furthermore investigation of the behavior of the supporting system is not a concern of this study. In this way, analysis time is reduced and the finite element model is simplified.

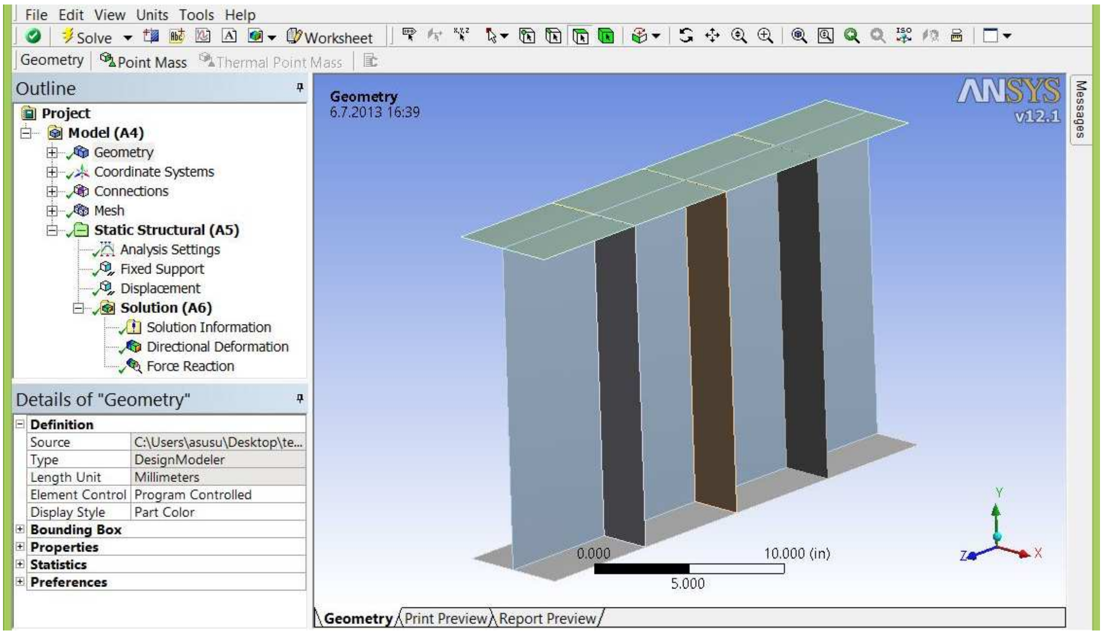

Fig. 4.2 Finite element model of Specimen 4

In order to determine the optimum mesh size in terms of both accuracy and computation time, the finite element model is meshed into 0.5 inch (12.7 mm), 1 inch (25.4 mm), 2 inches (50.8 mm) and 5 inches (127 mm) sized elements. Specimen 4 under various mesh refinement is analyzed under monotonic loading, and the results are compared in Fig. 4.3. Evident from this comparison, 2 inches mesh size provides an accurate and converged nonlinear response, thus further mesh refinement is unnecessary and would increase computation time (Fig. 4.4).

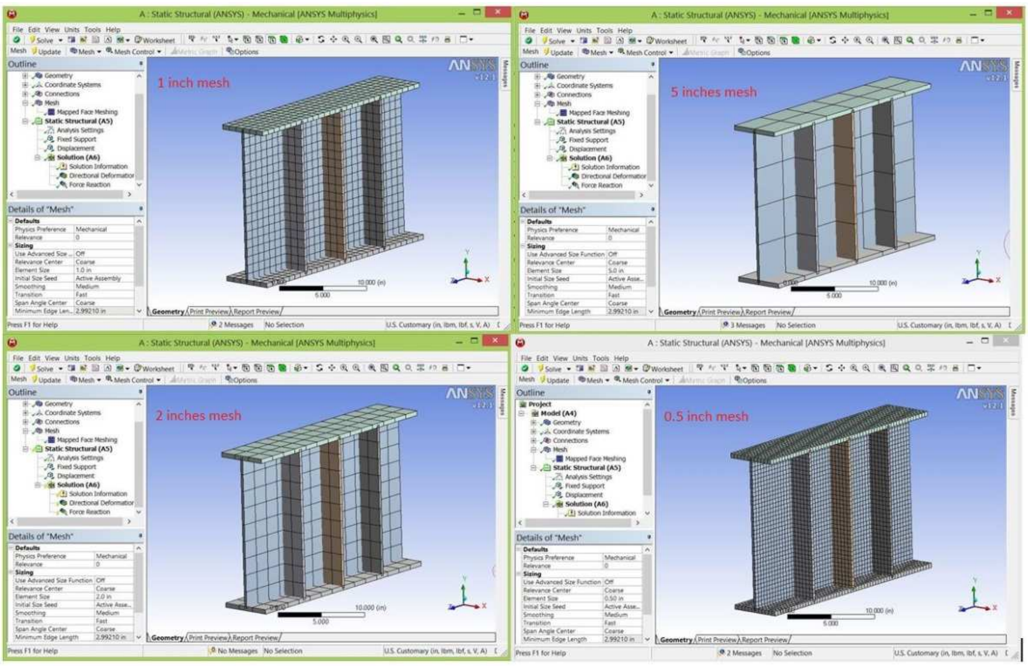

Fig. 4.3 Finite element models with different mesh sizes

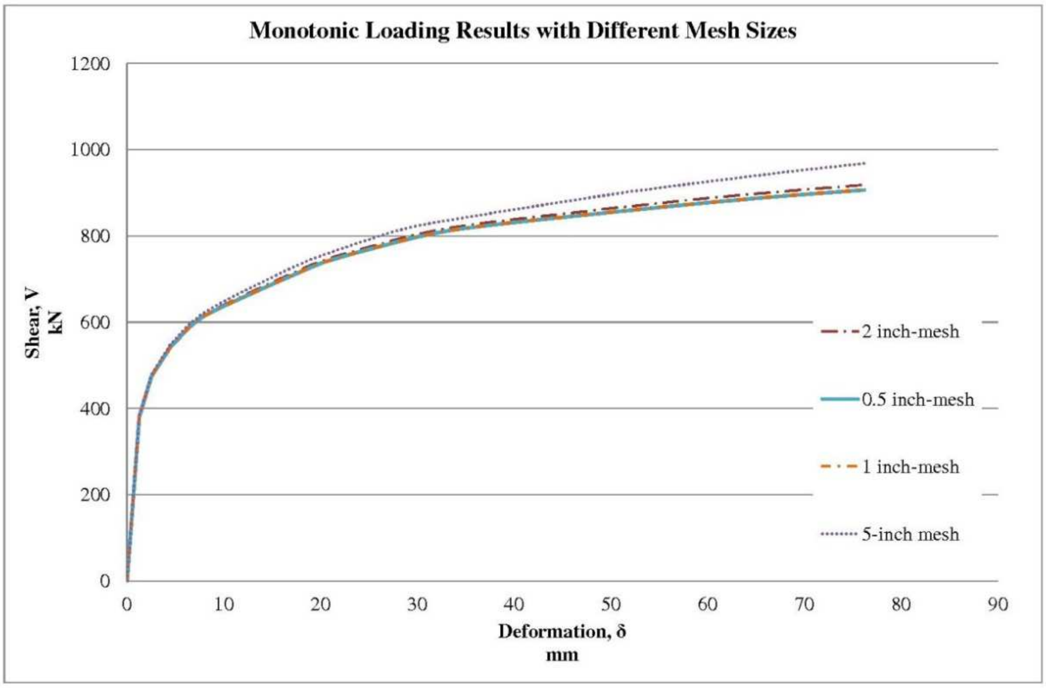

Fig. 4.4 Comparison of the results of the analysis of model (specimen 4 of Hjelmstad) with different mesh sizes

4.1.2. Material Models and Assumptions

Since high ductility is required for the specimens, Hjelmstad (1983) preferred ASTM A36 steel for specimens. The material properties of the specimens are determined from the coupon tests taken from flanges and webs of each specimen. For Specimen 4, the material properties reported by Hjelmstad are given in Table 4.1. In the table, σ_y is the yield strength, σ_u is the ultimate strength, ε_{sh} is the strain value at the beginning of hardening, ε_u is the strain value at the ultimate stress state and E is Young's modulus. The material used in the specimen presents the typical behavior of steel as shown in Fig. 4.5.

Table 4.1 Material properties of Specimen 4

Location	σ_y MPa	σ_u MPa	ε_{sh} mm/mm	ε_u mm/mm	E GPa
Web	272.34	414.37	0.018	0.22	195.12
Flange	241.32	403.34	0.014	0.24	193.05

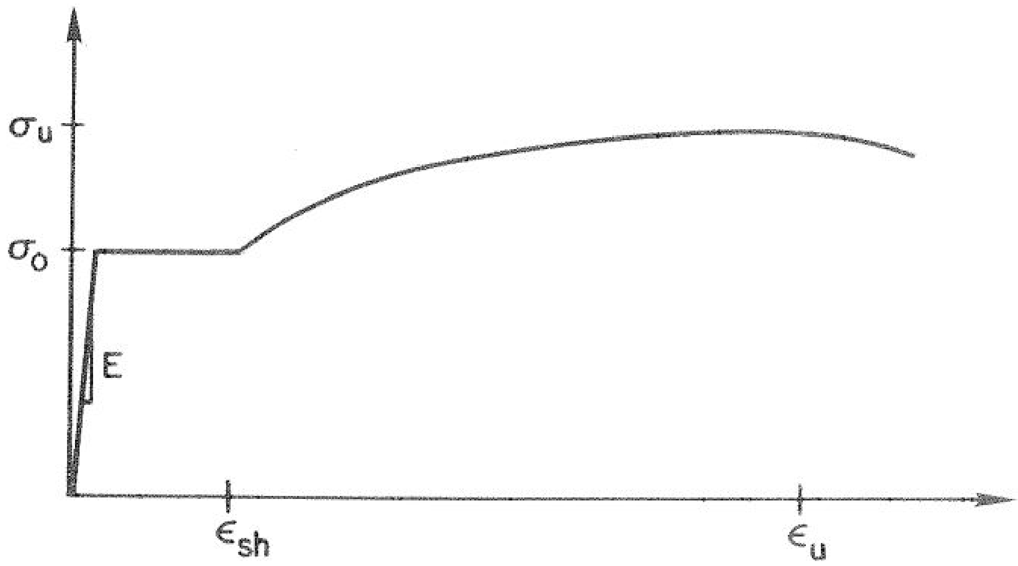

Fig. 4.5 Typical uniaxial stress-strain curve for steel

The typical behavior of steel represents a linear elastic range until the stress level reaches the yield stress, right after yielding a long plastic plateau and strain hardening region. Hjelmstad (1983) states that cyclic material properties can be quite different from the typical behavior of material and dominate the response of the links subjected to cyclic loading.

Because of the difference between the behavior of the material subjected to cyclic loading and monotonic loading, a calibrated material model is created for the finite element analysis in the light of the previous studies. Kaufmann et al. (2001) made experiments on A572, Gr.50, A913 Gr 50 and A36 steel sections to investigate the cyclic inelastic strain behavior. They plotted the strain stress diagrams of each specimen under cyclic loading and monotonic loading and fitted them into an equation of the form $\sigma = K \times \varepsilon^{n}$, where σ is stress, K is coefficient, ε is strain and n is the cyclic strain hardening exponent (Fig. 4.6). They performed the experiments on every specimen with the strain interval of 2%, 4%, 6% and 8% with 2-3 or 4-5 cycles and represented the results of experiments with strain interval of 2%. Della Corte et al. (2013) conducted their numerical analysis with calibrated material model based on the experimental studies on cyclic and monotonic behavior steel of Kaufmann et al. (2001) and got compatible results with the experiments. With the help of the studies of Kaufmann and Della Corte, the stress-strain diagrams of both flange and web of Specimen 4 is calibrated in the this thesis. Until strain value of 0.04, the calibration made is according to the study of Kaufmann and after this value an asymptotical approach to the ultimate stress level is followed to prevent overshooting the ultimate stress.

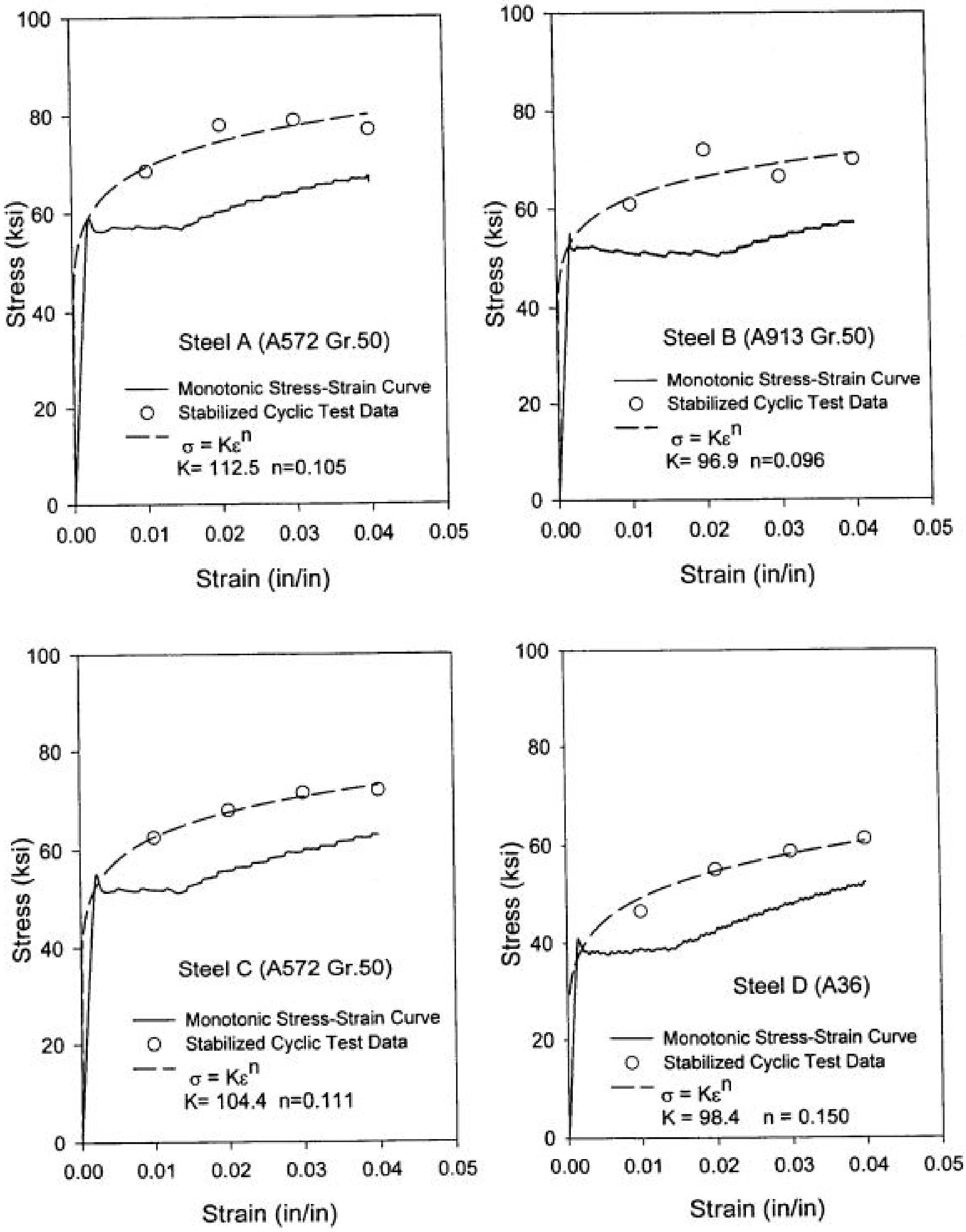

Fig. 4.6 Comparison of monotonic and cyclic stress-strain behavior of the four steels (Kaufmann et al. (2001))

In this study, two different material models are developed for flanges and webs of the specimens and it is assumed that stiffeners remain elastic during the loading. Comparison of the material data given by Hjelmstad (1983) in Table 4.1 and calibrated material data is given in Fig. 4.7 and Fig. 4.8.

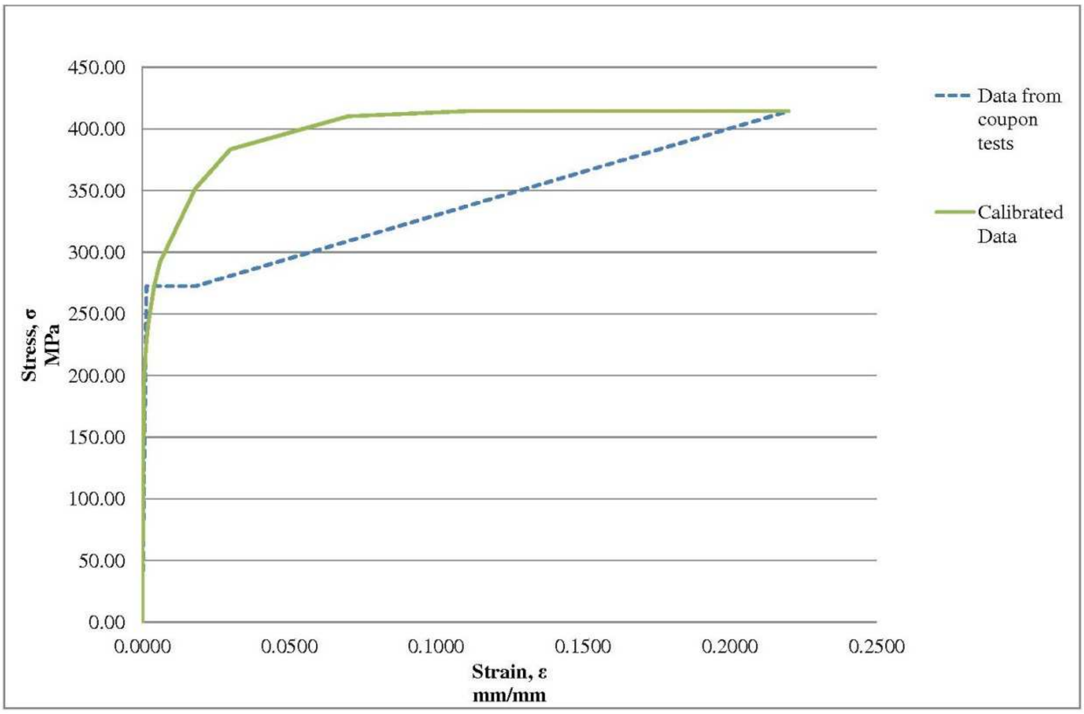

Fig. 4.7 Calibrated stress-strain diagram of the material used in the web of the specimen

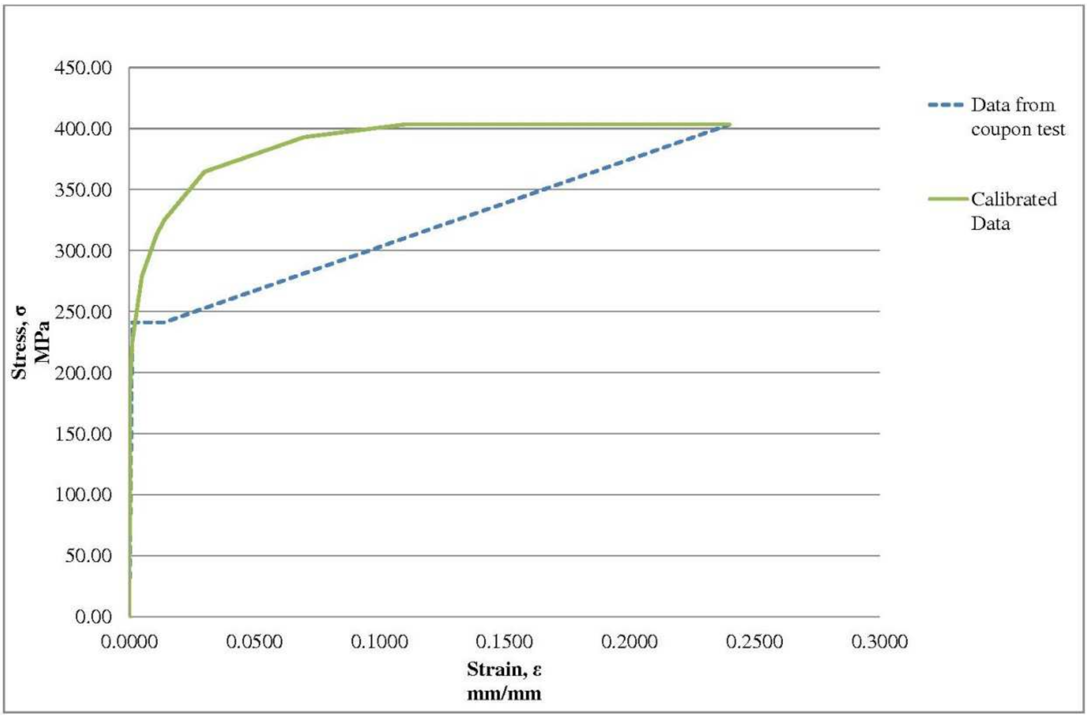

Fig. 4.8 Calibrated stress-strain diagram of the material used in the flange of the specimen

Since the stress-strain diagram of the material has multi slopes, multi-linear kinematic hardening is preferred rather than bilinear kinematic hardening to define the data precisely. The elastic and plastic properties are individually defined in ANSYS Workbench. Information on isotropic elasticity is used by the program until the stress level reaches the yield stress and after this point the material shows plastic properties. The plastic stress-strain relationship should be defined starting from the stress that material yields and corresponding strain value should be edited as 0 in multi-linear kinematic hardening tool as shown in Fig. 4.9.

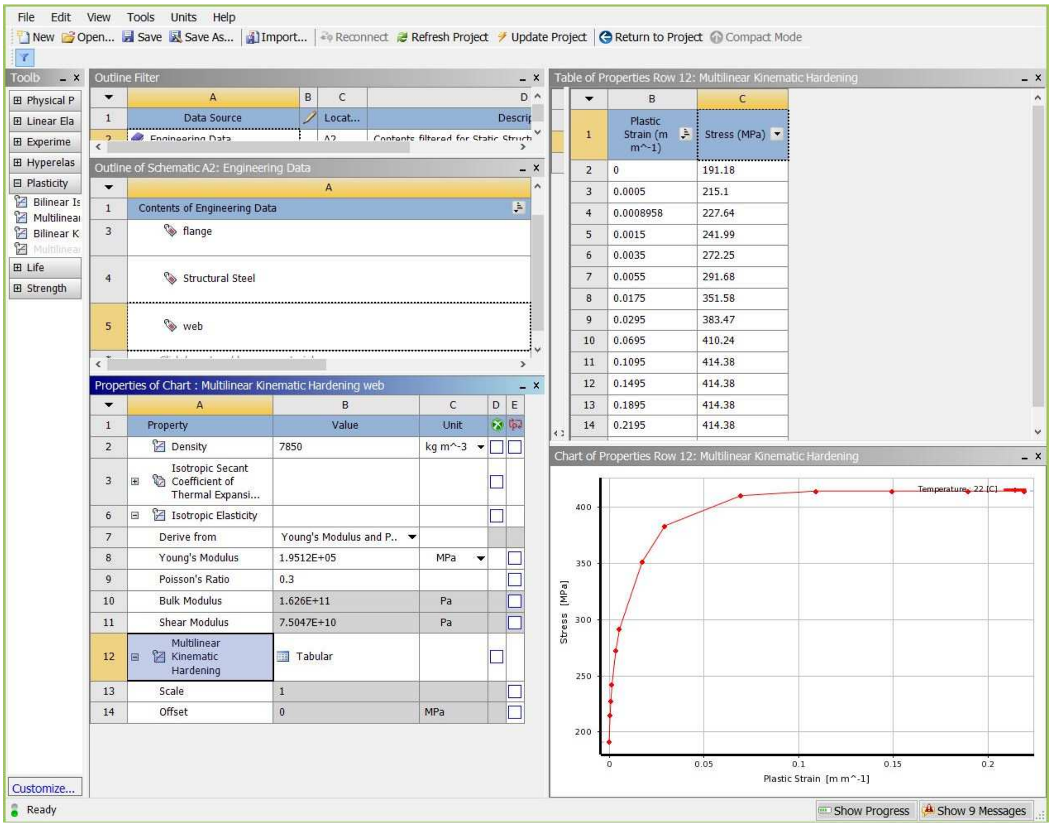

Fig. 4.9 Description of plastic material data in ANSYS Workbench

4.1.3. Loading Protocol

The aim of the study of Hjelmstad (1983) is to determine the response of shear-links under earthquake loads. Therefore, cyclic displacements were applied to the specimens in the plane of the web of the specimens to simulate earthquake loading. Loading history was started with first one cycle that had a magnitude of half inches (12.7 mm) then continued with double cycles of magnitude of one inch (25.4 mm), one half inches (38.1 mm), two inches (50.8 mm) etc. The loading was applied until failure of the specimen initiated.

In finite element simulation conducted in this thesis, the displacement is defined in only the y-direction which is normal to the plane of the flanges and displacements in other directions are restraint to illustrate the experimental setup (Fig. 4.10).

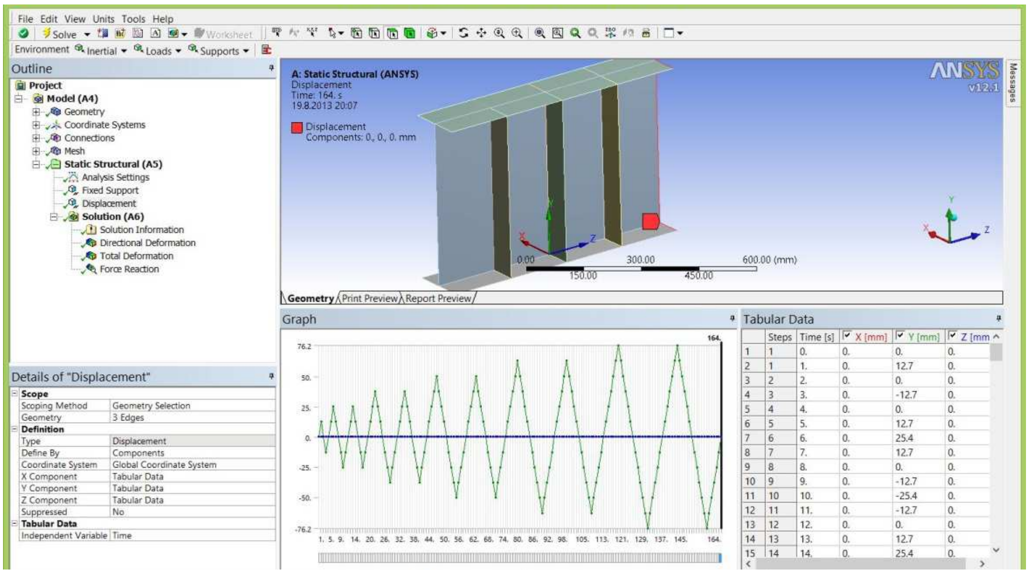

Fig. 4.10 Description of cyclic loading data in ANSYS Workbench

4.1.4. Results

Hjelmstad (1983) stated that after the failure of Specimen 4, slight web buckling was observed and it was stated that energy dissipation of the link was fulfilled through inelastic shearing strains rather than inelastic web buckling (Fig. 4.11). Shear force versus transverse displacement data for Specimen 4 was plotted as given in Fig. 4.12.

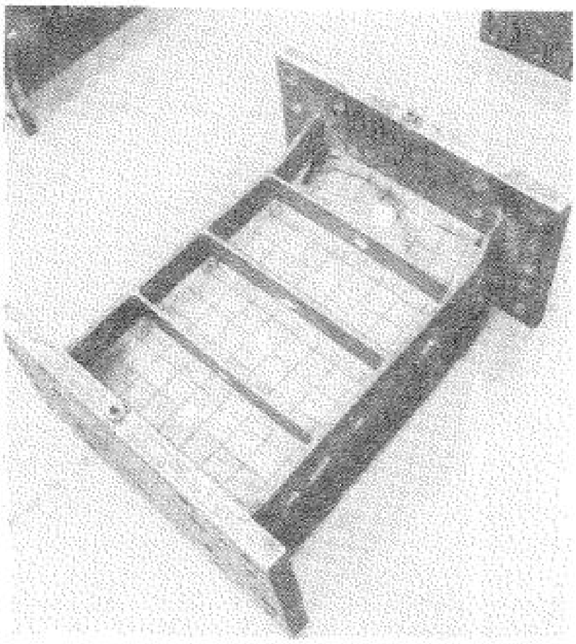

Fig. 4.11 Specimen 4 after failure (Hjelmstad (1983))

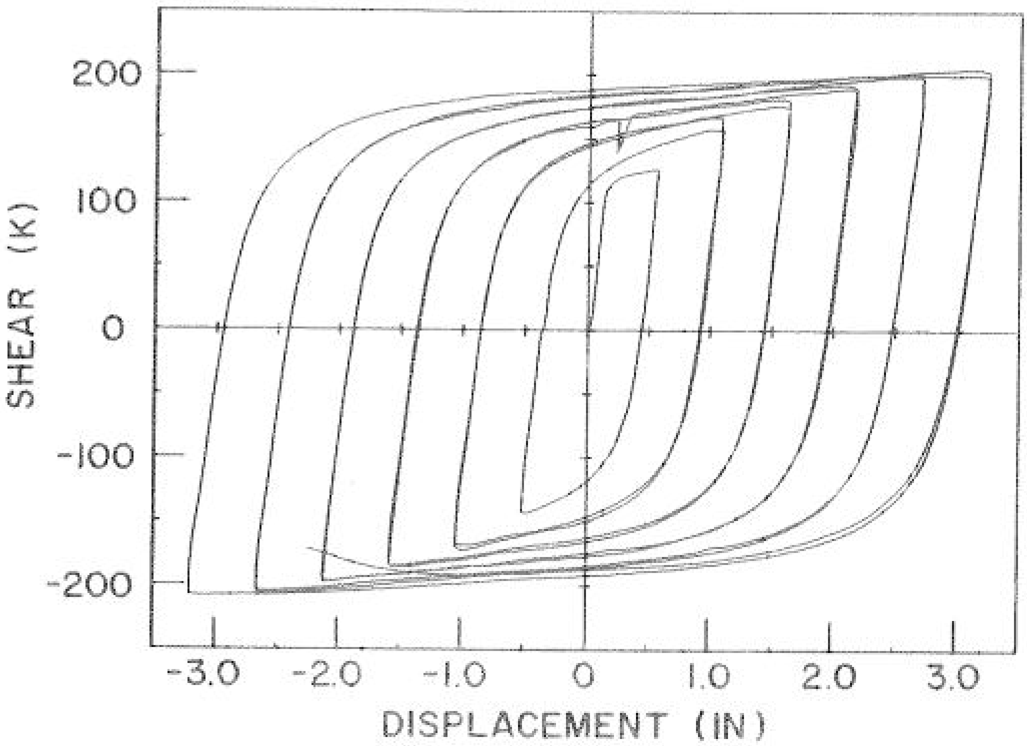

Fig. 4.12 Shear force vs. transverse displacement of Specimen 4 (Hjelmstad (1983))

To verify the accuracy of the finite element model that is created in ANSYS Workbench, the shear force vs. imposed displacement curve obtained after the analysis is plotted and compared with the results of Hjelmstad. Evident in Fig. 4.13, the results almost agree with each other from the point of energy dissipation capacities and ultimate strengths, but some discrepancies are observed at unloading parts. A slight difference between the stiffness provided by the supporting system in the experiments vs. analytical model could have been the reason of this mismatch. Another discrepancy that takes attention is shear force values at first cycle of deformation. Analysis results give a higher shear capacity at first 12.7 mm (0.5 inch) displacement possibly as a result of the calibrated material model. Since the calibration is made according to the procedure outline by Kaufmann et al. (2001), which are performed for a strain range of 2% and with 4-5 loading cycles, the adjusted stress values according to Kaufmann's studies exceed the expected stress level at low strains. The purpose of such a calibration is to accurately capture the overall cyclic properties of steel material at higher inelastic strain hysteresis. In order to both capture lower and higher cycles of inelastic straining accurately, it is imperative to adopt a much more sophisticated 3d steel material model as suggested by Ucak and Tsopelas (2010); however, such a steel material model is not currently available in ANSYS.

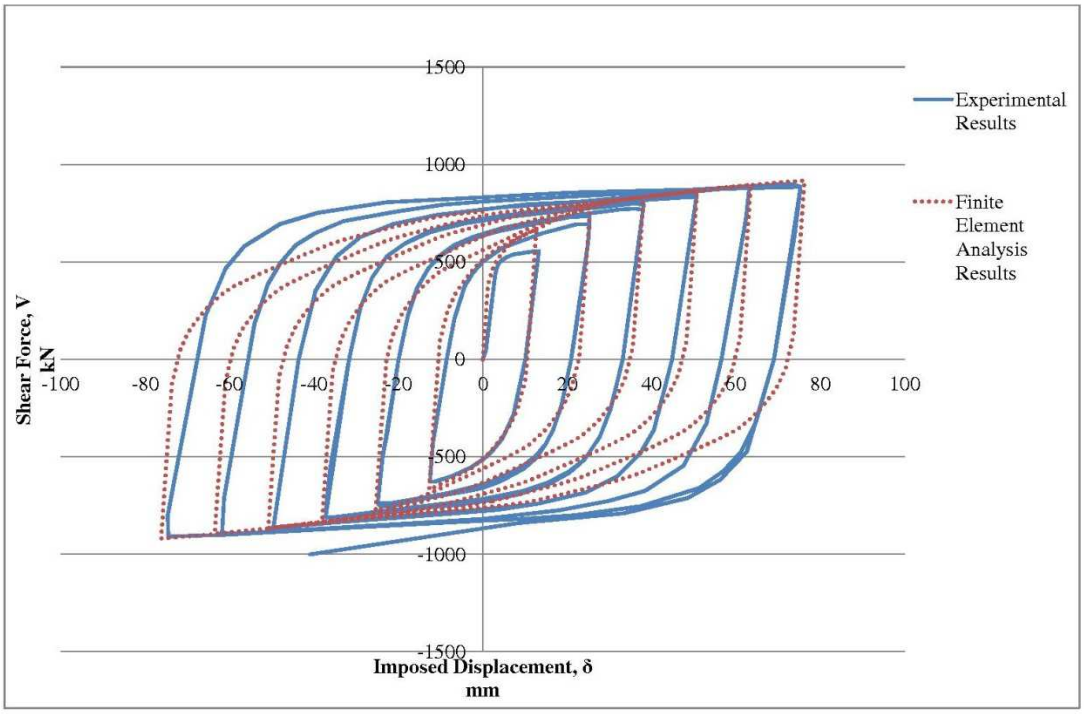

Fig. 4.13 Comparison of experimental data and analysis results

4.2. Kasai's Experiments

4.2.1. Specimens and Test Setups

Kasai (1985) conducted tests on 7 different shear-link specimens, and used W8x10 section for all the specimens. Web and flange thicknesses of W8x10 section are 4.32 mm and 5.28 mm, respectively. Total height of the section is 202.44 mm and total width of the flange is 100.6 mm.

The aim of the tests on the specimens was to create and study more realistic loading conditions that would be present shear-link ends. It is expected that the moment value at the end of a shear-link close to column could be greater than the other end of the shear-link in an EBF system such as shown in Fig. 2.1.b. To illustrate this behavior the test setup shown in Fig. 4.14 was used by Kasai (1985). In this test setup a long removable beam that had the same cross section with the shear-link was located between the support and the link, and equal displacements were applied at both the end of the link and the beam.

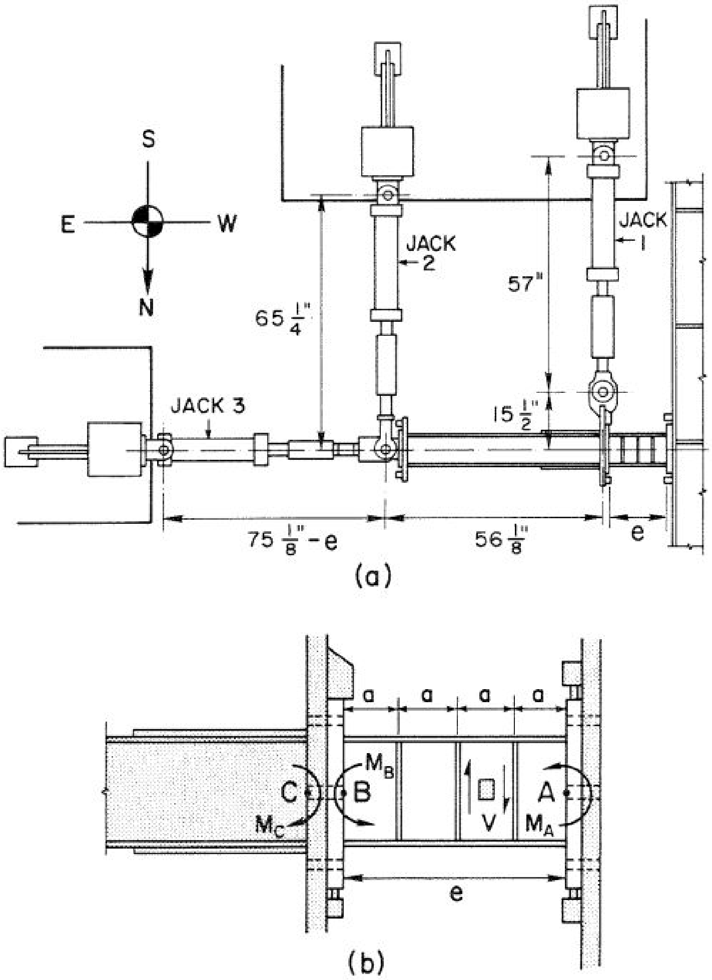

Fig. 4.14 Test setup used in Kasai's experiments Kasai (1985)

In this thesis, since specimens that performed stable hysteresis loops as a result of web stiffener use is studied, Specimens 3 and 5 from Kasai are selected. Geometric properties of these specimens can be found in Table 4.2. The thickness of stiffeners used in links is 6.35 mm. The stiffeners are placed equally spaced at both sides of the link symmetrically and welded to both flanges and web.

Table 4.2 Dimensions of the Specimen 3 and 5

Specimen No.	e (mm)	Panel Zones		
		Number	a (mm)	a/t_w
3	368.3	4	92.202	21.3
5	444.5	5	88.900	20.6

The boundary conditions of specimens used in experiments of Kasai (1985) is defined as fixed connection at the column connection end and at the other end connected to the long beam behaves like pin connection. Also, at the other end of the long beam, rotation is allowed. The simple sketch of the specimen 5 is shown in Fig. 4.15, where imposed displacements are marked.

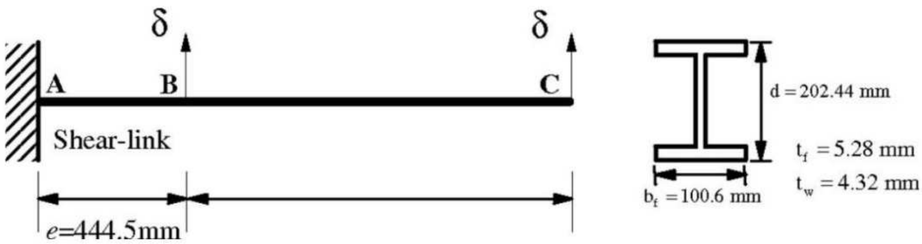

Fig. 4.15 Geometry of Specimen 5 of Kasai (Saritas and Filippou (2009a))

Both of the specimens 3 and 5 are modeled with 2d surface (shell) elements in ANSYS Workbench. All welded connections between the parts of the specimen are defined as bonded connection. In addition, the connection of link and long beam is also defined as bonded connection. In order to shorten the analysis time, the end plates are not included into the model. In both models, 28 mm sized meshes are used as shown in Fig. 4.16 and Fig. 4.17, where this mesh discretization resulted in an accurate and converged nonlinear response.

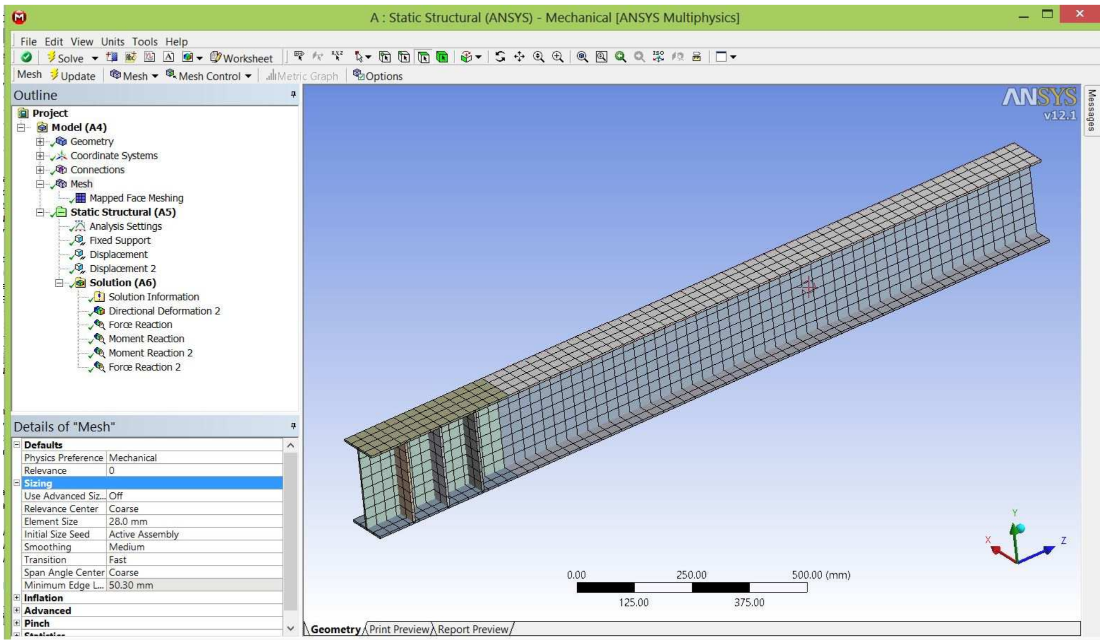

Fig. 4.16 Finite element model of Specimen 3

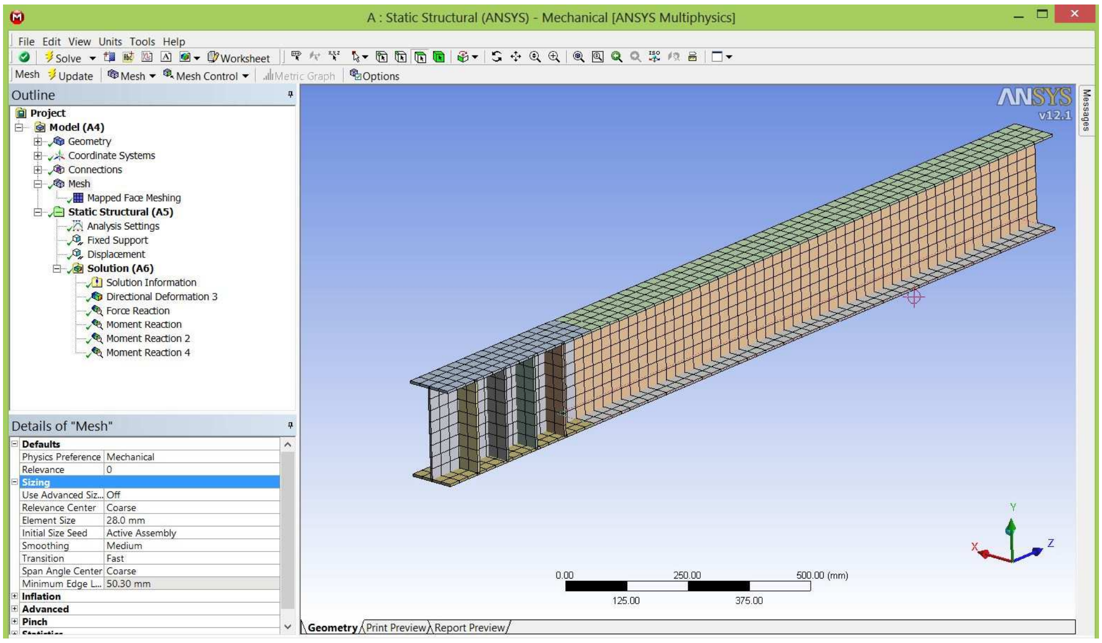

Fig. 4.17 Finite element model of Specimen 5

4.2.2. Material Models and Assumptions

Kasai (1985) used ASTM A36 steel in shear-link specimens. Coupon tests conducted by Kasai are reported in Table 4.3. These values represent uniaxial monotonic loading response of steel material tested from the web and flange of Specimens 3 and 5.

Table 4.3 Material properties of Specimens 3 and 5

Location	σ_0 MPa	σ_u MPa	ε_{sh} mm/mm	ε_u mm/mm	E GPa
Web	417.82	550.89	0.031	0.163	206.85
Flange	361.29	487.46	0.026	0.198	214.55

The material properties, which are obtained from the coupon tests, of web and flange are calibrated to fit the cyclic stress-strain values as suggested by Kaufmann et al. (2001), and this calibration is shown in Fig. 4.18 and Fig. 4.19 for both specimens 3 and 5.

In ANSYS Workbench, multi-linear kinematic hardening option is used to model the plasticity of steel material. The elastic properties are edited to the elastic isotropy part, and then to define the behavior of the material after the yield point, calibrated values are used in the model (Fig. 4.20).

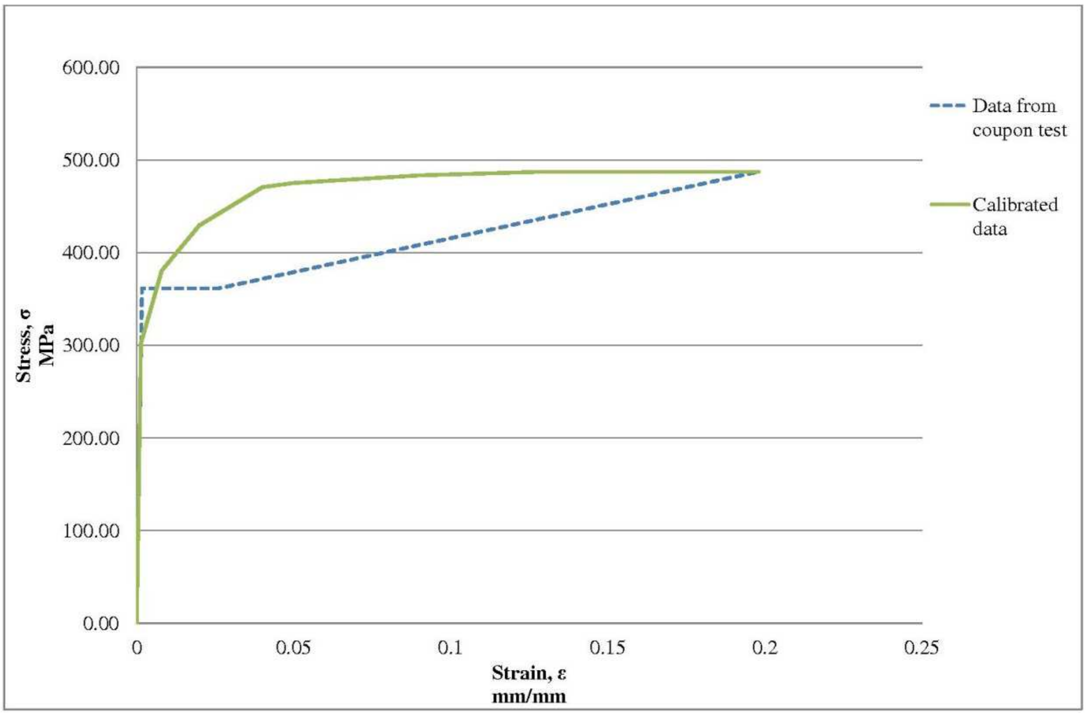

Fig. 4.18 Calibrated stress-strain diagram of the material used in the flange of the both specimens

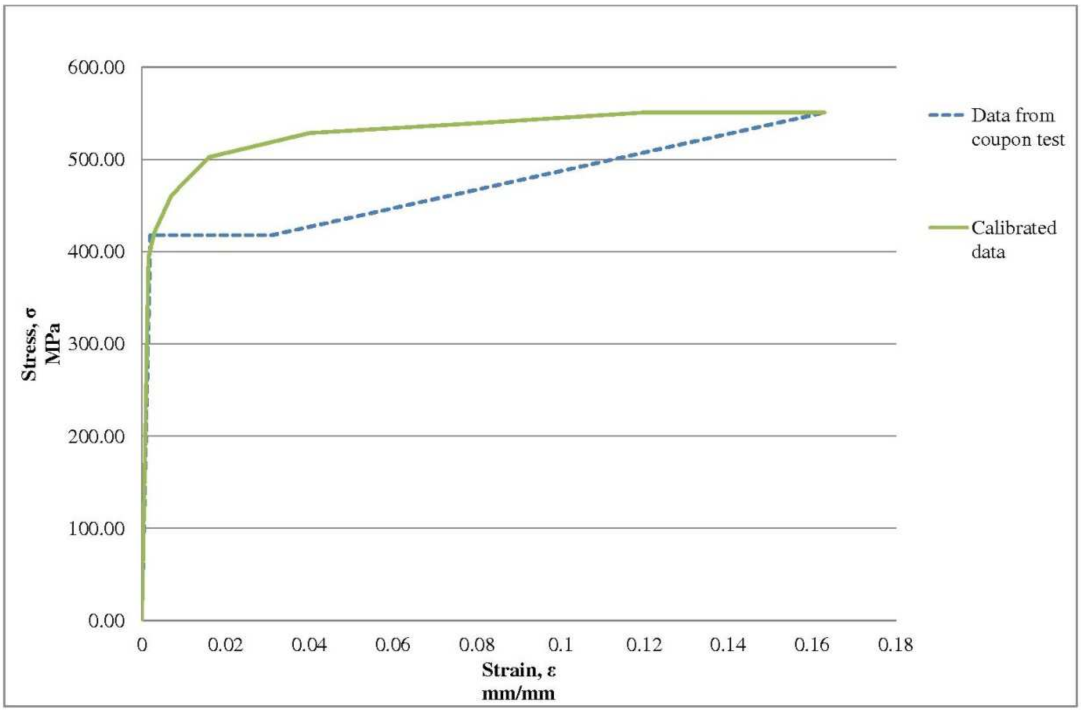

Fig. 4.19 Calibrated stress-strain diagram of the material used in the web of the both specimens

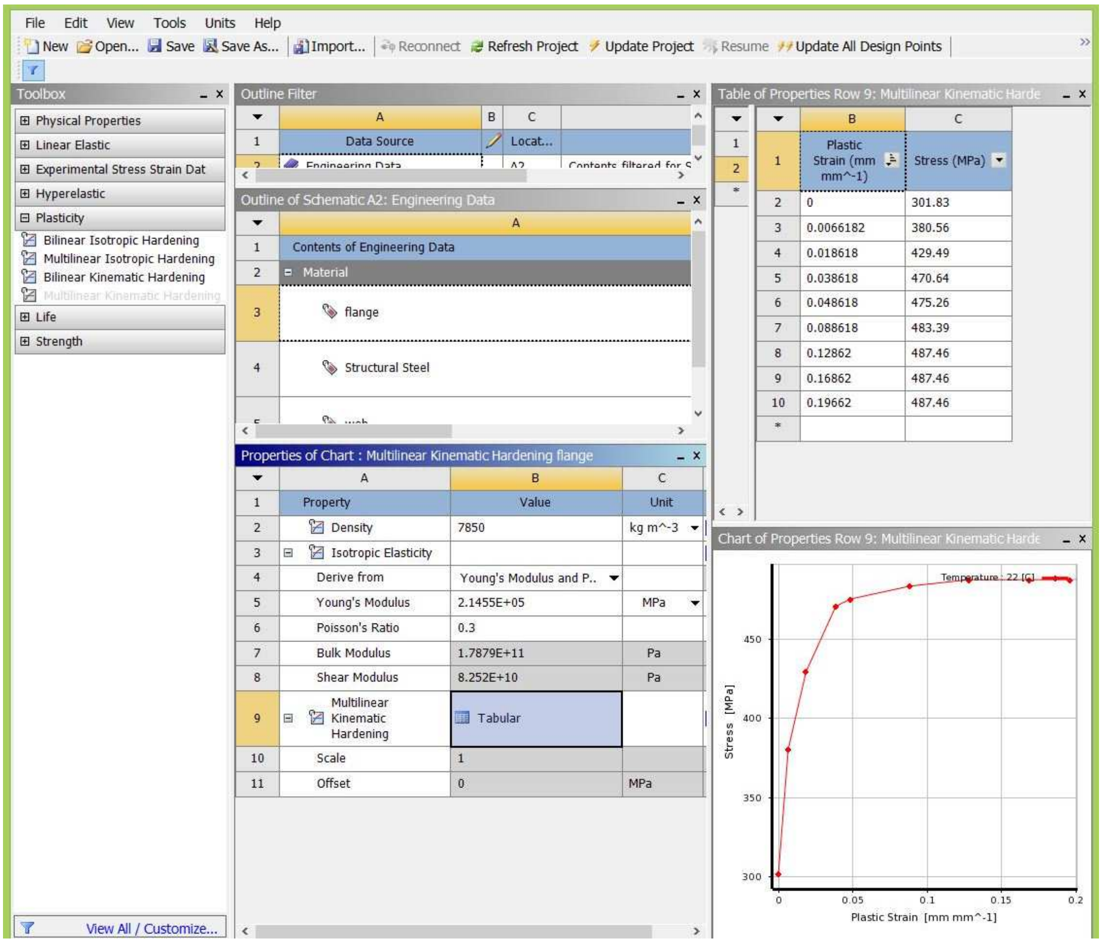

Fig. 4.20 Description of plastic material data in ANSYS Workbench

4.2.3. Loading Protocol

Kasai (1985) considered cyclic and monotonic loadings on the specimens, and in addition, presence of axial forces on shear-link specimens was also studied. For Specimens 3 and 5, loading type was symmetric cyclic type and did not contain any axial force effects. The cyclic displacement history consisted of one cycle of 0.25 inches (6.35 mm) and continued with double cycles at 0.5 inches (12.7 mm), 0.75 inches (19.05 mm) etc.

The cyclic displacement is applied both to the link-beam connection and to end of the beam in the plane of the web, in y-direction. At the end of the beam and the link-beam joint, the rotation about the x axis was allowed since the specimen was pinned at the beam end as shown in Fig. 4.14.

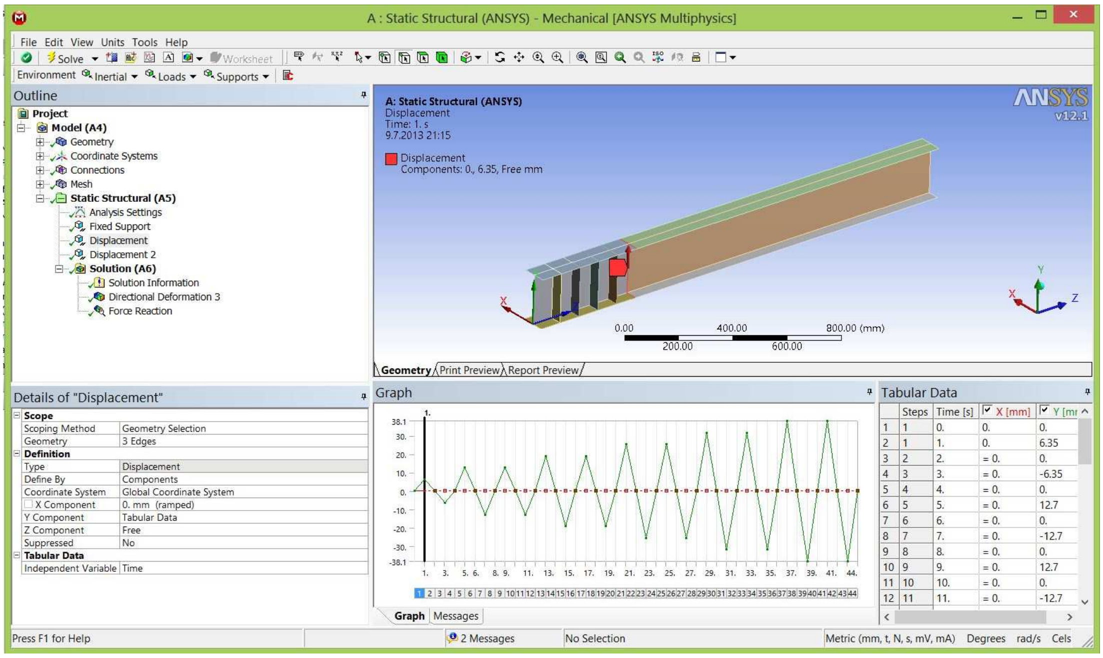

Fig. 4.21 Description of cyclic loading data in ANSYS Workbench

4.2.4. Results

The experimental data and results reported by Kasai (1985) on Specimens 3 and 5 provided not only the link shear force versus displacement plots but also the variation of link end moments through cyclic loading. Furthermore, detailed pictures taken from the specimens were also available through the loading history. At first cycle of loading, yielding of both specimens was observed. At the end of the experiment, a slight web buckling and symmetric flange buckling of Specimen 3 and no web buckling and symmetrical flange buckling of Specimen 5 was present.

In this study a detailed comparison is performed for verification of the finite element model set up as part of the study conducted in this thesis. Kasai (1985) presented the deformed shapes of the specimens during the tests. At same cycles and displacement values, the deformed shapes of the finite element model are captured to compare with the deformed shapes of the tested specimen. Close match between the numerical and experimental results can be observed when Fig. 4.22 and Fig. 4.23 are compared with each other.

The comparison of shear force versus imposed displacement curves in Fig. 4.24 shows excellent agreement between finite element model and the experimental results. In overall, analysis results give similar ultimate shear capacities and stiffness values for both loading and unloading parts as well as energy dissipation characteristics with the experimental results. However, at first 3 cycles an overshooting in shear capacities is observed. As observed in the comparison of results with Kasai (1985), the main reason of the discrepancy is the calibration of material model.

In Fig. 4.25 and Fig. 4.26, the comparisons of the moments at the ends of the link show that similar stiffness values are captured in both hysteretic diagrams. Variation of moment through cyclic loading obtained from analysis shows slight differences when compared with experimental results. The analysis results give higher moment capacities at column end and lower capacities at link-beam joint. A possible reason of this situation is the differences in boundary conditions considered in the finite element model and the exact boundary conditions present at the ends of the physical specimen. Since the end plates are not modeled and the column end of the link is directly assigned as fixed support, moment capacity at this end naturally increased. However, despite this discrepancy, it should be emphasized that the obtained results present much better numerical results for moment variations when previous analytical results on this specimen are considered (Ramadan and Ghobarah (1991),Ricles and Popov (1994), Saritas and Filippou (2009a)).

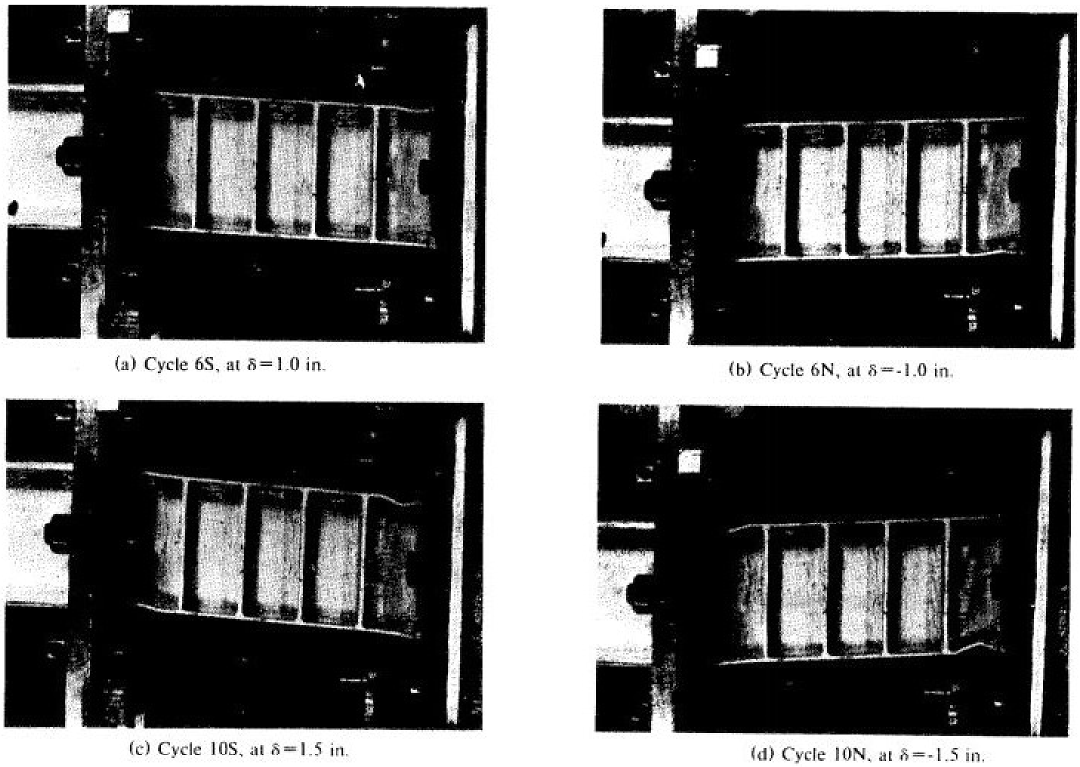

(a) Cycle 6S, at $\delta=1.0$ in.

(b) Cycle 6N, at $\delta=-1.0$ in.

(c) Cycle 10S, at $\delta=1.5$ in.

(d) Cycle 10N, at $\delta=-1.5$ in.

Fig. 4.22 Photos of Specimen 5 during the test by Kasai (1985)

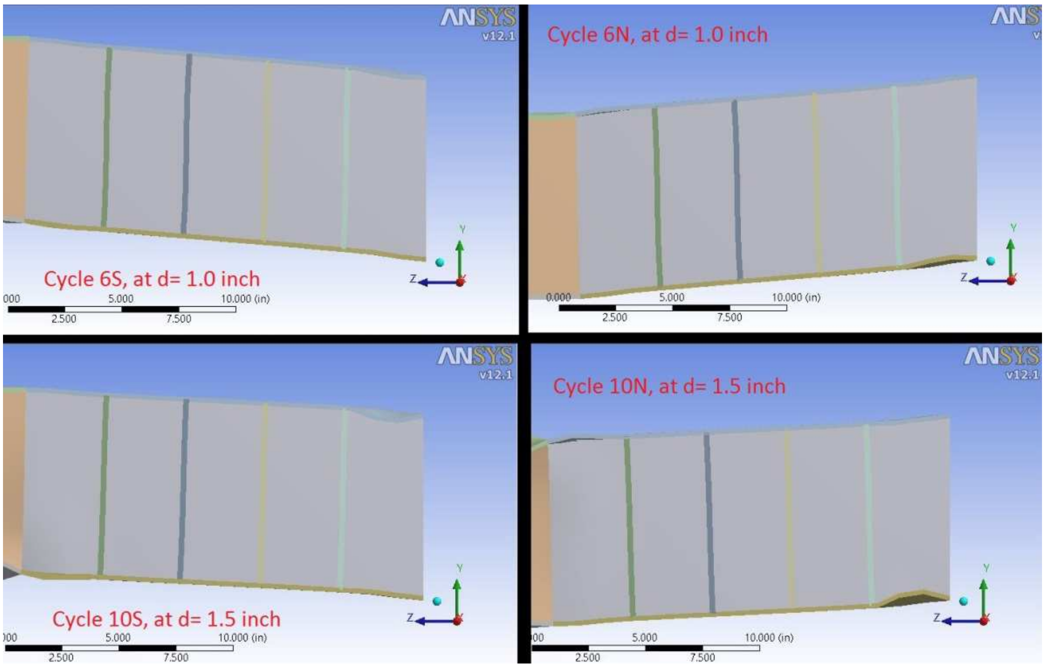

Fig. 4.23 Deformed shapes of Specimen 5 at different steps of the analysis

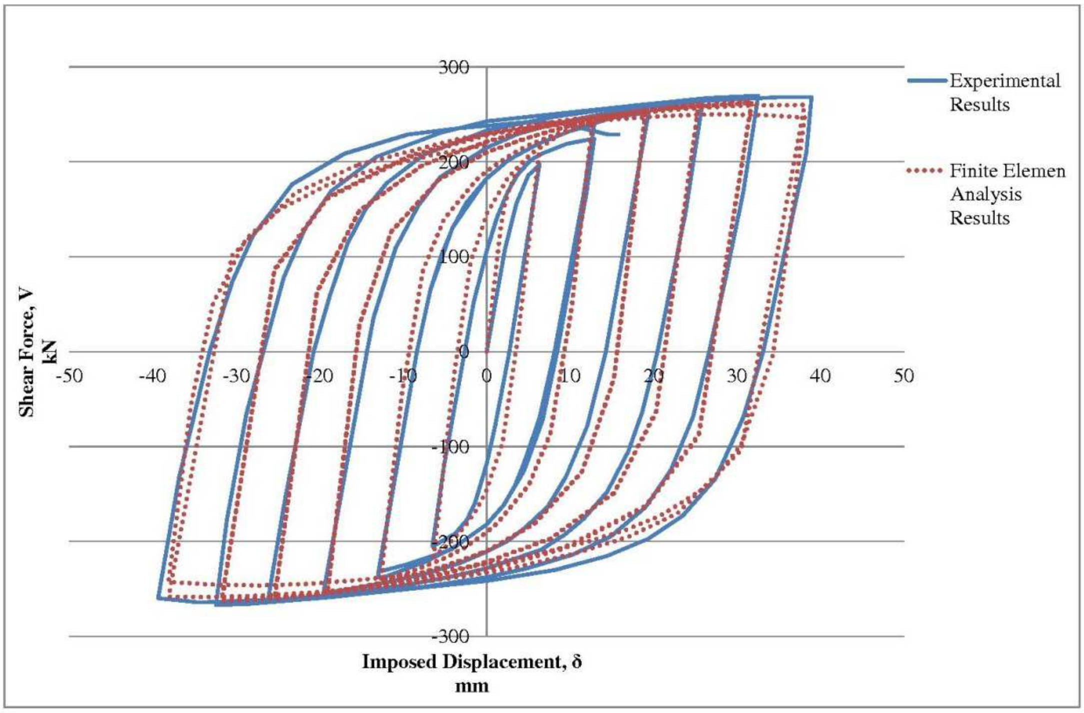

Fig. 4.24 Comparison of the shear-imposed displacement curves of experiment and finite element analysis for specimen 5

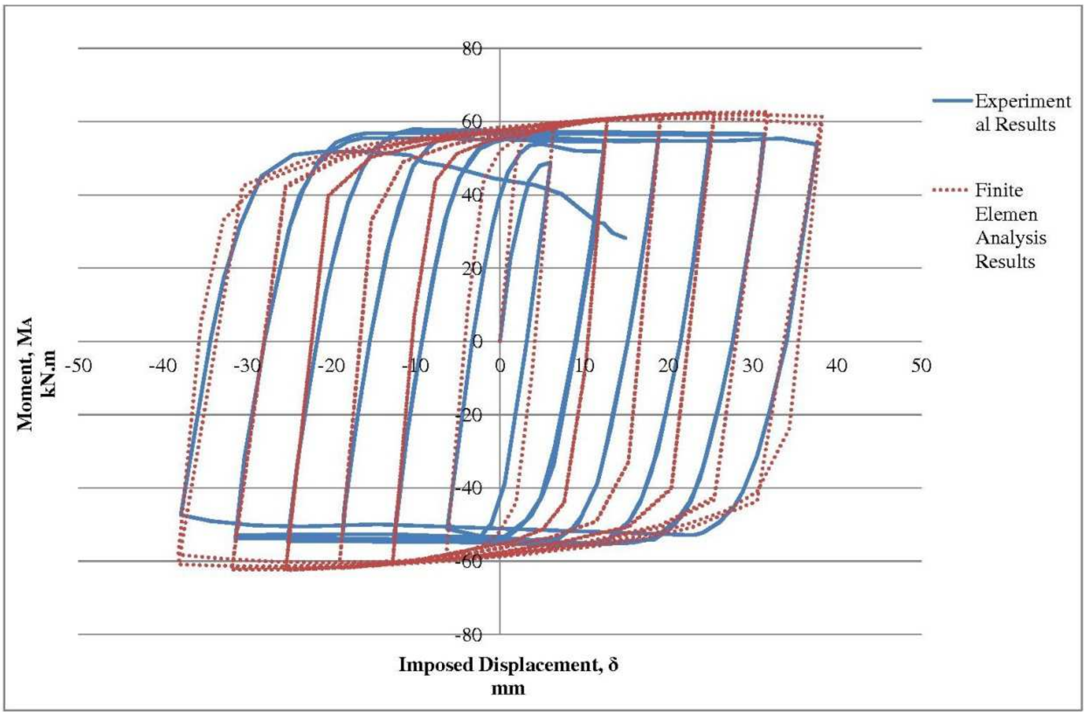

Fig. 4.25 Comparison of the moment at column end of the link versus imposed displacement curves of experiment and finite element analysis for Specimen 5

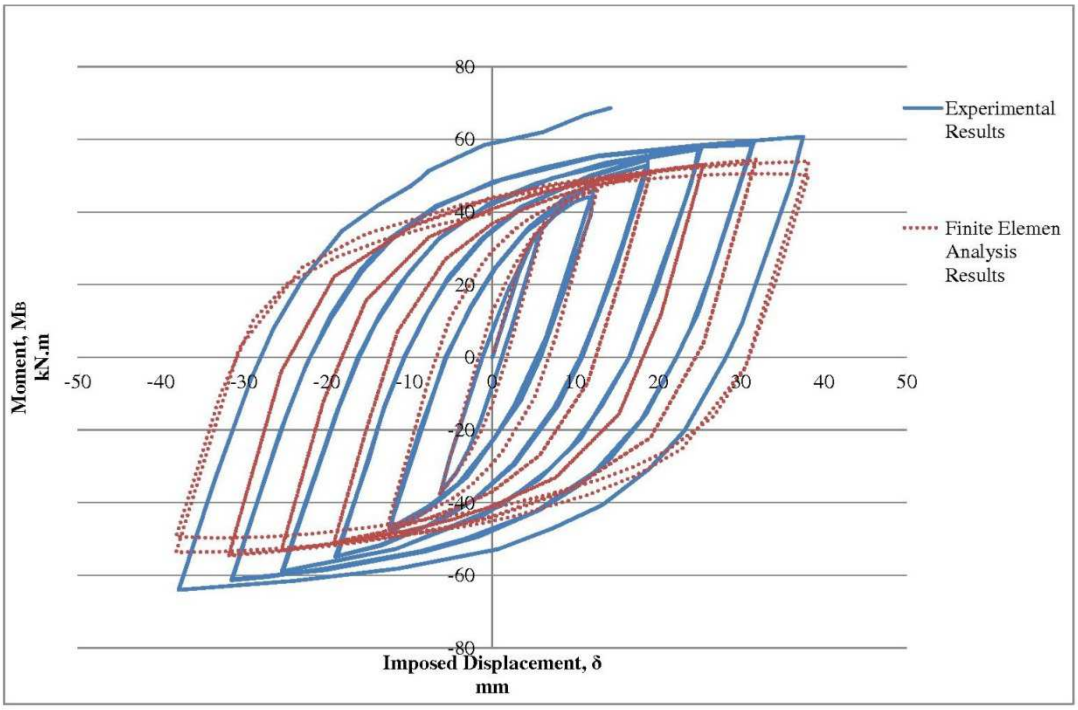

Fig. 4.26 Comparison of the moment at beam joint end of the link versus imposed displacement curves of experiment and finite element analysis for Specimen 5

As a second comparison of the tests conducted by Kasai (1985), Specimen 3 is considered where the length of Specimen 3 is shorter than Specimen 5 and everything else is basically the same. The shear force versus imposed displacement curves obtained from finite element simulation for Specimen 3 is compared with the experimental results in Fig. 4.27. Although the stiffness slopes of analysis and experiment at the unloading parts agreed well with each other, slight discrepancies are visible in the curves resulting in slight underestimation of energy dissipation capacity captured by the numerical model. In addition to this comparison, the deformed shape of the specimens at various points during analysis matched with the experimental deformed shapes.

Variations of end moments obtained from numerical analysis for Specimen 3 are presented in Fig. 4.28 and Fig. 4.29. The moment-imposed displacement curves of the links obtained from analysis have similar loading and unloading slopes with the experimental results, but moment capacities are underestimated at both ends in the finite element model. It is important to point out that, prior numerical studies on this specimen gave further discrepancies in capturing the distribution of end moments; thus in this regards, the current study is an improvement over prior studies.

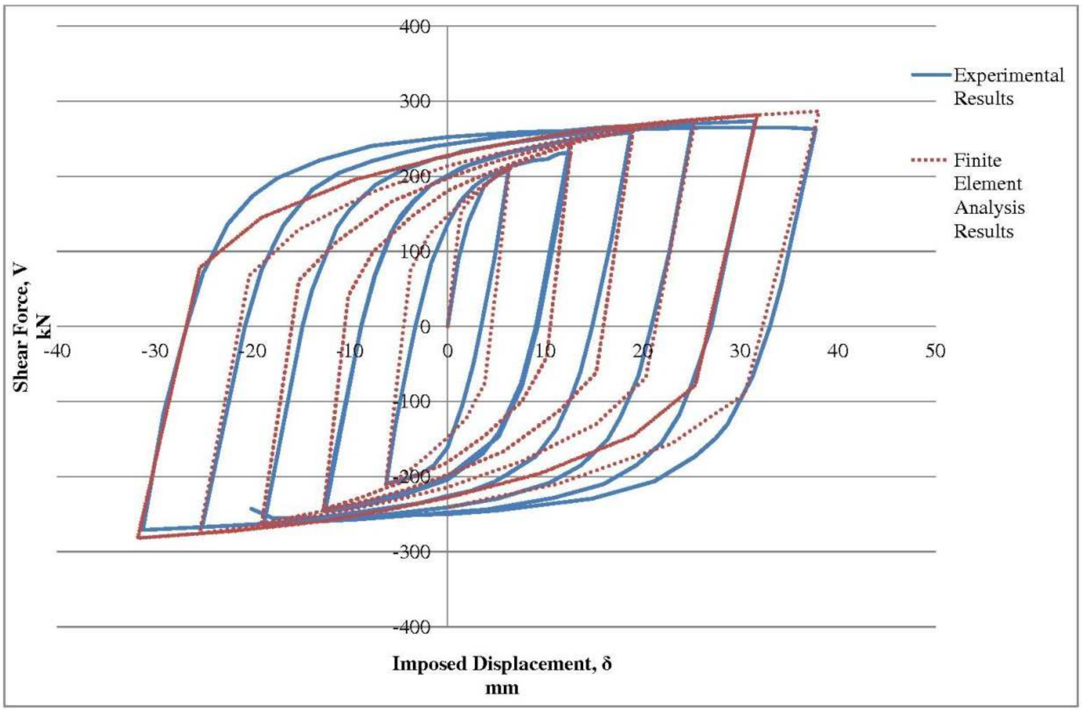

Fig. 4.27 Comparison of the shear-imposed displacement curves of experiment and finite element analysis for Specimen 3

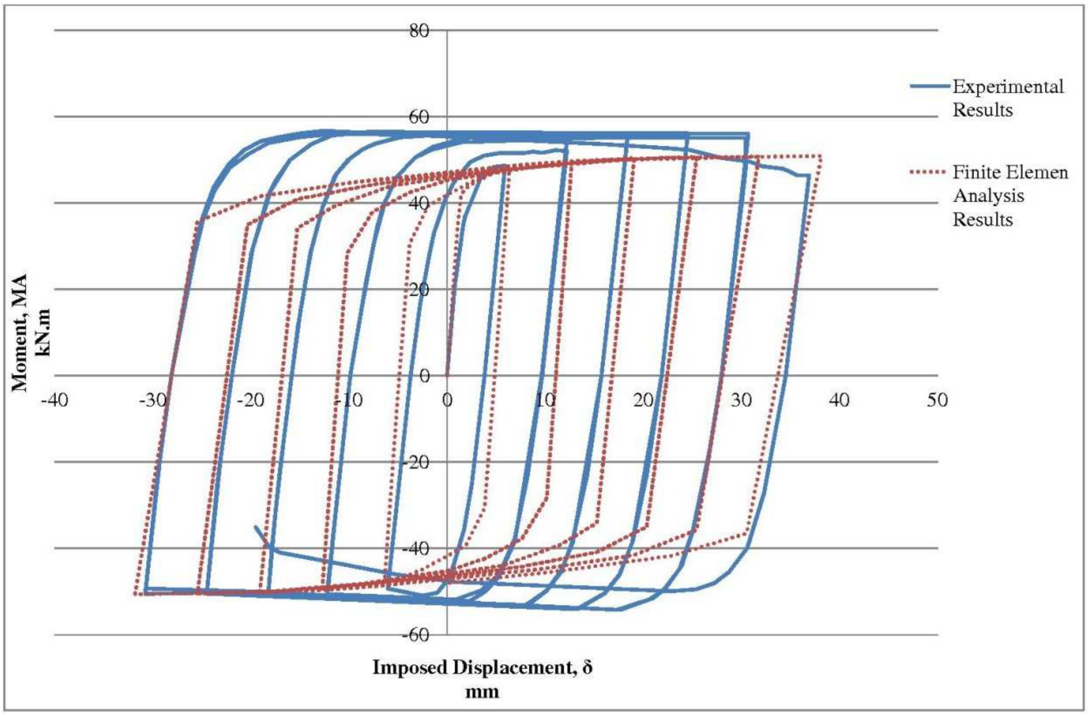

Fig. 4.28 Comparison of the moment at column end of the link-imposed displacement curves of experiment and finite element analysis for Specimen 3

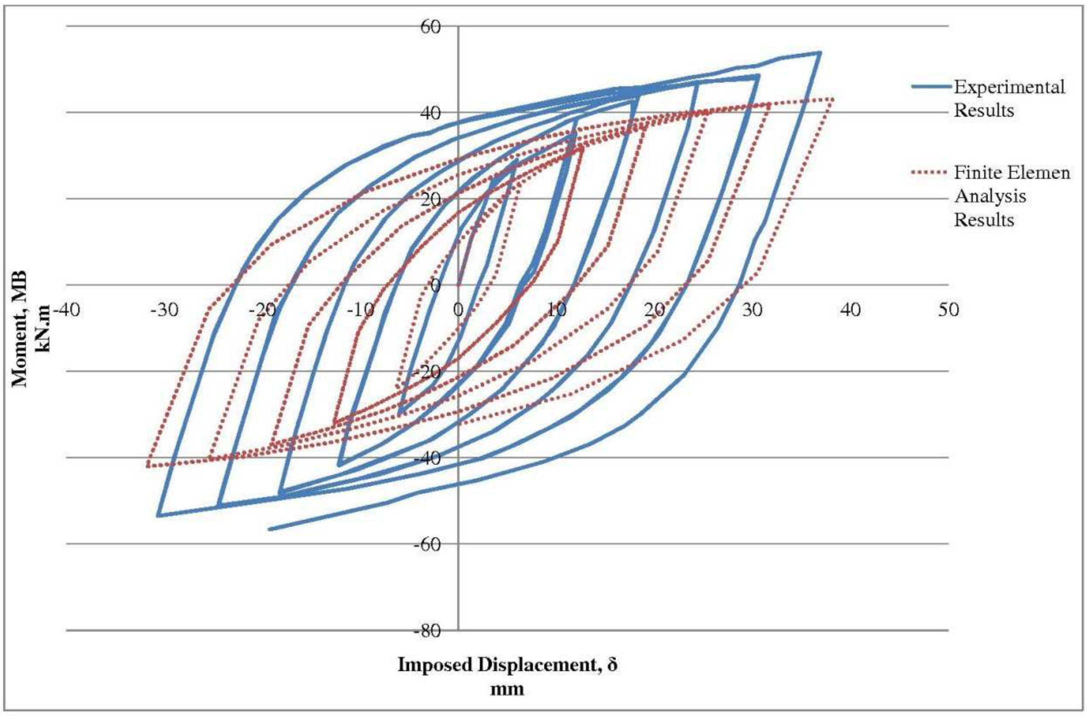

Fig. 4.29 Comparison of the moment at beam joint of the link-imposed displacement curves of experiment and finite element analysis for Specimen 3

4.3. Remarks on Numerical Analysis

In the light of the comparative studies conducted in this chapter, good agreement is captured overall between the finite element analysis results and experimental results, despite the presence of slight discrepancies.

The finite element models of the specimens are created adhering to real dimensions and properties indicated in the studies of the researchers to illustrate realistic models. However, some assumptions about the test setup and boundary conditions might have caused the slight deviations in the results when the numerical and experimental data are compared. Besides that, uncertainties and insufficient data about the behavior of the material subjected to cyclic loading will definitely cause further discrepancies between the experimental and analysis results.

After all, the comparisons of the results between the experiments and analyses show that the detailed finite element modeling approach employed in this thesis is verified in terms of capturing the overall nonlinear behavior and energy dissipation characteristics of various shear-link specimens. The accuracy of numerical simulations gives assurance to investigate the behavior of the links in more detail with finite element models. In the upcoming chapters, a comparative study is undertaken in order to assess the influence of flange thickness on the over-strengthening of shear-link specimens and furthermore, unsymmetrical cyclic loading protocols will be studied in terms of their influence on nonlinear response. The results obtained from the numerical simulations will be compared with a frame finite element model developed by Saritas and Filippou (2009a).

CHAPTER 5

FRAME FINITE ELEMENT MODEL

In this chapter, the frame finite element model proposed by Saritas and Filippou (2009a) is presented. The current study conducted in this thesis provides slight enhancement to the flange shear strain distribution on the section model employed by Saritas and Filippou (2009a) and Saritas and Filippou (2009b), thus in this regards, this effort contains improvements in the formulation of that frame element. Furthermore, the presentation of the frame finite element is cast by using principle of virtual forces rather than the use of a three-field variational formulation as done by Saritas and Filippou (2009a).

In the second part of the chapter, numerical response of the frame finite element under cyclic loading conditions is demonstrated with the experiments of Hjelmstad (1983) and Kasai (1985). The frame finite element will be used in the next chapter for the comparative numerical study with more refined finite element models employed in ANSYS Workbench.

5.1. Description of Frame Finite Element Model

Derivation of the frame finite element can be started from the differential equations of equilibrium that are written as follows:

$$N' + w_x(x) = 0; \quad M' + V = 0; \quad V' + w_y(x) = 0 \qquad (5)$$

where N, M, and V are the axial force, bending moment and shear force at a section, respectively (Fig. 5.1), and w_x and w_y are the axial and transverse components of the distributed element load acting along the beam, respectively.

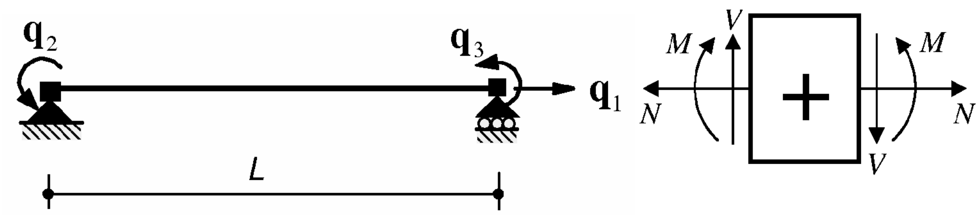

Fig. 5.1 Basic forces and deformations of beam element

Under linear geometry, above equation can be solved independent of the displacements and of the material response. The boundary values in above figure are used as the basic element forces **q**, and the equilibrium for the beam element with length L is expressed as follows

$$\mathbf{s}(x)=\begin{pmatrix} N(x) \\ M(x) \\ V(x) \end{pmatrix}=\begin{bmatrix} 1 & 0 & 0 \\ 0 & x/L-1 & x/L \\ 0 & -1/L & -1/L \end{bmatrix}\begin{pmatrix} q_1 \\ q_2 \\ q_3 \end{pmatrix}+\mathbf{s}_{\mathrm{p}}(x)=\mathbf{b}(x)\mathbf{q}+\mathbf{s}_{\mathrm{p}}(x) \tag{6}$$

where $\mathbf{s}(x)$ is the vector of the section forces, and $\mathbf{b}(x)$ is the matrix of force interpolation functions. For uniform distributed element loading, the particular solution $\mathbf{s}_{\mathrm{p}}(x)$ can be easily found from equilibrium, and added to the right hand side of Eq. (6). The particular solution for uniform distributed element loading is presented by Saritas and Filippou (2009b).

The compatibility statement of the element is obtained from principle of virtual forces. From the equality between the external and internal work done as a result of the application of a virtual force system, i.e. $\delta\mathbf{s}(x)=\mathbf{b}(x)\delta\mathbf{q}$, the basic element deformations $\mathbf{v}$ are obtained in terms of the section deformations $\mathbf{e}(x)$ along the beam length L.

$$\mathbf{v}=\int_L \mathbf{b}^{\mathrm{T}}(x)\,\mathbf{e}(x)dx \tag{7}$$

where $\mathbf{e}(x)$ is the vector of section deformations with following terms in given order: the axial deformation $\varepsilon_a(x)$, curvature $\kappa(x)$, and shear deformation $\gamma(x)$.

Element flexibility matrix can be calculated through differentiation of end deformations with respect to end forces:

$$\mathbf{f}=\frac{\partial\mathbf{v}}{\partial\mathbf{q}}=\int_L \mathbf{b}^{\mathrm{T}}(x)\frac{\partial\mathbf{e}(x)}{\partial\mathbf{s}(x)}\frac{\partial\mathbf{s}(x)}{\partial\mathbf{q}}dx=\int_L \mathbf{b}^{\mathrm{T}}(x)\,\mathbf{f}_s(x)\,\mathbf{b}(x)dx \tag{8}$$

where $\mathbf{f}_s$ is section flexibility matrix.

In a standard finite element analysis program, all elements are expected to present themselves as if they are displacement-based, i.e. element resisting forces in a displacement-based formulation are a function of element end deformations, $\mathbf{q}=\mathbf{q}(\mathbf{v})$, and the response of an element is resisting forces and stiffness matrix. Since a standard finite element program imposes displacements on an element, element state determination is straightforward with displacement-based elements. However, in a force-based element such a direct relation cannot be obtained; because the current deformations can only be expressed as a function of the element resisting forces, $\mathbf{v}=\mathbf{v}(\mathbf{q})$. Due to this mismatch, the state determination of the force-based element requires a rather complicated solution algorithm.

The element response is obtained from the fact that the element deformations that are sent from the finite element program to the element, let's call it $\hat{\mathbf{v}}$ to signify that this is imposed on the element, should be equal to the element deformations compatible with element forces, i.e. $\hat{\mathbf{v}}-\mathbf{v}(\mathbf{q})=\mathbf{0}$. The solution to this equality is achieved by linearization, and the following updating scheme with an iteration counter j is obtained.

$$\Delta \underset{\sim}{\mathbf{q}}^{(j+1)} = \left[\underset{\sim}{\mathbf{f}}^{(j)} \right]^{-1} \left(\hat{\underset{\sim}{\mathbf{v}}} - \underset{\sim}{\mathbf{v}}^{(j)} \right) \quad \text{and} \quad \underset{\sim}{\mathbf{q}}^{(j+1)} = \underset{\sim}{\mathbf{q}}^{(j)} + \Delta \underset{\sim}{\mathbf{q}}^{(j+1)} \tag{9}$$

where **v** in Eq. (9) is obtained from Eq. (7) with numerical integration at discrete sections.

Constitutive relations at the section level are mostly derived from section deformations, $\hat{\mathbf{s}} = \hat{\mathbf{s}}(\mathbf{e})$, where the hat notation signifies that these section forces are deformation dependent. However, the section forces of the force-based element are given by the basic element forces in Eq. (6), and we denote this as $\mathbf{s} = \mathbf{b}\mathbf{q} + \mathbf{s}_{\mathrm{p}}$. These two relations should be equal to each other in order to obtain a compatible section response for given element forces, i.e. $\mathbf{s} - \hat{\mathbf{s}}(\mathbf{e}) = \mathbf{0}$. The solution to this equality is achieved by linearization again. Iterations at the section and element level can be done in a nested fashion as suggested by Spacone et al. (1996). Therefore, the section iteration counter is selected to follow the element iteration counter, *j*.

$$\Delta \mathbf{e}^{(j+1)} = \left[\mathbf{k}_s^{(j)} \right]^{-1} \left(\mathbf{b}\mathbf{q}^{(j+1)} + \mathbf{s}_{\mathrm{p}} - \hat{\mathbf{s}}(\mathbf{e}^{(j)}) \right) \quad \text{and} \quad \mathbf{e}^{(j+1)} = \mathbf{e}^{(j)} + \Delta \mathbf{e}^{(j+1)} \tag{10}$$

where $\mathbf{k}_s$ is the section stiffness matrix.

In depth discussion on above solution algorithms is presented by Saritas and Soydas (2012). In that work, the element state determination algorithms for the force formulation elements are derived from a three-field variational principle presented by Taylor et al. (2003).

When a section deformation is calculated through above solution algorithm, section response should be then obtained so that solution can proceed. Calculation of section response is denoted as section state determination, and for this purpose fiber discretization model is used by Saritas and Filippou (2009a).

5.1.1. Section Response

Compatible strains along section depth can be calculated from plane sections remain plane assumption modified for the presence of distributed shear strains as follows:

$$\boldsymbol{\varepsilon} = \begin{Bmatrix} \varepsilon_x \\ \gamma_{xy} \end{Bmatrix} = \mathbf{a}_{\mathrm{s}} \mathbf{e}, \quad \text{where} \quad \mathbf{a}_{\mathrm{s}} = \begin{bmatrix} 1 & -y & 0 \\ 0 & 0 & \psi(y) \end{bmatrix} \tag{11}$$

For an I-section a non-dimensional parabolic shear strain distribution can be used on the web region as suggested by Saritas and Filippou (2009a):

$$\psi(y) = \beta \phi(y)$$

$$\phi(y) = \left((1+2\alpha) - 4\frac{y^2}{d^2} \right); \quad \beta = \left(\frac{2}{3}(1+3\alpha) \right) \Big/ \left((1+2\alpha)^2 - \frac{2}{3}(1+2\alpha) + \frac{1}{5} \right) \tag{12}$$

where α is the ratio of the flange area to the web area, i.e. $\alpha = (2t_f b_f)/(t_w d)$. The distribution $\phi(y)$ ignores the presence of shear strain on the flanges and assumes that shear is carried by the web (known as sandwich beam theory in mechanics). A coefficient β is needed to be used due to the non-dimensionality of this distribution. In order to calibrate the parabolic distribution of shear strain, energy approach can be followed as suggested by Saritas and Filippou (2009a), where matching the elastic shear strain energy simply yields the calibration parameter β, thus changing the shear strain distribution on the flange as given in above equation.

Section forces derived from section deformations and the corresponding section tangent stiffness matrix are obtained from the following expressions

$$\hat{\mathbf{s}} = \begin{bmatrix} \hat{N} & \hat{M} & \hat{V} \end{bmatrix}^{\mathrm{T}} = \int_A \mathbf{a}_{\mathrm{s}}^{\mathrm{T}} \boldsymbol{\sigma}\, \mathrm{d}A \quad \text{and} \quad \mathbf{k}_{\mathrm{s}} = \frac{\partial \hat{\mathbf{s}}}{\partial \mathbf{e}} = \int_A \mathbf{a}_{\mathrm{s}}^{\mathrm{T}} \mathbf{k}_{\mathrm{m}} \mathbf{a}_{\mathrm{s}}\, \mathrm{d}A \qquad (13)$$

where $\boldsymbol{\sigma}_{\mathrm{m}}$ is the stress vector with normal and shear stress components, i.e. $\boldsymbol{\sigma}_{\mathrm{m}} = \begin{bmatrix} \sigma_{xx} & \sigma_{xy} \end{bmatrix}^{\mathrm{T}}$, and $\mathbf{k}_{\mathrm{m}}$ is the material tangent stiffness ($\mathbf{k}_{\mathrm{m}} = \mathrm{d}\boldsymbol{\sigma}/\mathrm{d}\boldsymbol{\varepsilon}$) at the material point.

5.1.2. Approximation of Shear Strain Distribution on Flanges

In the study by Saritas and Filippou (2009a), flange shear strain was assumed as negligible for shear-link specimens used in eccentrically braced frames. This is a relatively safe assumption when the flange thickness is rather small as observed in the specimens tested by Hjelmstad (1983) and Kasai (1985). When the flange thickness gets larger, this assumption should be modified.

Determination of the shear strain distribution on the flanges for a beam finite element model is a complicated and difficult task to undertake. In a relatively simplified finite element modeling approach such as a beam finite element, it would actually be unrealistic to expect the same level of accuracy attained from a 3-D solid and even 2-D shell finite element modeling approach. In this regards, an approximation that suits the needs for the estimation of shear strain on the flanges of a typical steel shear-link member would be a satisfactory path to follow.

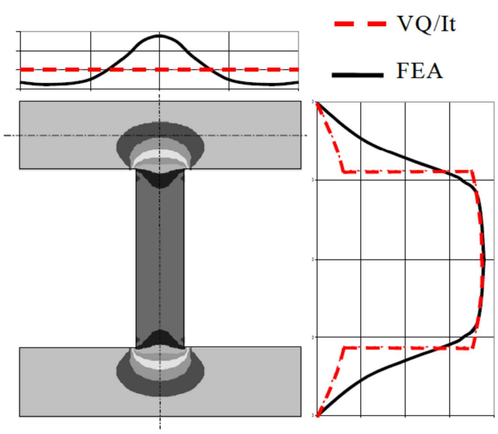

Fig. 5.2 Comparison of vertical shear strain distributions by Iyer (2005)

A shear strain distribution can be obtained under linear elastic conditions, just as the same bases of assumption made in plane sections remain plane assumption. The distribution of vertical shear strain on a wide-flange section can be obtained from $(VQ)/(It)$ approximation. In order to obtain a more accurate distribution of shear strain on the section, either theory of elasticity or 3d finite element models can be employed. In the study by Iyer (2005), vertical shear strain distribution obtained from 3d finite element analysis (FEA) was compared with $(VQ)/(It)$ approximation as shown in Fig. 5.2.

It is evident from Fig. 5.2 that mechanics of materials estimation provides good match for the web region; however there are significant discrepancies on the flange portion. Furthermore, vertical shear strain distribution on flanges not only changes along the thickness of the flange but also along the width of the flange. Considering such a complicated strain distribution for a beam finite element model will not be pursued here. Instead, a constant shear strain will be used on the flanges.

An initial reference value of flange shear strain, which may be used for further modification, can be calculated from the junction of the web and flange by the use of Equation 14 as follows:

$$\gamma_{flange} = \frac{t_{web}}{b_{flange}} \psi(d/2)\gamma = \frac{4t_f}{d}\beta\gamma \tag{14}$$

where γ is the section shear deformation.

For a wide flange section approaching to a rectangular section, β coefficient goes to 5/4. As flange area increases, i.e. α increases, value of β drops as given in Table 5.1.

Table 5.1 Variation of parameter β for various wide-flange sections

α	0	0.25	0.5	1	2	3
β	1.250	0.805	0.581	0.370	0.213	0.150

In this thesis, the constant flange shear strain value in Equation 14 is modified in order to get a better match in the comparative study that is presented in Chapter 6. The justification for this modification comes from the complexity of the shear strain distribution under various loading and boundary conditions, as well as due to nonlinear material behavior. It should be recalled that depth to length ratio of a shear-link member actually violates the mechanics of materials calculations due to Saint Venant's principle.

As a conclusion of the study conducted in this thesis, the following constant flange shear strain is suggested for use on shear-link specimens as a multiple of shear deformation acting on the section:

$$\gamma_{flange} = \eta\gamma \quad \text{where} \quad \eta \cong \frac{2t_f}{d} \tag{15}$$

where η can also be associated with the length ratio of total flange thickness to depth of the section. By the way, further research on the determination of a more exact value of flange shear strain acting on thick-flanged shear-link members is recommended.

5.1.3. Material Response

For the description of stress-strain relations of steel material model under cyclic loading conditions, a nonlinear kinematic hardening model should be used in order to accurately capture Bauschinger effect. In the study by Saritas and Filippou (2009a), the generalized plasticity material model proposed by Lubliner et al. (1993) was implemented. This material model in reality is similar to the bilinear hardening model; however, instead of a sharp change from elastic to plastic, a gradual evolution is prescribed through two parameters: the distance ϕ that measures this transition in stress space and the asymptotic transition parameter, called yield radius δ.

The original model by Lubliner et al. (1993) was modified by Saritas and Filippou (2009a) in order to get better match for Bauschinger effect for reinforcing steel specimens tested under uniaxial cyclic loading, and the following model properties were suggested: elastic modulus E was set to be the same as the elastic modulus of steel documented in a coupon test; the radius of yield function σ_y of generalized plasticity material model was taken to be equal to 50% of the yield strength f_y measured in a coupon test; the distance ϕ from the asymptotic yield surface to the yield function was used as 65% of ($f_u - 0.5 f_y$), where f_u is the ultimate strength measured in a coupon test; the transition parameter from the yield function to the asymptotic yield surface was expressed as $\delta = 0.25E$; the isotropic hardening modulus was set as $H_i = 0.0002E$; the kinematic hardening modulus was set as $H_k = 0.005E$; and Poisson's ratio is taken as 0.3.

It is important to realize that the study conducted in this thesis uses a multi-linear kinematic hardening material model calibrated as presented in Chapter 4 with the methodology suggested by Kaufmann et al. (2001). Differences in material model types and the calibration techniques employed for multi-linear kinematic hardening model for ANSYS and the generalized plasticity material model for frame finite element analysis will definitely result in slight differences in cyclic loops and energy absorption characteristics for the steel material model. It should also be reminded that the differences in the nonlinear response of shear-link members would not just be due to the use of different material models but also due to the use of shell versus frame elements, as well. With these in mind, the results obtained by the use of frame finite element model are presented in the next section.

5.2. Verification of Frame Finite Element

The following results were previously presented in the paper by Saritas and Filippou (2009a), and they are given here once more for completeness of documentation for the demonstration of the accuracy provided by the frame finite element in capturing the nonlinear response of Hjelmstad's and Kasai's specimens.

Specimen 4 by Hjelmstad was modeled with single element, and Specimen 3 and Specimen 5 by Kasai were modeled by two elements. For each element in all simulations, four monitoring sections with positions determined from Gauss-Lobatto integration rule were used to capture spread of plasticity. On each section, 8 layers were used on web and 4 layers are used on each flange, where midpoint integration rule was used in obtaining section forces and stiffness matrices. Yield strength, ultimate strength and stiffness values on the web and flange were used as given in the experiments. A 3-D generalized plasticity material model was implemented to capture Bauschinger effect in steel. Material parameters were calibrated as discussed in depth by Saritas and Filippou (2009a) in order to get close match with experimental data.

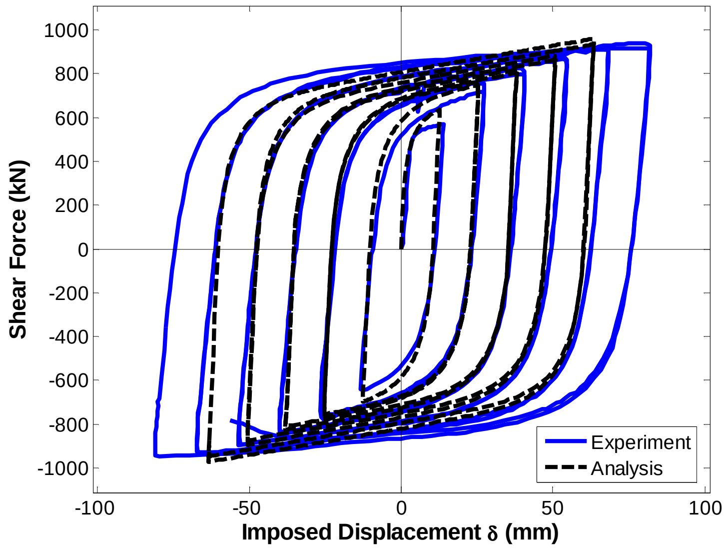

Fig. 5.3 Analytical vs. experimental results for Specimen 4 by Hjelmstad (1983)

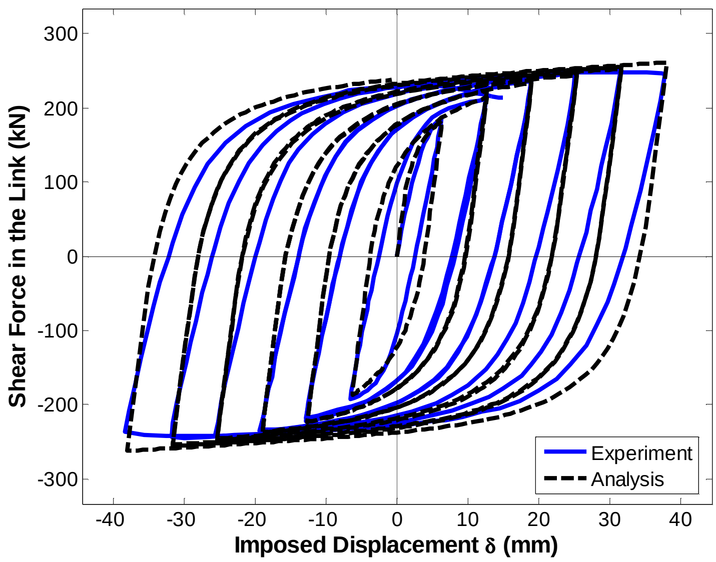

Fig. 5.4 Analytical vs. experimental results for Specimen 5 by Kasai (1985)

Shear force versus imposed displacement responses of the frame finite element model are compared with the experimental data of Specimen 4 by Hjelmstad in Fig. 5.3, Specimen 5 of Kasai in Fig. 5.4, and Specimen 3 of Kasai in Fig. 5.5. While Hjelmstad's specimen is a fairly short shear-link, specimens by Kasai are much longer and actually contain both shear and flexure yielding mechanisms; furthermore, experimental loading and boundary conditions in the specimens are much different. Despite these variations, it is evident that the frame finite element model provides very good match in terms of estimating both shear force capacities and energy dissipation characteristics of the specimens.

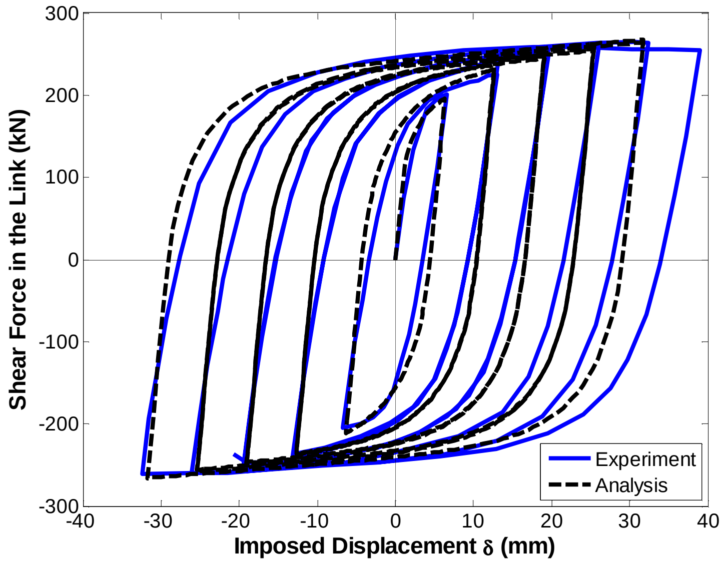

Fig. 5.5 Analytical vs. experimental results for Specimen 3 by Kasai (1985)

CHAPTER 6

COMPARATIVE STUDY WITH THE USE OF DIFFERENT ANALYTICAL MODELS

In this chapter, two different comparative studies are undertaken for the assessment of the accuracy of numerical models in capturing cases other than tested in the experiments. First the contribution of flange to the shear load carrying capacity of the link will be investigated, and then the behavior of the links under unsymmetrical cyclic loading protocols will be studied. To achieve these studies, not only the finite element models created in ANSYS Workbench are used but also the frame finite element discussed in Chapter 5 is also taken into account.

6.1. Influence of Flange Thickness

6.1.1. Parametric Values and Loading

For typical wide flange sections used in eccentrically braced frames, most of the shear force is resisted by the web; however, as the flange thickness increases, shear force carried by the flange under inelastic loading conditions may overstrength the response of a shear-link. In order to assess this increase, Specimen 4 of Hjelmstad (1983) is considered for a comparative finite element study. As part of this numerical study, shell and solid finite element models available in ANSYS are considered in modeling Specimen 4, where the material model and parameters for these simulations is exactly the same as employed in the verification study done for this specimen in Chapter 4. By the way, the same specimen is also modeled with the frame finite element proposed by Saritas and Filippou (2009a), where the material model is the same as employed in the numerical study by Saritas and Filippou (2009a). In this regards, there is not only a difference in terms of finite element modeling approach, but also in terms of material modeling approach, as well. Despite expected discrepancies due to modeling differences, comparison of the overstrengthening values obtained from different finite element models will provide means for verification of frame finite element model with respect to much more accurate shell and solid finite element models. The main deficiency of the frame finite element model is the lack of an accurate representation of flange shear strain.

Table 6.1 Flange thicknesses of the specimens used in parametric analysis

	Original Flange Thickness mm	20 % increase mm	50 % increase mm	80 % increase mm	100 % increase mm
Specimen 4 of Hjelmstad	13.23	15.876	19.845	23.814	26.46

In order to conduct the comparative finite element study on Specimen 4 of Hjelmstad (1983), the flange thickness of this specimen is increased with by 20%, 50%, 80%, and 100% as given in Table 6.1 by keeping the depth of web constant. The right end of this specimen is monotonically loaded until reaching 3 inches (76.2 mm) displacement.

In ANSYS, conducting a parametric study is relatively easy. The models with different thicknesses are created automatically with the help of parameter option in ANSYS Workbench (Fig. 6.1).

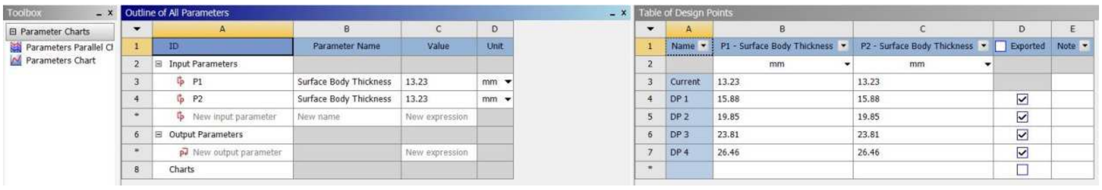

Fig. 6.1 Parameters for Specimen 4 of Hjelmstad

6.1.2. Results and Remarks

In Chapter 4, verification study conducted for Specimen 4 of Hjelmstad (1983) was done through the use of shell elements instead of solid finite elements. The reason for this selection actually based on trial analyses in order to estimate the accuracy provided by the use of shell elements over more accurate solid elements. First, shell and solid finite element modeling approaches in ANSYS will be compared, and the accuracy of the use of shell elements for this specimen will be validated, where this specimen had 13.23 mm flange thickness. The finite element mesh for the shell simulation was given in Figure 4.3, where only single layer shell was considered along the thickness direction of the flange. For modeling the response of the same specimen with solid elements, single mesh (Fig. 6.2) is used along the thickness direction, as well.

After this comparison, flange thickness value is increased for both the shell end solid finite element models. For thicker flanges, mesh refinement along the flange thickness direction is considered (Fig. 6.3).

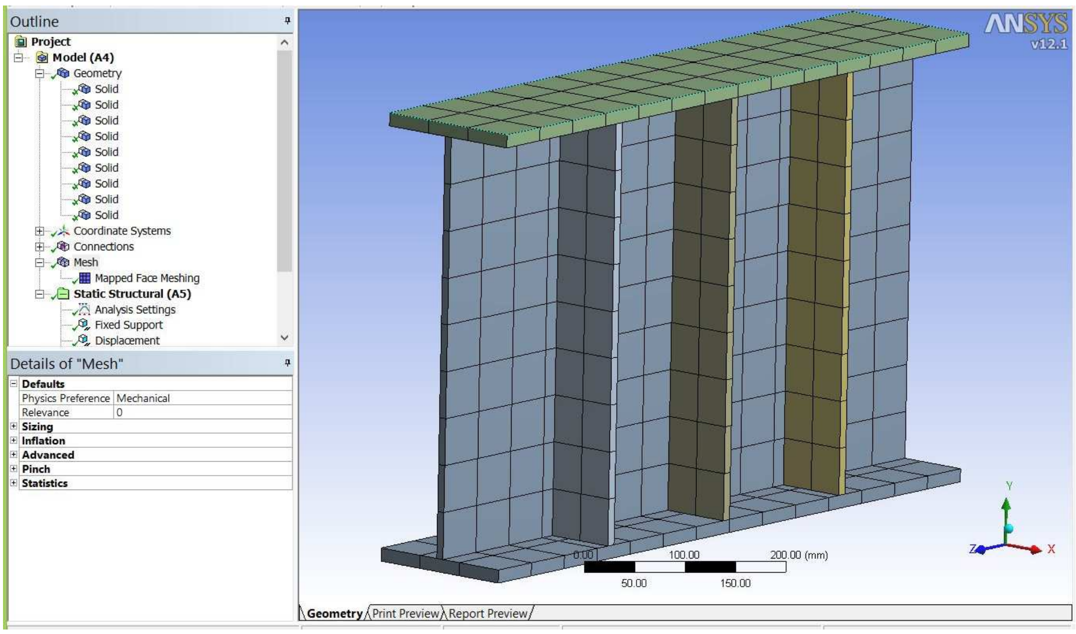

Fig. 6.2 Solid finite element model created in ANSYS Workbench

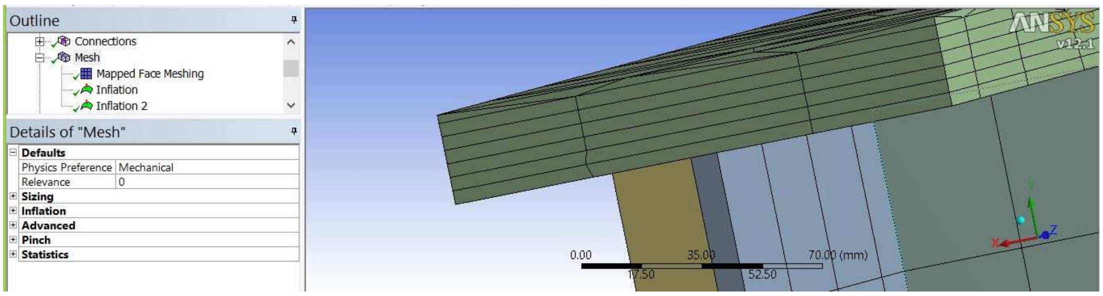

Fig. 6.3 The meshes created along the flange thickness for solid finite element model

For Specimen 4 with flange thickness 13.23 mm, i.e. the original Specimen 4 of Hjelmstad, very small difference is present in the shear force levels reached at the end of loading with the use of shell element with single layer over the use of solid finite element (Fig. 6.4). The main reason of the similarity in response is due to the small flange thickness of the original specimen. As a result, it can be concluded that shell elements sufficiently represent the nonlinear spread of plasticity both in terms of normal and shear stresses for most shear-link members employed in eccentrically braced frames.

As mentioned in Chapter 3 of in this thesis, ANSYS Workbench as default uses the 4 node shell element called as “SHELL181”. To increase the accuracy of the results the analysis of the shear link models with thicker flanges also conducted with another type of shell called as “SHELL281” which is an 8-node shell element and has 6 degrees of freedom at each node. The user interface of the ANSYS Workbench version 12.1 does not provide an option to change the shell type preferred for the model, but the shell type can be changed from the input script file for analysis by writing “SHELL281” over “SHELL181” manually at appropriate locations and ANSYS Workbench can be forced to use “SHELL281” instead of

“SHELL181” through this method. However, analysis with “SHELL281” did not result in any change with respect to the analysis with SHELL181.

As the flange thickness increases from 13.23 mm to 26.46 mm (i.e. 100% increase), the use of shell element results in more pronounced deviations with respect to the solid finite element results as shown in Fig. 6.4. In the same plot, it is also evident that the use of single meshing along flange thickness is sufficient for the solid model to get the same level of accuracy attained from seven layers of solid element meshing along flange thickness direction.

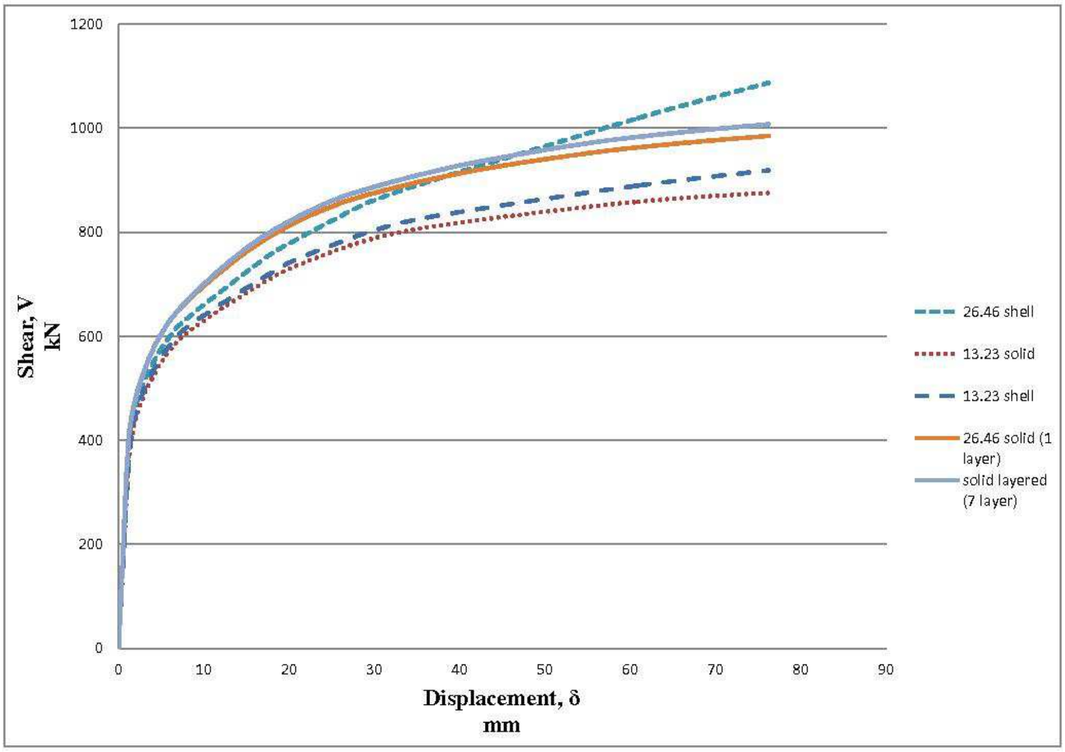

Fig. 6.4 Comparison of the shell and solid finite element model results

In the light of the results, the solid model with single layer discretization along flange thickness directions is chosen for the parametric analysis due to its accuracy. Fig. 6.5 represents the over-strengthening in shear capacity as flange thickness increases with solid models. The ratio of the shear capacities of each model to the original model are shown in Fig. 6.6. It is observed that the shear capacity of the link with 26.26 mm (100% flange thickness) is 12% more of the shear capacity of the original specimen in the inelastic region.

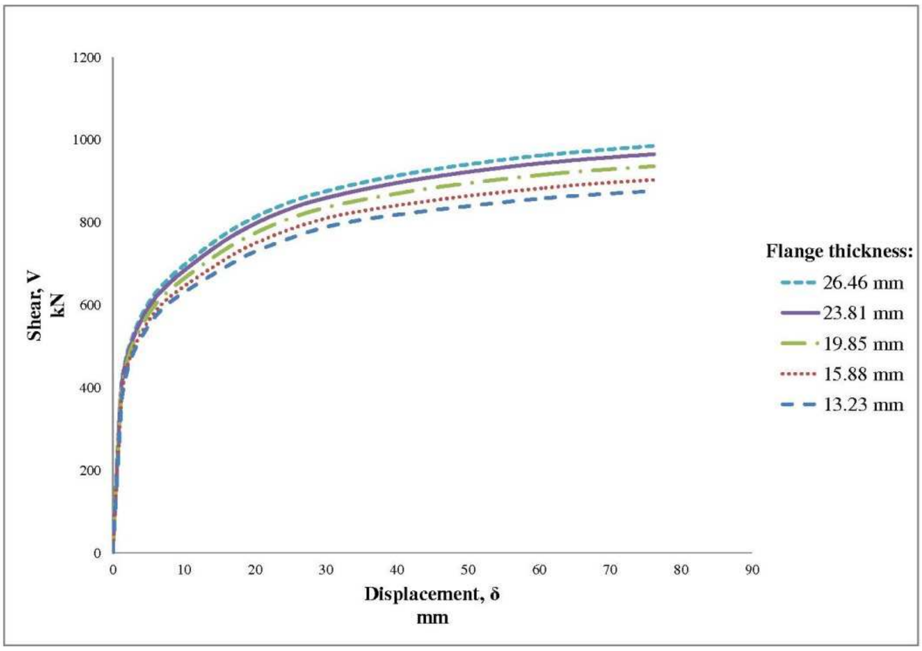

Fig. 6.5 Comparison of solid models created in ANSYS Workbench with different flange thicknesses

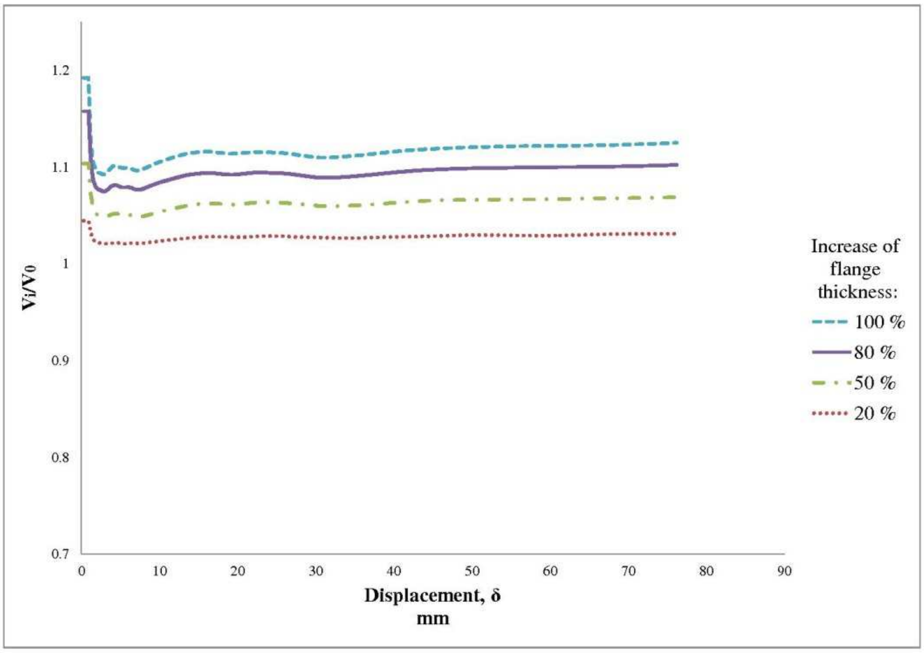

Fig. 6.6 Increase in shear capacity where V_i is the shear capacity of each model, V_o is the shear capacity of the original specimen

For the frame finite element model, shear force versus end displacement for the shear-links under varying flange thicknesses are presented in Fig. 6.7. A one to one direct comparison of the load-displacement plots between the solid and frame finite element models could be misleading in the sense that calibration of the material parameters were done totally in a different manner in both models. Despite this remark, the shear force estimation at 3 inches

(76.2 mm) displacement in the solid model is 875.5 kN (Fig. 6.5), and in the frame model including flange shear strain effect is 857.8 kN, and the frame finite element provides a close value with respect to solid element. This small difference is not only due to the use of 1-D (frame) element modeling approach versus 3d (solid) finite element modeling approach, but also due to the difference in the implemented materials models and the calibration of material parameters.

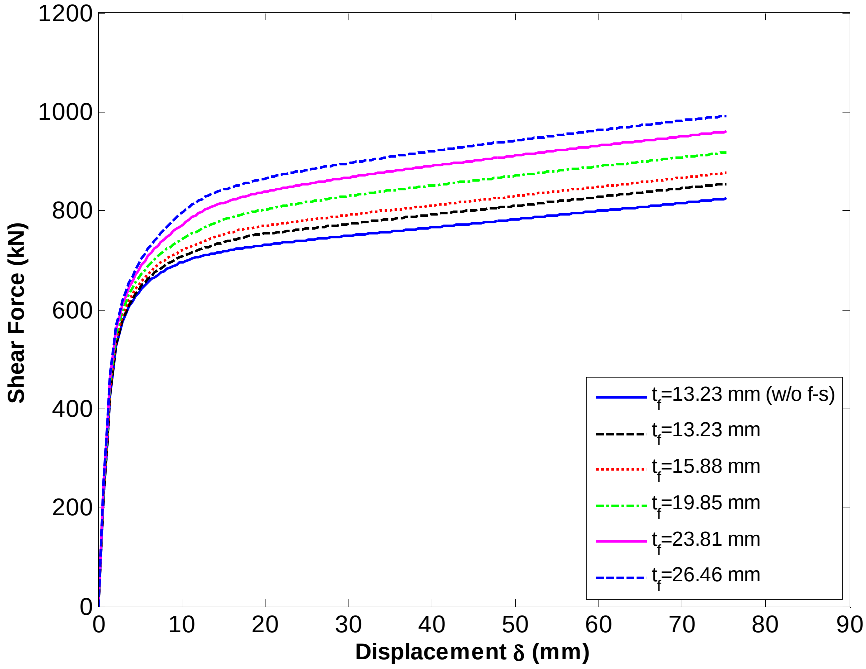

Fig. 6.7 Comparison of frame finite element models with different flange thicknesses

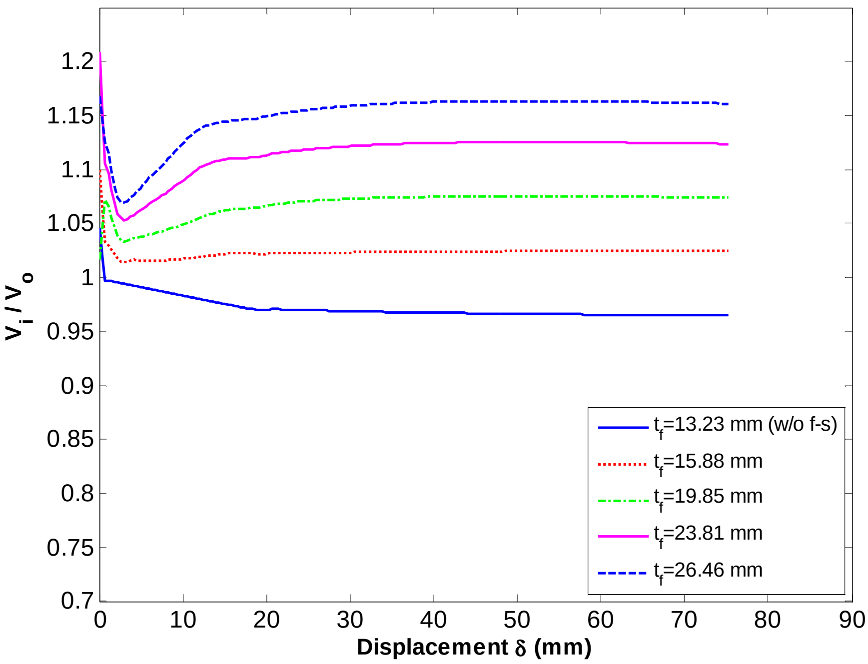

Fig. 6.8 Increase in shear capacity where V_i is the shear capacity of each model, V_o is the shear capacity of the original specimen with flange shear included

A much more important comparison between the frame finite element model and the solid finite element model can be made with regards to the over-strengthening of the shear force carrying capacities estimated by both models as flange thickness increases. As shown in Fig. 6.8, the frame finite element model estimates 15% increase with respect to the original specimen's shear force capacity as the flange thickness increases 100% with respect to the original specimen dimension, while the solid finite element model estimates 12% increase as shown in Fig. 6.6. While including flange shear strain is important as flange thickness increases, Fig. 6.8 also shows the fact that flange shear strain may be neglected in the original specimen's response. Setting flange shear strain equal to zero in the frame finite element model for the original specimen with 13.23 mm flange thickness only lowers the estimated shear force capacity by 3.5% as presented in Fig. 6.8.

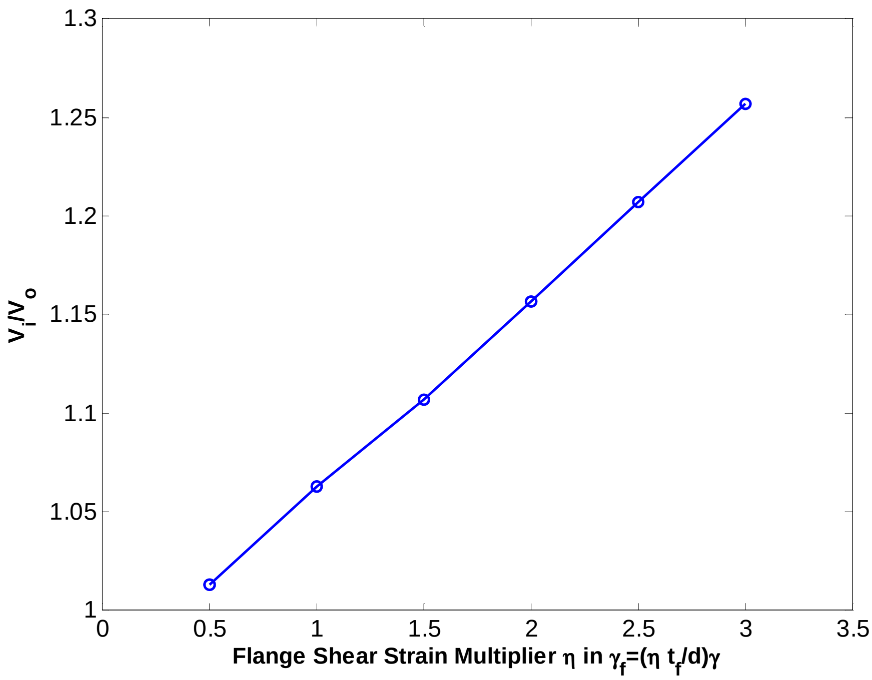

Fig. 6.9 Increase in shear capacity where V_i is the shear capacity of each model, V_o is the shear capacity of the original specimen for varying flange shear strain multiplier values

The estimation obtained by frame finite element in Fig 6.7 and Fig 6.8 assumes flange shear strain multiplier as 2 in the equation $\gamma_f = \left(2t_f / d\right)\gamma$ as given in Chapter 5. Changing the multiplier in the flange shear strain greatly influences the attained results. Fig. 6.9 presents V_i/V_o results for different multipliers of flange shear strain, where the increase fits a linear relationship. Apparent from Fig 6.9 selection of the multiplier as 1.5 instead of 2 gives a much closer match with respect to the increase obtained in solid finite element analysis. It is also worth knowing that overestimation would be an on the safer side result, especially since the force carried by the shear-link greatly influences the forces acting on the rest of the members in an eccentrically braced frame. An underestimation of shear force capacity of link members would cause an under design for the remaining members. Furthermore, since the boundary conditions of Hjelmstad's experimental setup provides more uniform loading along a shear-link member, adjustment of the flange shear strain value through this specimen is also considered as a safe approach. As a result, the current study suggests the use of

$\gamma_f = \left(2t_f/d\right)\gamma$ flange shear strain value for frame finite elements used towards nonlinear analysis of shear-link members.

6.2. Near Fault Loading and Nonlinear Behavior of Shear-Links

The purpose of using eccentrically braced frame is to provide lateral stiffness to the structure as well as sufficient energy dissipation capacity to overcome the seismic forces. Earthquake excitations create inherently cyclic and random forces and in addition to this the resulting cyclic displacements of a structure are usually not symmetric at all. To understand and predict the behavior of the shear links under different loading conditions, especially cyclic loading, the experimental studies are very important. But such kind of experiments is generally not pursued in assessing the behavior of structural members during static cyclic loading tests. On the other hand, availability of such data could be important in terms of assessing the accuracy of a numerical model employed for structural analysis. In Chapter 4, comparison of the finite element analysis results with the experimental results showed that the finite element models created in ANSYS Workbench gives very close estimates with experimental data and can be used for further analysis for comparison purposes with frame finite element analysis.

6.2.1. Loading Protocols

The near-fault loading protocol considered in this thesis was originally proposed by Krawinkler et al. (2000) for the evaluation of performance of steel moment resisting frames subjected to near-fault ground motions. The near-fault loading protocol includes a large one sided impulse and afterwards followed by many small cycles as shown in Fig. 6.10. In the study of Krawinkler et al. (2000), this protocol is constructed based on the reactions of SAC model buildings to the SAC near-fault ground motions for Los Angeles.

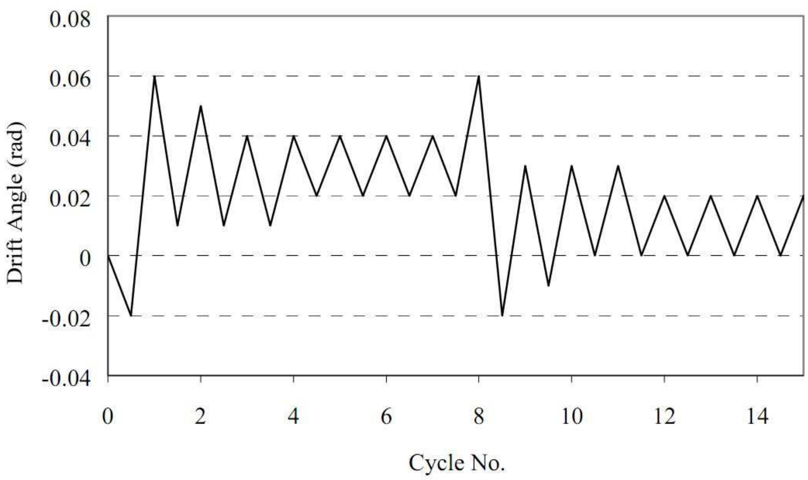

Fig. 6.10 SAC Near-fault (Krawinkler (2009))

Krawinkler et al. (2001) developed another near-fault loading protocol for the testing of wood framed structures as part of CUREE Wood Frame Project. This protocol is for short period wood framed structures and begins with little cycles and continues with bigger impulses as shown in Fig. 6.11.

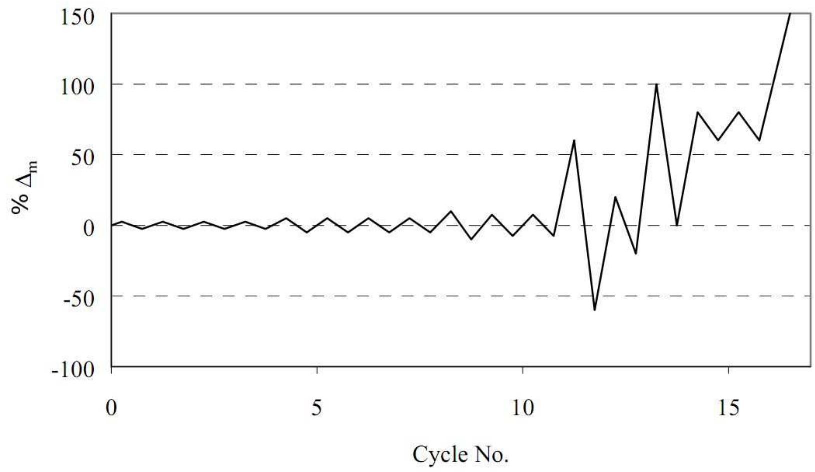

Fig. 6.11 CUREE Near-fault (Krawinkler (2009))

The loading histories used in the current study are constructed based on SAC and CUREE near-fault loading protocols, and modifications are introduced in order to reduce the amount of computation time by eliminating some of the cycles of displacements. The aim of using repetitive cycles in experiments is to inflict damage in structure and to observe possible isotropic hardening or low cycle fatigue effects. Reduction of cycles may be justified while such actions are not present or negligible in the inelastic response of a shear-link specimen. Reducing 4-5 cycles of same deformation to 2-3 cycles do not change the response of a well-designed shear-link member. The modified loading histories are applied on both Specimen 4 of Hjelmstad (1983) and Specimen 5 of Kasai (1985). For both specimens different loading protocols are constructed by considering the maximum displacements attained in the symmetric loading protocols of the original experiments, i.e. the displacement due to the largest impulse in near-fault loading protocols is set as the same value of the maximum displacement of the original experiment.

Fig. 6.12 and Fig. 6.13 represent the imposed displacement histories to the specimens in the finite element analysis. The loadings are applied both on the finite element model constructed in ANSYS Workbench and on the frame finite element model. The results obtained from the analysis are compared to each other in the next section.

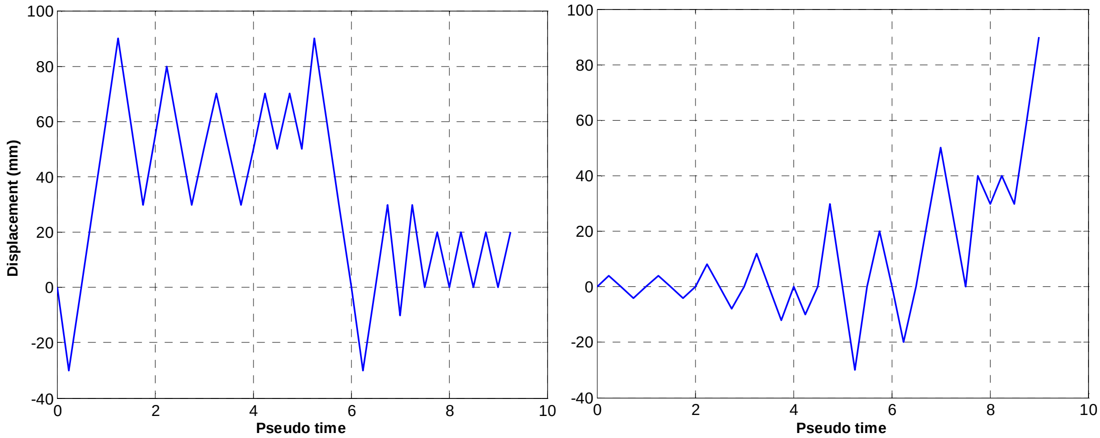

Fig. 6.12 Near-fault loading protocols for Specimen 4 of Hjelmstad:
SAC protocol (left), CUREE (right)

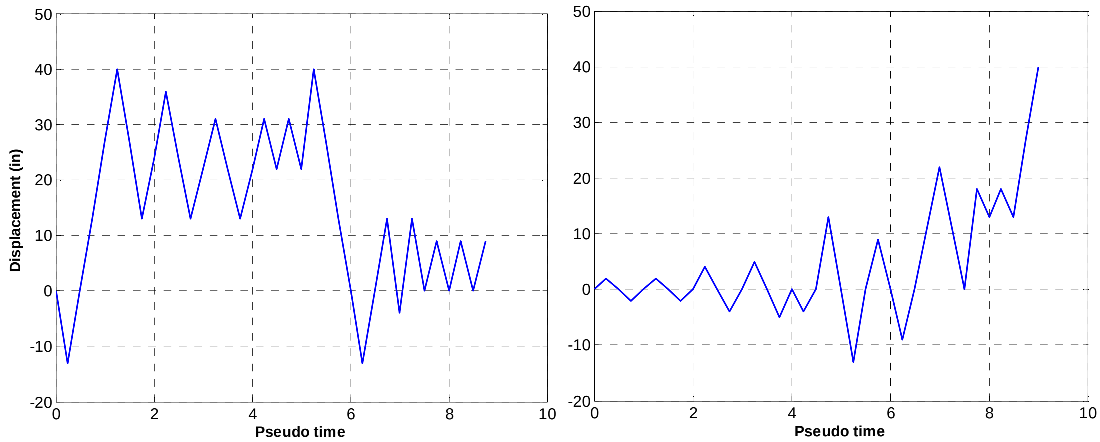

Fig. 6.13 Near-fault loading protocols for Specimen 5 of Kasai:
SAC protocol (left), CUREE (right)

6.2.2. Analysis Results and Remarks

Shear force versus imposed displacement responses obtained from SAC and CUREE loading protocols for Specimen 4 of Hjelmstad and Specimen 5 of Kasai are presented in Fig. 6.14 and Fig. 6.15, respectively. Despite the fact that the scale of finite element models are totally different and with the fact that the implemented material models and calibration of cyclic material parameters are not the same, the eventual shear force versus imposed displacement responses obtained from all near-fault loading protocols provide fairly close match between the frame and shell finite element models.

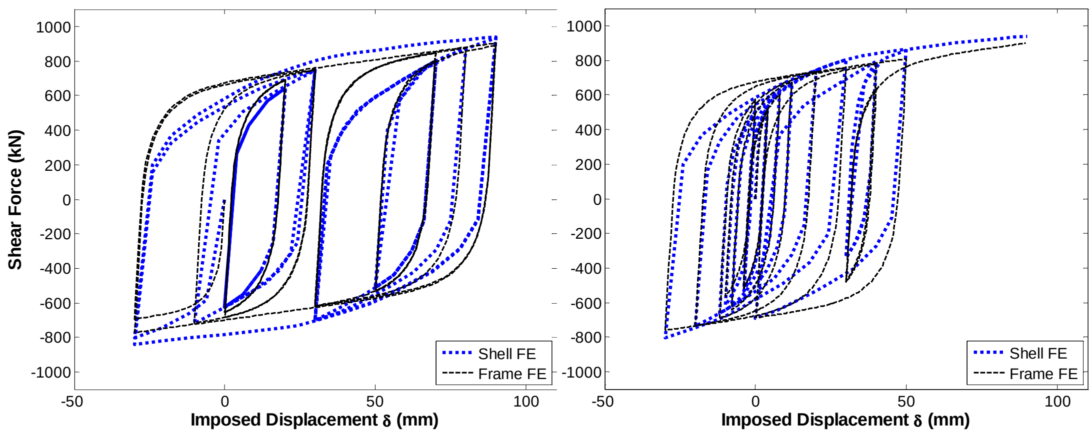

Fig. 6.14 Responses of Specimen 4 of Hjelmstad under SAC loading protocol (left) and CUREE loading protocol (right)

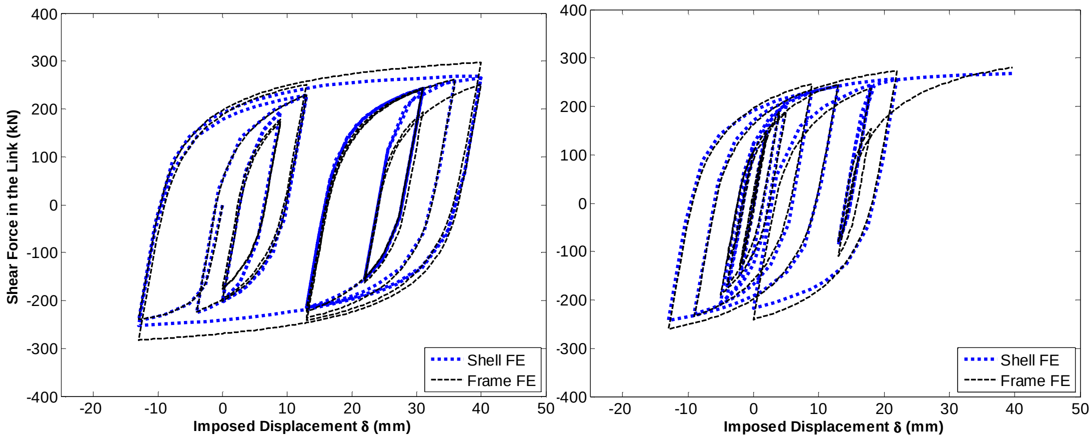

Fig. 6.15 Responses of Specimen 5 of Kasai under SAC loading protocol (left) and CUREE loading protocol (right)

It is worth to consider that the unsymmetrical loading protocols did not cause considerable divergences in the numerical results not only in terms of estimated shear force capacities but also in terms of dissipated energy. While the shell finite element models had 318 numbers of elements (450 nodes) for Hjelmstad's specimen and 1200 numbers of elements (1527 nodes) in Kasai's Secimen 5, frame finite element model only had 1 element (2 nodes) for Hjelmstad's specimen and 2 elements (3 nodes) for Kasai's specimen. The level of accuracy provided by the frame finite element with so few finite elements clearly demonstrates the robustness of the frame model and further strengthens its numerical efficiency in use towards nonlinear structural analysis.

CHAPTER 7

CONCLUSION

7.1. Summary

The study conducted in this thesis investigated finite element modeling of the nonlinear behavior of steel shear links, which constitute the most important part of an eccentrically braced steel frame system.

The first chapter presented an introduction to eccentrically braced frames and explained the scope and purpose of the study conducted in this thesis. The second chapter mentioned important points on the behavior and design of shear links and summarized both experimental and analytical past studies conducted on shear links. The third chapter documented in detail the procedure of modeling and conducting analysis in ANSYS Workbench, which is the finite element software package employed for the numerical simulations carried out in the thesis.

In the fourth chapter, first of all, the specimens that are chosen from the previous studies are presented and detailed information on modeling of those specimens in ANSYS Workbench is given. The material model used for the cyclic analysis of steel shear-links is based on the data given in the experimental studies; however, these values are obtained from coupon tests and can only describe the monotonic behavior of steel material under uniaxial tension. The behavior of steel material under cyclic loading conditions is very much different than monotonic loading conditions due to a phenomenon known as Bauschinger effect. Therefore, a cyclic calibration method is proposed in order to better capture energy dissipation characteristics of steel material. After the suggested calibration method, finite element models are analyzed and the results of analyses are compared with the experimental data. A good agreement is captured between analysis and experimental results, thus it is concluded that the finite element model constructed in ANSYS Workbench is reliable and suitable for further research.

In the fifth chapter, a frame finite element model is introduced for the analysis of shear-links. In this chapter, formulation of the frame element is briefly summarized and approximation of shear strain distribution on the flanges of the link is presented. The chapter concludes with the verification of the frame finite element response with experimental data. As seen from the comparisons in this chapter, frame element model gives good response independent of the boundary conditions and the loading history.

In the sixth chapter, a comparative study towards capturing the nonlinear behavior of shear-links with different finite element modeling approaches and for cases that are not covered as part of an experimental study is undertaken. This comparison highlights the accuracy provided by a much simpler finite element modeling approach, which is a frame finite element, over more complex finite element modeling approaches, which are shell and solid finite elements. First a parametric analysis is performed with the models by changing the flange thickness to observe the flange contribution to shear carrying capacity of shear links. In this part of the study, the suitability of the 2-D (shell) elements to model shear-links with thick flanges is also examined. In this part, since the shell finite element has some difficulties to catch the behavior of steel with increased flange thickness, the analysis are performed with 3-D (solid) finite element models. As part of the comparative study, various unsymmetrical cyclic loading conditions are generated and used in order to assess and compare the responses of the finite element models for loading histories that are much more different than the proposed ones in the shear-link experiments. Once again, the accuracy provided by the frame finite element model over ANSYS models are elaborated.

7.2. Conclusion

The following conclusions are obtained from this thesis,

- Accuracy provided by the force (mixed) based frame finite element under both linear and nonlinear conditions is achieved by a single element discretization per member. On the other hand, the use of shell and solid elements necessitate great increase in the number of element discretization. It is known that increase in mesh size significantly influences matrix calculations and storage of data and this will place a burden on calculations if a much larger framed type structural system is analyzed with shell and solid elements versus frame finite element presented in this thesis.
- Shell (2-D) elements are suitable for modeling beams with I-sections with thin flanges, but for rolled or built-up sections with thick flanges, the accuracy attained by shell elements should be investigated carefully and solid finite elements should be preferred.
- The frame finite element with proposed flange shear strain assumption provides very close match when compared with the solid finite element results for shear-link specimens with thicker flanges.
- Influence of shear strain acting on the flanges of a thin flanged shear-link member is on the order of 3% of total shear force carried by the member. Thus, for a frame finite element formulation of a shear-link member, it is safe to assume the sandwich beam theory assumptions, i.e. the web carries all of the shear force.
- For nonlinear analysis of shear-link members with frame finite elements, the use of flange shear strain value $\gamma_f = \left(2t_f/d\right)\gamma$ is observed to provide a realistic and on the safe side capture of over strengthening observed in shear-link specimens with thicker flanges. However, further research on the determination of a more exact value of flange shear strain acting on thick-flanged shear-link members is recommended.
- The proposed calibration technique to represent cyclic behavior of steel in ANSYS by the use of multi-linear kinematic hardening material model gives

very close estimation of the nonlinear behavior of shear-link members. For the presented frame finite element, generalized plasticity material model proposed in literature was employed, and the capability of that material model in reflecting the cyclic behavior of steel has also resulted in overall close estimation of nonlinear response and energy dissipation characteristics of shear-link members.

- Under unsymmetrical loading conditions, the results attained by the frame finite element closely matches with the results obtained with the use of shell finite elements. Despite this close match, experimental specimens tested under more complex loading histories are needed in order to verify the reliability of finite element models in capturing the energy dissipation characteristics of structural members. Further work may be necessary especially in using a more complex steel material model that captures monotonic loadings, as well as various symmetrical and unsymmetrical loading conditions. Such a material model is actually not available in ANSYS. In this regards, further research work focusing on the development of more elaborate steel material models are needed.

REFERENCES

AISC (2005). Seismic provisions for structural steel buildings, American Institute of Steel Construction.

AISC (2010). Seismic provisions for structural steel buildings, American Institute of Steel Construction.

ANSYS, I. (November, 2009). ANSYS Workbench User's Guide. Canonsburg, PA.

Berman, J. W. and M. Bruneau (2007). "Experimental and analytical investigation of tubular links for eccentrically braced frames." Engineering Structures **29**(8): 1929-1938.

Della Corte, G., M. D'Aniello and R. Landolfo (2013). "Analytical and numerical study of plastic overstrength of shear links." Journal of Constructional Steel Research **82**: 19-32.

Engelhardt, M. D. and E. P. Popov (1989). "On design of eccentrically braced frames." Earthquake Spectra **5**(3): 495-511.

Engelhardt, M. D. and E. P. Popov (1992). "Experimental Performance of Long Links in Eccentrically Braced Frames." Journal of Structural Engineering-ASCE **118**(11): 3067-3088.

Ghobarah, A. and T. Ramadan (1990). "Effect of Axial Forces on the Performance of Links in Eccentrically Braced Frames." Engineering Structures **12**(2): 106-113.

Hjelmstad, K. D. (1983). Seismic Behavior of Active Beam Links in Eccentrically Braced Frames Ph.D., University of California.

Hjelmstad, K. D. and E. P. Popov (1983). "Cyclic Behavior and Design of Link Beams." Journal of Structural Engineering-ASCE **109**(10): 2387-2403.

Hjelmstad, K. D. and E. P. Popov (1984). "Characteristics of Eccentrically Braced Frames." Journal of Structural Engineering-ASCE **110**(2): 340-353.

Inc., A. (2009). ANSYS Workbench Finite Element Analysis Program. Canonsburg, PA.

Itani, A. M., C. Lanaud and P. Dusicka (2003). "Analytical evaluation of built-up shear links under large deformations." Computers & Structures **81**(8): 681-696.

Iyer, H. (2005). The Effects of Shear Deformation in Rectangular and Wide Flange Sections. M.S., Virginia Polytechnic Institute and State University.

Kasai, K. (1985). A Study of Seismically Resistant Eccentrically Braced Frame Systems Ph.D., University of California.

Kasai, K. and E. P. Popov (1986a). "Cyclic Web Buckling Control for Shear Link Beams." Journal of Structural Engineering-ASCE **112**(3): 505-523.

Kasai, K. and E. P. Popov (1986b). "General Behavior of Wf Steel Shear Link Beams." Journal of Structural Engineering-ASCE **112**(2): 362-382.

Kasai, K. and E. P. Popov (1986c). A study of seismically resistant eccentrically braced steel frame systems, Earthquake Engineering Research Center, College of Engineering, University of California.

Kaufmann, E., B. Metrovich and A. Pense (2001). "Characterization of Cyclic Inelastic Strain Behavior On Properties of A572 Gr. 50 and A913 Gr 50 Rolled Sections." ATLSS Rep(01-13).

Krawinkler, H. (2009). Loading histories for cyclic tests in support of performance assessment of structural components. The 3rd International Conference on Advances in Experimental Structural Engineering.

Krawinkler, H., A. Gupta, R. Medina and N. Luco (2000). Development of loading histories for testing of steel beam-to-column assemblies, Stanford University.

Krawinkler, H., F. Parisi, L. Ibarra, A. Ayoub and R. Medina (2001). Development of a testing protocol for woodframe structures, CUREe Richmond, CA.

Lubliner, J., R. L. Taylor and F. Auricchio (1993). "A New Model of Generalized Plasticity and Its Numerical Implementation." International Journal of Solids and Structures **30**(22): 3171-3184.

Malley, J. O. and E. P. Popov (1983). "Design considerations for shear links in eccentrically braced frames." NASA STI/Recon Technical Report N **84**: 30136.

Malley, J. O. and E. P. Popov (1984). "Shear Links in Eccentrically Braced Frames." Journal of Structural Engineering-ASCE **110**(9): 2275-2295.

Okazaki, T. (2004). Seismic Performance Of Link-To-Column Connections in Steel Eccentrically Braced Frames. Doctor of Philosophy, The University of Texas at Austin.

Okazaki, T. and M. D. Engelhardt (2007). "Cyclic loading behavior of EBF links constructed of ASTM A992 steel." Journal of Constructional Steel Research **63**(6): 751-765.

Prinz, G. and P. Richards (2009). "Eccentrically braced frame links with reduced web sections." Journal of Constructional Steel Research **65**(10): 1971-1978.

Ramadan, T. and A. Ghobarah (1991). "Prediction of the Ultimate Capacity of Wide Flange Link Beams under Cyclic Loading." Computers & Structures **40**(2): 409-418.

Ricles, J. M. and E. P. Popov (1987a). Dynamic Analysis of Seismically Resistant Eccentrically Braced Frames, Earthquake Engineering Research Center, University of California, Berkeley.

Ricles, J. M. and E. P. Popov (1987b). Experiments on eccentrically braced frames with composite floors, Earthquake Engineering Research Center, University of California.

Ricles, J. M. and E. P. Popov (1994). "Inelastic link element for EBF seismic analysis." Journal of Structural Engineering **120**(2): 441-463.

Roeder, C. W. and E. P. Popov (1977). Inelastic Behavior of Eccentric Braced Frames, Earthquake Engineering Research Center, University of California, Berkeley.

Roeder, C. W. and E. P. Popov (1978). "Eccentrically Braced Steel Frames for Earthquakes." Journal of the Structural Division-ASCE **104**(3): 391-412.

Saritas, A. (2006). Mixed Formulation Frame Element for Shear Critical Steel and Reinforced Concrete Members, Ph.D. Dissertation, University of California, Berkeley.

Saritas, A. and F. C. Filippou (2009a). "Inelastic axial-flexure-shear coupling in a mixed formulation beam finite element." International Journal of Non-Linear Mechanics **44**(8): 913-922.

Saritas, A. and F. C. Filippou (2009b). "Inelastic axial-flexure–shear coupling in a mixed formulation beam finite element." International Journal of Non-Linear Mechanics **44**(8): 913-922.

Saritas, A. and O. Soydas (2012). "Variational base and solution strategies for non-linear force-based beam finite elements." International Journal of Non-Linear Mechanics **47**(3): 54-64.

Spacone, E., F. C. Filippou and F. F. Taucer (1996). "Fiber Beam-Column Model for Nonlinear Analysis of RC Frames: I: Formulation." Earthquake Engineering and Structural Dynamics **25**(7): 711-725.

Taylor, R. L., F. C. Filippou, A. Saritas and F. Auricchio (2003). "Mixed finite element method for beam and frame problems." Computational Mechanics **31**(1-2): 192-203.

Ucak, A. and P. Tsopelas (2010). "Constitutive model for cyclic response of structural steels with yield plateau." Journal of Structural Engineering **137**(2): 195-206.